

Ministry of Water Resources



Bangladesh Water Development Board

Coastal Embankment Improvement Project, Phase-I (CEIP-I)

Long Term Monitoring, Research and Analysis of Bangladesh Coastal Zone (Sustainable Polders Adapted to Coastal Dynamics)



FINAL SUBSIDENCE REPORT

JUNE 2022



Ministry of Water Resources



Bangladesh Water Development Board

Coastal Embankment Improvement Project, Phase-I (CEIP-I)

**Long Term Monitoring, Research and Analysis of
Bangladesh Coastal Zone (Sustainable Polders Adapted to
Coastal Dynamics)**

FINAL SUBSIDENCE REPORT

JUNE 2022

Long Term Monitoring, Research and Analysis of Bangladesh Coastal Zone

Office: Flat #3/B, House #4, Road #23/A, Banani, Dhaka 1213, BANGLADESH

Phone +880 1307 693299

Memo No: CEIP/LTMRA/0622/184

30 June 2022

Project Management Unit
Coastal Embankment Improvement Project, Phase-I (CEIP-I)
Pani Bhaban, Level-10
72, Green Road, Dhaka-1205

Attn: Mr. Syed Hasan Imam, Project Director

Dear Mr Imam,

Subject: Submission of Final Subsidence Report (D-4B).

It is our pleasure to submit herewith five copies of the "**Final Subsidence Report**".

This report focuses on the project components related to subsidence and cover the efforts to obtain new data and numerical modeling to better understand the rates and distribution of subsidence in the coastal zone of Bangladesh.

The longest running datasets analyzed for this report include 8 years of measurements in the Sundarbans mangrove forest at Sorbothkhali and Polder 32 at the village of Shrinagar. For the RSET-MH installed for this project, plots of surface elevation and vertical accretion are shown in the figures of Chapter 7.

Thanking you,

Yours sincerely,



Dr Ranjit Galappatti
Team Leader

Copies: Engineer Fazlur Rashid, Director General, BWDB
Dr. Zia Uddin Baig, ADG (Planning), BWDB
Dr Kim Wium Olesen, Project Manager, DHI
Ms. Sonja Pans, Deltares Project Manager
Mr Zahirul Haque Khan, Deputy Team Leader
Mr AKM Bodruddoza, Procurement Specialist
Swarna Kazi, Sr. Disaster Risk Management Specialist, World Bank

Contents

1	Introduction	1
1.1	Regional Setting	4
2	Compaction Processes.....	9
2.1	Previous Estimates of Subsidence in the GBD.....	10
2.2	Estimates of Subsidence in the GBD under this Project	15
2.3	Discussion.....	26
3	Subsidence Maps.....	31
4	Implications for Coastal Change	33
5	Summary	39
6	References	41
7	Supplemental Material.....	47
8	Additional References	59

List of Figures

Figure 1. Summary of the processes inducing subsidence in the Ganges-Brahmaputra Delta along an east-west cross-section of the delta. The maximum sediment thicknesses in the basin are approximately 20 km.....	3
Figure 2. Location map of Bangladesh and the Ganges-Brahmaputra Delta showing major tectonic and sedimentary boundaries, and the significant rivers. The Hinge Zone is the transition between the Indian craton and the Bengal Basin with up to 20 km of sediments. The Topographic Break is the boundary between the Fluvial Fan Delta to the north and the flatter Fluvial-Tidal Delta to the south (Wilson and Goodbred, 2015). K = Kolkata, Kh = Khulna, Dh = Dhaka, S = Sylhet, H = Hazipur-1 well, SoNG = Swatch of No Ground Canyon. The inset shows the regional topography with the outline of the drainage basin of the Ganges, Brahmaputra and Meghna River basins outlined in black and the rivers in white. The red box shows the location of the detailed figure.	5
Figure 3. Water level data from the Khepupara tide gauge. The top shows hourly data from the Bangladesh Inland Water Transportation Authority (BIWTA) in red and a tidal model from t_tide (Pawlowicz, 2002) in blue showing a mean sea level rise rate of 9.2 mm/y, indicated by a white line. However, examination of the data shows variable rates of sea level rise. The middle shows fits to the three distinct regimes with the rates noted below each segment. The bottom shows the more limited publicly-available time series from PSMSL. It corresponds approximately to the central portion of the longer times series when the apparent sea level rise rate was greatest.	10
Figure 4. Photo of the ~400 year old Shakher Temple in the Sundarbans with a closeup of our interpreted plinth level in the lower left.	11
Figure 5. Map of Ganges-Brahmaputra Delta from Grall et al., 2018, showing average subsidence rates over the Holocene (last 10,000 years) derived from radiocarbon dates samples of a suite of over 400 tube wells and a very high resolution seismic line along the Jamuna River (heavy black line). The subsidence rates increase southeast from the Hinge Zone to a maximum of ~4.5 mm/y. The subsidence rates in Sylhet may be underestimated because of the underfilling of the region by sediments. Tectonically induced subsidence is identified between the Dauki and Dapsi Faults near the Shillong Massif. Note the lack of subsidence north of Dhaka corresponding to the Madhupur Tract. The thin black line outlines the area imaged by InSAR in Higgins et al. (2014). Superimposed are the locations of the river gauges (Becker et al., 2020) as colored dots with the corresponding average rates on subsidence over a 20-year period for each set. The K indicates the position of the tide gauge at Khepupara.....	13
Figure 6. Results from the KHLC compaction meter. A) plot showing the decrease in compaction with depth. The blue dots show the shortening rate of the different length fibers and teal dots show the differential rate between pairs of fibers. Approximate exponential curves to the data for the total compaction and its derivative are shown. Note that all of the compaction is occurring in the Holocene sediments and there is effectively none in the Pleistocene. B) Google Earth image of the KHLC site. The wells were installed on the river bank in the red box. The double arrow shows the width of the river before 1989. Notice the large concrete bridge SE of KHLC over the now small river. C) photo of the marker at the base of one of the monuments taken in 2017 with a cm scale. The lower section shows ~6 cm of tidalites deposited over 4 monsoon seasons. Above are 4-6 cm of muddy deposits in the 2 years since the March 2015 dredging.....	14
Figure 7. Map of Bangladesh showing the location of tube wells drilled by our team over recent years. The wells circled in red were drilled as part of this project.	16
Figure 8. Average lithology across the lower delta along transects labeled in Figure 5.....	17
Figure 9. GPS antenna mounted on roof of	18
Figure 10. Map of GPS and RSET sites installed, upgraded or serviced in July 2019. All GPS sites now have cellular connections for data downloads. Previously HRNP point data was downloaded by the RSET team when they serviced the RSET.	18
Figure 11. Map of SW Bangladesh showing subsidence rates obtained from GNSS and historic sites. Size of fonts for GNSS sites are proportional to the length of the time series as a proxy for their reliability.	19
Figure 12. Map on the left shows the position of the 278 geodetic monuments installed by the SoB. The map above is a close up of the field area showing the 55 monuments targeted for reoccupation. 47 sites were successfully remeasured (green). The yellow circles are the positions of our continuous GPS installations.	20
Figure 13. Plots of the time series for two of the reoccupied campaign sites. For the site on the left, the three measurements are colinear. For the site on the right, the third measurements yielded uplift	

relative to the long-term trend. We suspect that this site has slumped and is now shifting vertically with the rice field. This supports our inference of monument stability. 21

Figure 14. Subsidence rates from the SoB monuments projected along a profile N160°E, perpendicular to the subsidence contours in Grall et al. (2018). Our initial interpretation is that the sites with rate of 18 mm/yr and higher are due to poor monument stability. The remaining rates show systematic trend on increasing from the NW to the SE. However, where there is overlap, the survey rates are about twice as large as the continuous GPS rates. These results require further investigation. 22

Figure 15. Schematic diagram (not to scale) of the RSET-MH method that is used to quantify shallow subsidence in wetland settings (from Bomer et al., 2019). The RSET measures interannual elevation change, and vertical accretion is measured using either marker horizons (brick dust or glitter) or sediment tiles. This method is modified in polder settings by burying aluminium plates at depth to measure vertical accretion. Shallow subsidence is measured from the difference in vertical accretion and surface elevation change. The bottom photo shows an installed RSET with glitter marker horizon. Above, the sediments accumulated on a tile are measured. At the top, the measurement rods are attached to the RSET and the surface elevation is being measured. 23

Figure 16. Inter-annual change in (A) surface elevation, (B) vertical accretion, and (C) shallow subsidence in the Sundarbans mangrove forest near Polder 32 (PD32, location shown in Fig 4) from Bomer et al. (2019). Positive values of shallow subsidence occur from compaction and dewatering of the shallow subsurface, and negative values represent expansion in the subsurface (i.e., clay shrink-swell, belowground biomass production-decay, etc.). Error bars are the standard error for all measurements. 25

Figure 17. Cartoon presenting a synthesis of subsidence versus depth based on combining measurements from multiple instruments, each of which measure compaction or subsidence over a different depth range. GPS on building and tide gauges measure subsidence below the building or gauge foundations and miss shallow compaction. The RSET-MH and KHLC compaction meter measure compaction above the base of their instruments. The campaign GPS on SoB monuments measures both shallow and deep subsidence. Combining the results, the synthesis column shows a preliminary estimate of subsidence in each depth range. The long-term rates correspond to the sum of the two deeper brown layers. 27

Figure 19. Map of subsidence rates for the Bangladesh coastal zone based on continuous GPS measurements, tide gauges and historic sites. The red dots are the locations of the sites used to construct the maps. 32

Figure 18. Map of subsidence rates for the Bangladesh coastal zone based on campaign GPS measurements. The red dots are the locations of the sites used to construct the maps. 32

Figure 20. Total cumulative subsidence estimated for 25, 50 and 100 years in the future based upon the subsidence rate map in Figure 18. 34

Figure 21. Land cover change 1989 - 2020. Landsat-derived continuous land cover fraction map (A) shows areal percent of soil/sediment substrate, vegetation (trees & crops) and water at 30 m resolution for February/March 2020. Continuous land cover change map (B) shows increase in areal percent of each land cover type between 1989 and 2020. Discrete land cover change classification (C, on following page) shows increases in land cover fraction > 20% between 1989 and 2020. Shoreline movement from erosion and deposition within the Bangladesh Sundarbans appear as elongate bands of increased tree cover (green) and water (blue) along channels and on island peripheries. Rank-size distributions (C inset) of spatially contiguous areas of > 20% increase observed within the Sundarban show more and larger changes related to bank erosion (water increase) and forest expansion (trees increase). Growth of tidal flats (substrate increase) is underrepresented because intertidal mud flats are much darker than dry soil and generally fall below the 20% increase threshold. The large increase in forest area is an indication of the rapid colonization of stable tidal flats by vegetation. Increases in vegetation and water outside the Sundarbans reflect increases in aquaculture and dry season agriculture, as well as significant expansion of tree cover on polder embankments north and east of the Sundarbans. 36

List of Tables

Table 1: Mean annual rates (\pm standard error) of surface elevation, vertical accretion measured by sediment tiles (ST) and marker horizons (MH), and shallow subsidence among study sites in the Sundarbans mangrove forest near Polder 32 (from Bomer et al., 2019). Shallow subsidence values are based on the difference between surface elevation change and vertical accretion from the sediment tile method, as Bomer et al., (2019) observed crab bioturbation led to slightly greater MH measurements..... 26

1 Introduction

Bangladesh is situated at the confluence of three great trans-Himalayan rivers, the Ganges, the Brahmaputra or Jamuna, and the Meghna, which form the Ganges-Brahmaputra Delta (GBD). While over 90 percent of the catchment of the GBD system lies outside of Bangladesh, more than 200 rivers and tributaries and distributaries of the GBD system drain through the country via a constantly changing network of channels, tidal inlets and creeks, forming the most active large delta on the planet. The coastal land mass is shaped by the interaction of large volumes of sediment laden water with the moderate to high tides of the Bay of Bengal.

Land in the coastal zone is built up by the deposition of river sediments in the tidal delta, including the mangroves of the Sundarbans, the largest mangrove forest in the world. The deposits of sand, silt, clay and organic material form the land mass, which despite subsidence due to continuous consolidation of layers many kilometers deep, is kept around the level of the highest tides by the continuing deposition of sediments.

The coastal zone of Bangladesh spans over 710 km of coastline and is subject to multiple threats. Sixty-two percent of the coastal land has an elevation less than 3 meters above mean sea level. With a sediment supply of 1 billion tons per year, this is the delta with the largest sediment supply in the world. This leads to continuing accretion of the land area in the coastal zone (5-10 km²/year), mainly in the Meghna Estuary, but also erosion of the coast farther west. It has been observed that the land subsidence rate may vary from place to place due to anthropogenic factors such as drainage and ground water extraction as well as the properties and depth of underlying strata. On top of this there are tectonic plate movements, particularly in the eastern delta, that give rise to other changes in ground level.

The coastal lands, particularly in SW Bangladesh, being subject to regular flooding by saline water during high tides, could not be used for normal agricultural production in a country with a very high demand for land. The Coastal Embankment Project (CEP) was initiated in the 1950s and 1960s to build polders surrounded by embankments preventing the spilling of saline water onto the land at high tides. These embankments were built along the larger rivers and across the smaller rivers and creeks which then formed the drainage system within each polder and connected to the peripheral rivers via appropriately sized flap gate regulators, that open at low tide to let the drainage water out.

The Coastal Embankment Project made possible the reclamation of large tracts of land for agriculture from 1960 onwards. Polder building proceeded continuously until today. We now have 1.2 million hectares reclaimed in 139 active polders in the coastal zone of Bangladesh.

In over half century of its existence, a number of challenges have surfaced that threaten the long-term safety and even the very existence of the polder system as a viable and sustainable resource. These are:

- Sea level rise and changes in precipitation and water discharge due to climate change
- Threats of damming and diversion to the delivery of river sediments from upstream

- Subsidence of land and structures founded on existing land. In places, this is compensated where land has been allowed to be rebuilt by natural or tidal flooding.
- Drainage congestion due to accumulation of silt in some peripheral waterways around polders
- Changes in tidal hydrodynamics and related river erosion and siltation in the peripheral rivers of polders
- Increasing vulnerability to cyclones and storm surges

The main objective of the “long-term monitoring, research and analysis of the Bangladesh coastal zone” project is to create a framework for polder design, based on understanding of the long-term and large-scale dynamics of the delta and sustainable polder concepts. The field and modelling work within the project is carried out to improve our understanding of the long-term and large-scale dynamics of the Ganges-Brahmaputra Delta (GBD). There is insufficient knowledge about sediment budget in the delta involving sediment transport within the estuaries, sediment sources and sediment distribution into the river system. Sediment and tidal dynamics are important for river and coastal erosion, land reclamation, and delta development. Subsidence of the land alters the topography and hydrodynamics, and increases flooding, coastal erosion and salinization. The knowledge on sediment dynamics, distribution, subsidence, erosion-deposition processes and sediment management at present and in the future under climate change, land use changes and proposed interventions in the upstream reaches of the Ganges and Brahmaputra River systems are essential for the framework of polder design. This report focuses on the project components related to subsidence and cover the efforts to obtain new data and numerical modeling to better understand the rates and distribution of subsidence in the coastal zone of Bangladesh.

Deltas, the low-lying land at river mouths, are dynamic environments in which the landscape is continually changing. Rivers and channels shift, both depositing and eroding sediments. The land is continually sinking due to compaction and isostasy creating space for new sediments. Furthermore, eustatic sea level is rising, threatening inundation of the land and increasing the vulnerability to cyclones and storm surges. Thus, they are particularly sensitive to the delicate balance between sea level rise, land subsidence and sedimentation (Milliman et al., 1989).

An estimated 350 million people globally inhabit these vulnerable landscapes (Edmonds et al., 2020), thus processes that control growth versus loss of land is vital to the stability of coupled human-natural deltaic systems (Syvitski et al., 2009; Tessler et al., 2015). Low-lying river delpalains grow by receiving sediments transported to the coast. On the other hand, the weight of the sediments causes compaction and isostatic loading that induces subsidence, which reduces the growth of the delta. Human modification, especially subsurface fluid withdrawal, can further exacerbate subsidence (e.g., Dixon et al., 2006; Akhter et al., 2009; Minderhoud et al., 2017; Erkens et al, 2016). Upstream damming and river diversions have substantially decreased the sediment supply to many deltas (e.g., Syvitski et al, 2005; Blum and Roberts, 2009; Giosan et al., 2014; Kondolf et al., 2014, Gebremichael et al, 2018). A detailed understanding of the balance between sea level rise, sedimentation and subsidence is critically important for assessing the sustainability of deltas. The elevation balance at deltas can be summarized by the following equation modified from Syvitski et al. (2009):

$$\Delta REL = -\Delta E - C_n - C_a - M + A \quad (1)$$

in which

Δ_{REL} = Rate of vertical change in delta surface elevation (m/yr)

ΔE = Eustatic Sea Level Rise Rate (m/yr),

C_n = Subsidence rate from Natural Compaction (m/yr),

C_a = Subsidence rate from Accelerated/Anthropogenic Compaction (m/yr),

M = Rate of Crustal Vertical Movement (m/yr),

A = Sediment Aggradation Rate (m/yr).

Thus, while sea level rise directly affects the elevation of the delta, subsidence compounds the effect by lowering the land surface. Sediments are then of critical importance in filling this newly created accommodation space to maintain the subaerial extent of the delta. As the boundary between land and sea, a number of studies have found that deltas are at risk from sea level rise and climate change, and are becoming increasingly vulnerable to flooding, erosion, and salinization (Ericson et al., 2006; Syvitski et al., 2009; Ostanciaux et al., 2012; Tessler et al., 2015, 2018). A recent study (Nienhuis et al., 2020) found globally deltas are still gaining land, but with accelerating sea level rise and anthropogenic changes this is likely not sustainable. However, most large and medium size deltas have insufficient sediment supply to maintain their current size (Giosan et al., 2014) and there is declining sediment supply to most major deltas due to climate change and human intervention (Dunn et al., 2019). In the Mississippi and Mekong Deltas, this decrease in sediment input is leading to significant land loss in the deltas (Kesel, 1988; Allison et al., 2016), which has also been predicted for the GBM delta with on-going and planned changes in the drainage basin (Higgins et al., 2018).

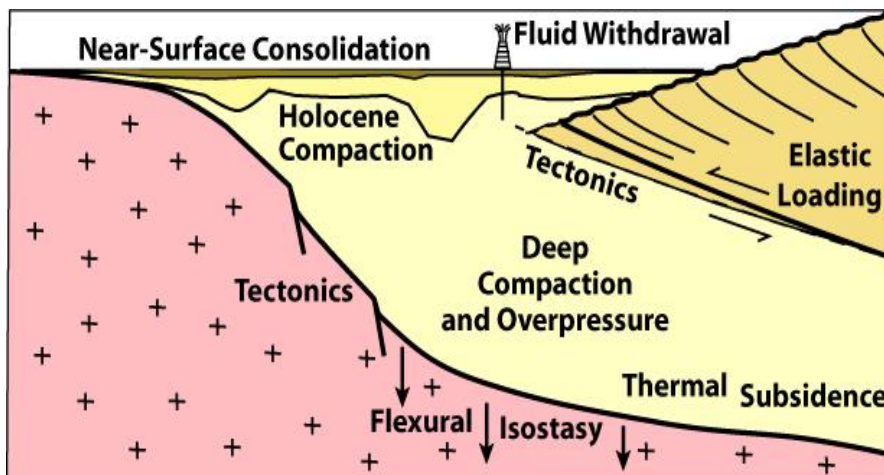


Figure 1. Summary of the processes inducing subsidence in the Ganges-Brahmaputra Delta along an east-west cross-section of the delta. The maximum sediment thicknesses in the basin are approximately 20 km.

Subsidence affects all deltas worldwide. It originates from a variety of processes including lithospheric cooling (thermal subsidence), faulting, isostatic loading by tectonic motions and the weight of the sediments, shallow and deep consolidation/dewatering/compaction of sediments, and oxidation of organic matter. Thermal subsidence is due to deep seated cooling and contraction of the lithosphere, the upper 125 km of the earth. Isostatic loading is the depression of the earth by the weight of sediments of tectonic loads, such as areas shifted by faulting. As sediments are buried, the weight of overlying sediment squeezed water out of the pore space so they take up less space, a process known as compaction. When organic matter is oxidized, it is mostly converted to carbon dioxide and water, resulting in significant volume reduction and therefore compaction of the hosting sediments. Figure 1 summarizes these

processes in a roughly east-west cross section of the Ganges-Brahmaputra Delta. Thus, elastic loading and tectonics primarily affects the eastern half of the country from Dhaka eastwards. Fluid withdrawal related subsidence is most severe in and around major cities, such as Dhaka.

While accurate estimations of ΔREL are critically needed for addressing the human sustainability in deltas, these estimates are plagued with difficulties, such as constraining all the parameters that play out both locally and regionally, and having sufficient long-term instrumental records that capture interannual variability. In order to fully understand ΔREL , a variety of measurements are required, as different instruments provide distinct information on compaction and subsidence. For example, different instrument anchoring depths yields different results (Keogh and Törnqvist, 2019). This can lead to a large variability in measurements, such that the regional pattern is difficult to distinguish. This is the case for the Ganges-Brahmaputra Delta (GBD), the largest delta in the world (Brown and Nicholls, 2015; Paszkowski et al., 2021). We present here a coherent synthesis of vertical elevation change, compaction, and subsidence in this region, revisit previously published data, and update this dataset with newly acquired data. Finally, we analyze these datasets together to extract significant information about the temporal and spatial variability of subsidence in the GBD, one of the most densely populated regions of the world.

1.1 Regional Setting

The GBD, the largest delta in the world, is formed by two of the world's major rivers (Fig. 2). The GBD has been highlighted as a region at risk from rising river and ocean water levels (e.g., Milliman et al., 1989; Ericson et al., 2006; Syvitski et al., 2009; Tessler et al., 2018). It receives $>3/4$ of the water and sediment drained from the Himalayas (Milliman and Farnsworth, 2011) creating a fertile and densely-populated delta in which >130 million people live. This low-lying land, with half of Bangladesh at elevations <10 m, undergoes riverine flooding every monsoon season: in a normal year, 20-25% of the land is submerged, but can reach 60-70% during an extreme flood (Mirza, 2003). The GBD is still net gaining land, with growth at the river mouth outpacing land loss along the coast farther west (e.g., Allison, 1998, Brammer, 2014). While parts of the delta near the Lower Meghna River mouth (Fig. 1) are receiving sufficient sediment and gaining land, other regions away from the major rivers are in decline (Wilson and Goodbred, 2015). In the tidal delta near the coast, sediment supply averages 11 mm/y in the Sundarbans (Rogers et al., 2013) and 23 mm/y farther east (Rogers et al., 2017) with large variability. Anthropogenic channel infilling in the delta interior also contributes to net land gain (Wilson et al., 2017). However, large tracts of coastal Bangladesh have been embanked (poldered), halting sediment delivery within the polders. This region, where natural and anthropogenically-enhanced subsidence is no longer offset by sedimentation, is where the land is at greatest risk (Wilson and Goodbred, 2015; Auerbach et al., 2015). This has exacerbated waterlogging of the embanked islands and a shift from rice cultivation to shrimp farming (Alauddin and Hamid, 1999).

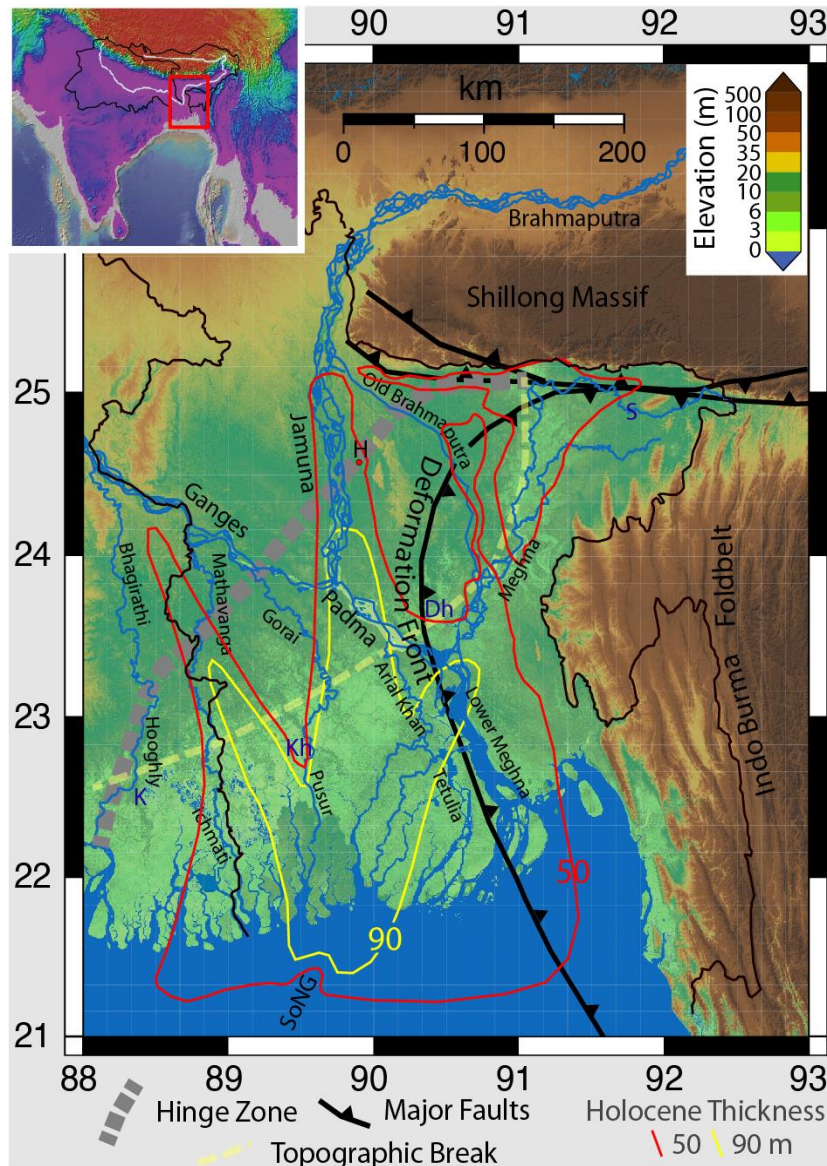


Figure 2. Location map of Bangladesh and the Ganges-Brahmaputra Delta showing major tectonic and sedimentary boundaries, and the significant rivers. The Hinge Zone is the transition between the Indian craton and the Bengal Basin with up to 20 km of sediments. The Topographic Break is the boundary between the Fluvial Fan Delta to the north and the flatter Fluvial-Tidal Delta to the south (Wilson and Goodbred, 2015). K = Kolkata, Kh = Khulna, Dh = Dhaka, S = Sylhet, H = Hazipur-1 well, SoNG = Swatch of No Ground Canyon. The inset shows the regional topography with the outline of the drainage basin of the Ganges, Brahmaputra and Meghna River basins outlined in black and the rivers in white. The red box shows the location of the detailed figure.

In the fluvial delta farther upstream, sedimentation is focused near the rivers while subsidence is distributed broadly. Elevation increases near rivers while areas farther away subside. This increasing elevation contrast through time drives river avulsions (Slingerland and Smith, 2004), thereby spreading the sediments delta-wide over sufficiently long (geologic) timescales (Reitz et al., 2015). Major tributaries to the upper delta, such as the Tista are also highly avulsive, in part associated with flexural loading across the hinge zone (Grimaud et al., 2020). The result is a dynamic landscape where sedimentation and subsidence patterns are continually in flux. Around the turn of the 19th century, there was the well-known westward avulsion of the Old Brahmaputra River to its present Jamuna channel (Fig. 1). This is one of several Holocene avulsions of the Brahmaputra, which averages avulsions every ~1800y (Reitz et al., 2015; Sincavage et al., 2017). The Ganges has also undergone avulsions. Prior to the mid 1600s, the Hooghly River (Fig. 1) was the main channel of the Ganges River (Eaton, 1993; Parua, 2010). The Mathabhanga, Gorai, Arial Khan, among others, were major distributaries to the east of the Hooghly. The shift of the Ganges to the Padma led to a reduction of water and sediment to these channels. The resulting increased salinity incursion in the lower delta plain led to the building of polders (embankments) in the 1960s and 70s to improve agricultural production. Now, the Farakka Barrage in India diverts water from the Ganges into the Hooghly and efforts have been made in Bangladesh to restore flow to the Gorai.

Sometime in the late 19th century the Ganges shifted from flowing down the Arial Khan and Tetulia channels to join the Brahmaputra in the Lower Meghna channel (Fig. 1). As a result, the Lower Meghna is widening while the Arial Khan and Tetulia are narrowing (Allison, 1998; Brammer, 2014).

The interplay of sedimentation, subsidence and sea level at the GBD is further complicated by active tectonics at the eastern half of the delta (Fig. 2). The IndoBurma subduction zone (IBSZ) is the along strike continuation of the Sumatra subduction zone. While most subduction zones are submarine, in Bangladesh the incoming plate is capped by the GBD with its 16-20 km of sediment (Singh et al., 2016; Mitra et al., 2018; Ismaiel et al., 2019) and as a result, the accretionary prism is entirely subaerial (Fig. 1). It encompasses to a >300 km area hosting a series of bivergent anticlines (Betka et al., 2018). The less well-developed frontal anticlines are blind and buried by the delta, but are known from gas exploration. The position of the deformation front (Fig. 1) is based on mapping these anticlines (Betka et al., 2018). East of the deformation front, there is additional subsidence from flexural loading, and uplift from shortening and thickening in the accretionary prism. Furthermore, the earthquake cycle produces cycles of subsidence and uplift through elastic loading of the megathrust underlying the entire area (Fig. 2). Akhter (2010) suggested that the avulsion of the Old Brahmaputra to the current Jamuna channel (Fig. 1) may have been due to tectonics, perhaps triggered by a 1787 earthquake. Furthermore, earthquakes can produce pulses of sediment delivery downstream. Enhanced sediment flux from the 1950 Assam earthquake has been documented (Goswami, 1985; Sarma, 2005; Sarker and Thorne, 2006) along with progressive changes in the Brahmaputra River width and braiding from the sediment pulse. Given these additional complexities, this paper's primary focus is on the components of elevation change, compaction, and subsidence in the non-tectonic part (i.e., west of deformation front, Fig. 1 and 2) of the GBD in southwest Bangladesh as defined by Grall et al. (2018).

The extensive natural and anthropogenic changes in the sediment distribution within the GBD illuminate the importance of addressing how subsidence is distributed across the delta, particularly on the lower tidal deltaplain. While sedimentation drives compaction and isostatic adjustment, the long timescales of these responses mean that they have significant lags and that subsidence continues after rivers have shifted their depocenters. This sets up a cycle of delta lobe progradation followed by degradation after abandonment, similar to the Mississippi Delta (Allison et al., 2003). However, reliable estimates of land subsidence and relative sea level rise (the combination of sea level rise and subsidence) at the GBD have been limited. Early global studies that included the GBD suggested high rates of relative sea level rise (Ericson et al., 2006; Syvitski et al., 2009; Tessler et al., 2018), while more recent local papers suggest modest rates (Pethick and Orford, 2013; Grall et al., 2018; Becker et al., 2020). Knowing the current rates of sediment compaction, tectonic land movement and isostatic loading (Fig. 2) is critical for understanding the sedimentation patterns in the GBD and the prospect for near future land loss and salinization. Recent studies (Karpytchev et al., 2018; Krien et al., 2019), suggest that isostatic loading by the sediments contribute significantly to the subsidence of the delta. The contribution of sediment compaction and organic matter degradation may be large at the GBD (Higgins et al., 2014) given the high sedimentation rates (Rogers et al., 2013, 2017) and thicknesses (Singh et al., 2016; Mitra et al., 2018; Ismaiel et al., 2019). While the GBD is predominantly considered a mineralogenic deltaplain, some organogenic wetland areas exist, and Higgins et al. (2014) documented that these fine-grained organic regions have experienced substantial subsidence after reclamation. In addition, groundwater extraction is significant near Dhaka (Akhter et al., 2009), but widespread irrigation is broadly lowering the water table (Shamsudduha et al., 2009).

Quantitative estimates of these multiple factors throughout the GBD are poorly known. Chamberlain et al. (2020) provided an overview of methods for quantifying the sedimentation and subsidence history of the GBD, and a summary of efforts to date.

Here we compile previous and recently published subsidence measurements with new evaluations of GNSS, tide gauge, and historical building measurements, and discuss the nuances between shallow vs deep and short- vs long-term processes. Our objective is to better quantify the magnitude, spatial variability, and depth variation of compaction and subsidence in the GBD to better evaluate the processes controlling it and the pattern of relative sea level rise in this vulnerable region.

2 Compaction Processes

As sediments are buried, they undergo a variety of sediment compaction and consolidation processes resulting in the loss of porosity and decrease in sediment layer thicknesses through time and with depth, inducing subsidence of the overlying strata (Fig. 1). With greater depth, sediment grains reorganize into more compact arrangements, particularly platy clay minerals that rotate to horizontal orientations. Smaller grains can fill pores between larger grains. With increasing pressure and temperature, grains can dissolve at inter-grain contacts and reprecipitate into pore spaces to further lower porosity. Additional dissolved minerals may be transported through the basin and contribute to cementation. Chemical reactions, such as dehydration of clays, further reduce the sediment water content. At still greater depth, metamorphic reactions reduce sediment volume. The progressive reduction of porosity with depth or lithostatic overburden has been modeled by a variety of empirical formulas, often with an exponential form (e.g., Athy, 1930; Terzaghi and Peck, 1967; Sclater and Christie, 1980; Gluyas and Cade, 1997; Kooi and DeVries, 1998; Bahr et al., 2001; Sheldon and Retallack, 2001; Kominz et al., 2011). The initial porosity of the sediments and its decay with depth depend strongly on the lithology of the sediments. Organic-rich clay and silt generally have higher initial porosities and undergo greater compaction than coarser sediments (Sheldon and Retallack, 2001; Meckel et al., 2007; van Asselen, 2011; Kominz et al., 2011). Another factor is that low permeability sediments, such as shale, may hinder the upward flow of fluids, slowing or halting compaction and creating overpressure in the sediments (e.g., Gluyas and Cade, 1997; Gordon and Flemings, 1998). In the GBD, extensive overpressure is present below depths of 3-5 km where sediments are mainly deeper-water shales (Zahid and Uddin, 2005).

Another important consideration impacting compaction is the incision of the delta during the last glacial maximum (LGM). While lowstand deltas are found offshore near the shelf edge (Palamenghi, 2012), within the GBD, a large valley 60-90m deep was incised into older Pleistocene-aged sediments during the LGM (Fig. 1, Pickering et al., 2014; Goodbred et al., 2014). Previously buried sediments do not significantly decompact with unloading (Chapman, 1983). Further compaction only occurs when the valleys are subsequently filled and overburden pressure exceeds the previously level. Thus, during the Holocene, compaction in the GBD has primarily occurred in the Holocene-aged sediments and not in the underlying older strata (Fig. 2).

At shallow depths, compaction of young sediments can be rapid, particularly for highly porous muddy sediments (Hedberg, 1936; Kominz et al., 2011; van Asselen, 2011). Peat and other organic rich soils undergo even more rapid compaction in the near surface than other soils (Sheldon and Retallack, 2001; van Asselen, 2011). Oxidation of peats due to groundwater lowering can cause significant subsidence (van Asselen et al., 2018). However, few true peats with very high percentages of organic matter are found in the GBD (Brammer, 1990; Goodbred et al. 2003, Best et al. 2007). Large water level fluctuations and biologic respiration lead to oxidation of most organic material before it is deeply buried. In addition, roots occupy soil volume, which can reach 10-20% in the Sundarbans mangrove forest in the near surface (Auerbach et al., 2015) leading to thickness loss as the plants senesce, dewater, and are oxidized with burial. Bioturbation and animal burrows can further increase the porosity at very shallow levels. These effects can contribute to a large amount of effective sediment compaction in the upper few meters of the sediment column.

2.1 Previous Estimates of Subsidence in the GBD

A limited number of studies have examined subsidence rates in the GBD. Alam (1996) and Hoque and Alam (1997) compiled radiocarbon dates on Holocene samples and obtained subsidence rates from 0.53 (Kolkata) to 5.48 mm/y (Khulna) (city locations in Fig. 2), but suggested that rates could reach 20-30 mm/y in places. Alam (1996) assigned the reported top of the Plio-Pleistocene Dupi Tila formation in the 1960 Hazipur-1 well (Fig. 2) as corresponding to the beginning of the Holocene. As a result, he estimated a subsidence rate of 22 mm/y that is likely too high (see Supplement 1). This was used in a global analysis of delta subsidence (Ericson et al., 2006) to suggest a high subsidence rate in the GBD. Radiocarbon data on auger and vibracores up to 7 m depth across the lower delta plain (Allison et al., 2003) indicated sediment accumulation rates of 1-7 mm/y and subsidence rates of 1-4 mm/y. A summary of the papers discussed in this section is provided in Table S1.

In a study of global deltas, Syvitski et al. (2009) suggested a GBD subsidence rate of up to 18 mm/y. Their estimate is based on a high rate of subsidence at the Khepupara tide gauge. However, our examination of the 1977-2010 record of this gauge using hourly Bangladesh Inland Water Transportation Authority (BIWTA) data shows several decadal-scale changes in rates (Fig. 3), with at least one change in 2000 corresponding to when the gauge was relocated based on local interviews. The publicly available data (1987-2000) from the Permanent Service for Mean Sea Level (PSMSL) corresponds closely to the period of high subsidence of the gauge, and thus should be regarded as an overestimate (Fig. 3). Ostanciaux et al. (2012) studied global trends of coastal vertical motion and estimated high rates at the GBD of 11-20 mm/y, again biased by the public Khepupara gauge data.

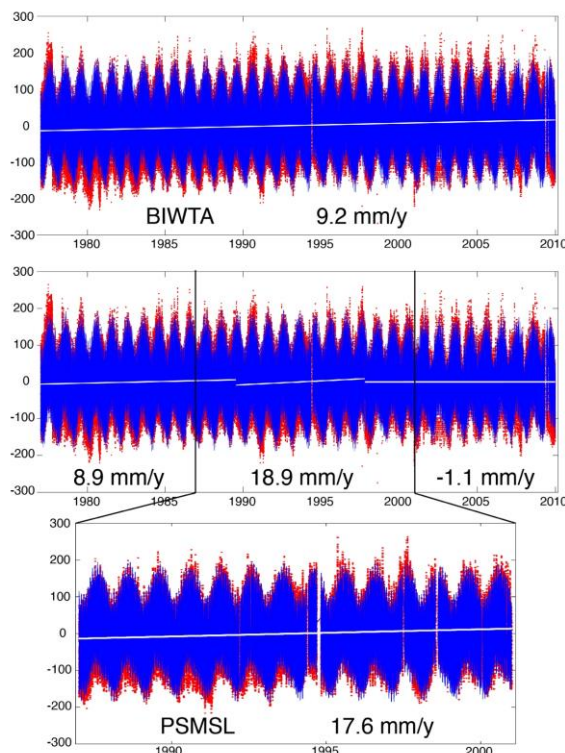


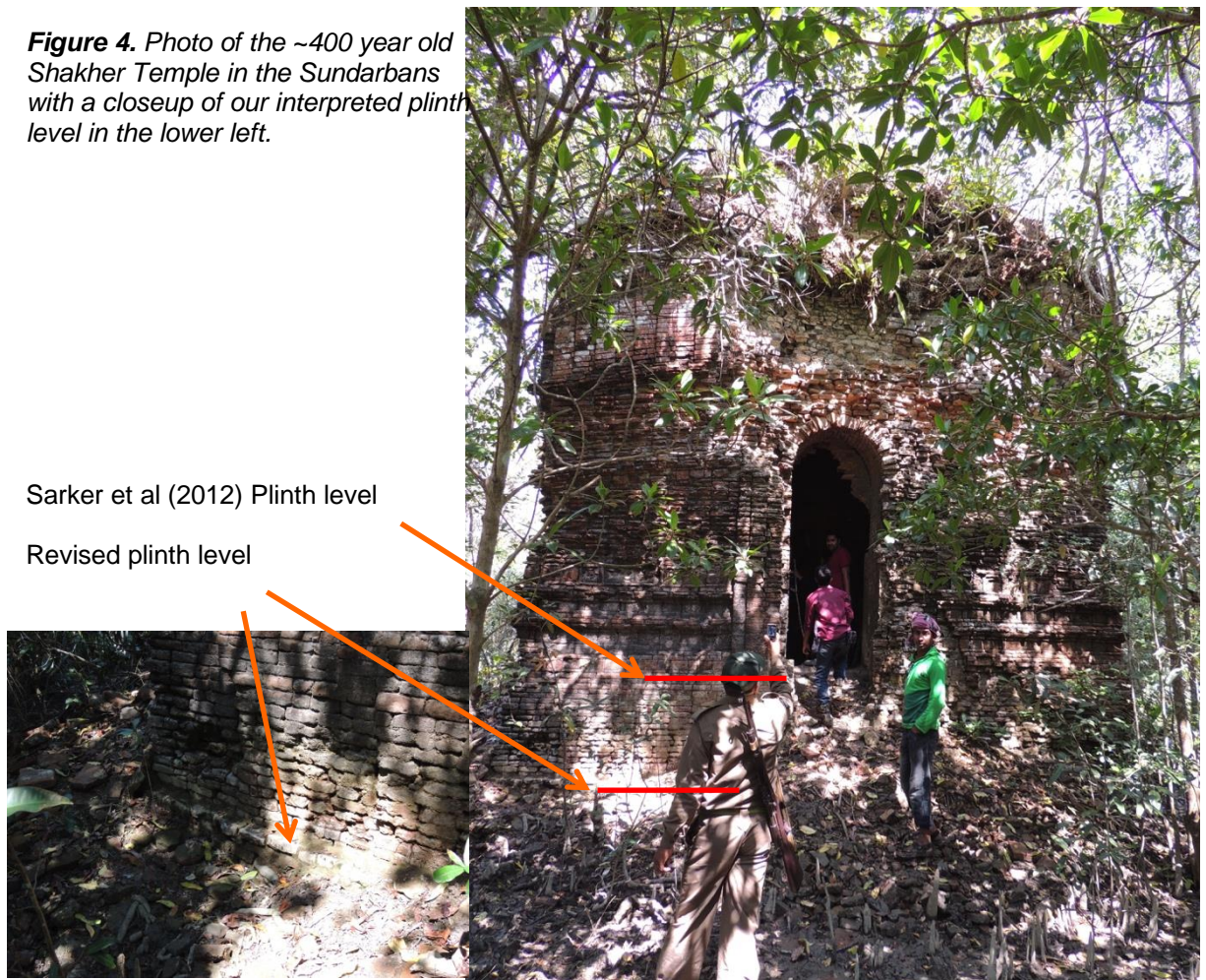
Figure 3. Water level data from the Khepupara tide gauge. The top shows hourly data from the Bangladesh Inland Water Transportation Authority (BIWTA) in red and a tidal model from t_tide (Pawlowicz, 2002) in blue showing a mean sea level rise rate of 9.2 mm/y, indicated by a white line. However, examination of the data shows variable rates of sea level rise. The middle shows fits to the three distinct regimes with the rates noted below each segment. The bottom shows the more limited publicly-available time series from PSMSL. It corresponds approximately to the central portion of the longer time series when the apparent sea level rise rate was greatest.

Based on the existing subsidence estimates available at the time, the CEIP-1 Design phase in 2011-2012 assumed a

uniform subsidence rate of 10 mm/y over the entire coastal area for designing embankments and the drainage systems for a design period of 30 years. This value is consistent with the published estimate at the times (Ericson et al., 2006; Syvitski et al., 2009; Ostanciaux et al., 2012) As discussed below, newer data, including the efforts in this project are refining these estimates and differentiating parts of the delta that are subsiding slower and more rapidly than this value.

In contrast, Sarker et al. (2012) examined plinth elevations relative to the surrounding ground levels at four historic sites that are 200-600 years old and determined low subsidence rates of 0-2.5 mm/yr. For the two 15th century mosques at Bagherat, subsidence is estimated as 1.9 ± 0.6 mm/y (Sarker et al., 2012). Lower rates of 1.25 mm/y and 0.14 ± 0.74 mm/y were found for the two ancient Hindu temples, the Shakher Temple and Doyamayee Mondir. Chamberlain et al. (2020) and Steckler et al. (2022) re-evaluated the subsidence at one of these temples during a visit (Fig. 4). They believe that the plinth level of the 400-year old the Shakher Temple in the Sundarbans was misidentified. In their analysis of the temple, Sarker et al. (2012) placed the plinth level at the entrance of the temple at the top of the stairs, even with the interior of the temple (Fig. 4). While Muslim mosques are communal prayer halls that often are open at ground level, Hindu temples are commonly raised, as they are the home to gods (in this case, the Goddess Kali). Thus, one ascends the temple to enter the home of the goddess (Sharma and Deshpande, 2017). We believe the previous evaluation (Sarker et al., 2012) missed this architectural feature. Instead, we located a ridge in the bricks near ground level (Fig. 4) that we associate with the plinth level (Chamberlain et al., 2020). In addition, augering discovered a buried brick layer 1.5m below the surface. We interpret the brick layer as the original TPL level minus any excavation for preparing and leveling the site for construction. The brick layer and revised plinth level are consistent and yield a new subsidence rate of 3.4 ± 0.5 mm/y (details in Supplement 3). We have not visited the other Hindu Temple, but it may have the same issue, so we exclude it from our calculations.

Figure 4. Photo of the ~400 year old Shakher Temple in the Sundarbans with a closeup of our interpreted plinth level in the lower left.



At Katka Beach in the Sundarbans, Hanebuth et al. (2013) discovered 300-year old salt kilns uncovered by coastal erosion. The kilns would have been built just above spring high tide level indicating 4.1 mm/y subsidence. Since then, the remains of many additional salt kiln sites in the region have been discovered (Hanebuth et al., 2021). The 108 kilns that they identified at 12 sites in the Sundarbans average 2.7 mm/y subsidence.

Brown and Nichols (2015) compiled a comprehensive suite of >200 measurements of subsidence in the GBD. Methodologies included carbon dating, borings/wells/auger logs, archaeological sites, InSAR, GNSS, optically stimulated luminescence dating, geomorphology, estimates of compaction from groundwater depletion, and magnetostratigraphic dating. However, by mixing multiple types of measurements with insufficient constraints on their settings, they obtained subsidence rates that varied from 44 to -1 mm/y, including broad ranges of values at individual sites. Their comprehensive mixture of samples with limited context also shows the “Sadler effect” (Sadler, 1981), with mean subsidence rates decreasing with increasing timescale of measurement. A critical problem is the need to distinguish between subsidence and sediment accumulation rates. For example, if incision by a river is followed by rapid deposition when the river migrates or avulses, the net effect is younger river channel sediments replaces older sediments. This “channel incision effect” yields incorrect high apparent subsidence rates. Grall et al. (2018) used >400 tube wells with almost 200 ¹⁴C dates (Fig. 5), as well as seismic data along the Brahmaputra River and offshore, to estimate average Holocene subsidence rates. The authors identified and removed samples affected by the channel incision effect, and distinguished components due to sediment accumulation, eustatic sea level rise and subsidence. Results revealed a systematic variation of subsidence rates across the delta. In the lower GBD, subsidence increases from near zero rates landward of the Hinge Zone to 4.5 mm/yr at the southern coast of Bhola Island (Fig. 4). The Hinge Zone is the track of the Eocene shelf edge, which also corresponds to the boundary between the thinly sediment-covered Indian craton and the thick sedimentary depocenter of the Bengal Basin (Fig. 2; Steckler et al., 2008).

Recently, Becker et al. (2020) analyzed groups of river and tide gauges to reconstruct subsidence rates in the delta. The averaging of 19-24 stations for each zone (dots and values in Fig. 5), along with the corrections and analysis in the paper, minimized the effect of poor tide gauges, such as Khepupara. They estimate a maximum of up to 7 mm/y subsidence for the period of 1993-2012. This is noticeably higher than the Holocene rates of Grall et al. (2018) (Fig. 5), but the pattern is generally coherent for the different morphodynamic units (Grall et al., 2018). In the tectonic areas east of the IBSZ deformation front, elastic loading by the locked megathrust (Steckler et al., 2016) is expected to contribute 2-3 mm/y of subsidence (Oryan, 2022) that would be countered by earthquake related uplift in the average Holocene rates, which are significantly lower.

GNSS geodesy provides another means of assessing current subsidence rates. Our GNSS stations in Dhaka and Sylhet showed locally high subsidence rates of 12 mm/y (Fig 2, Steckler et al., 2010). Reitz et al. (2015) expanded the results to include 18 stations. Sites in NW Bangladesh at or landward of the Hinge Zone showed subsidence rates <1 mm/y, while sites in Sylhet, a tectonically active basin, showed high rates (7-12 mm/y). The high subsidence rate in Dhaka at 12 mm/y from groundwater withdrawal was confirmed in the longer time series. Rates in the foldbelt farther east were variable depending on the structural position of the GPS site. Their three sites in the coastal belt showed moderate but variable rates of 3–8 mm/yr.

Higgins et al. (2014) used InSAR measurements with the ALOS-1 satellite to create a map of subsidence rates across a >10,000 km² swath of central Bangladesh (location in Fig. 4). They obtained rates from 0 to >18 mm/yr, with the lowest rates primarily in Pleistocene Madhupur Clay and the highest rates in Holocene organic-rich muds. One high subsidence area follows an eastern branch of the Lower Meghna that previously

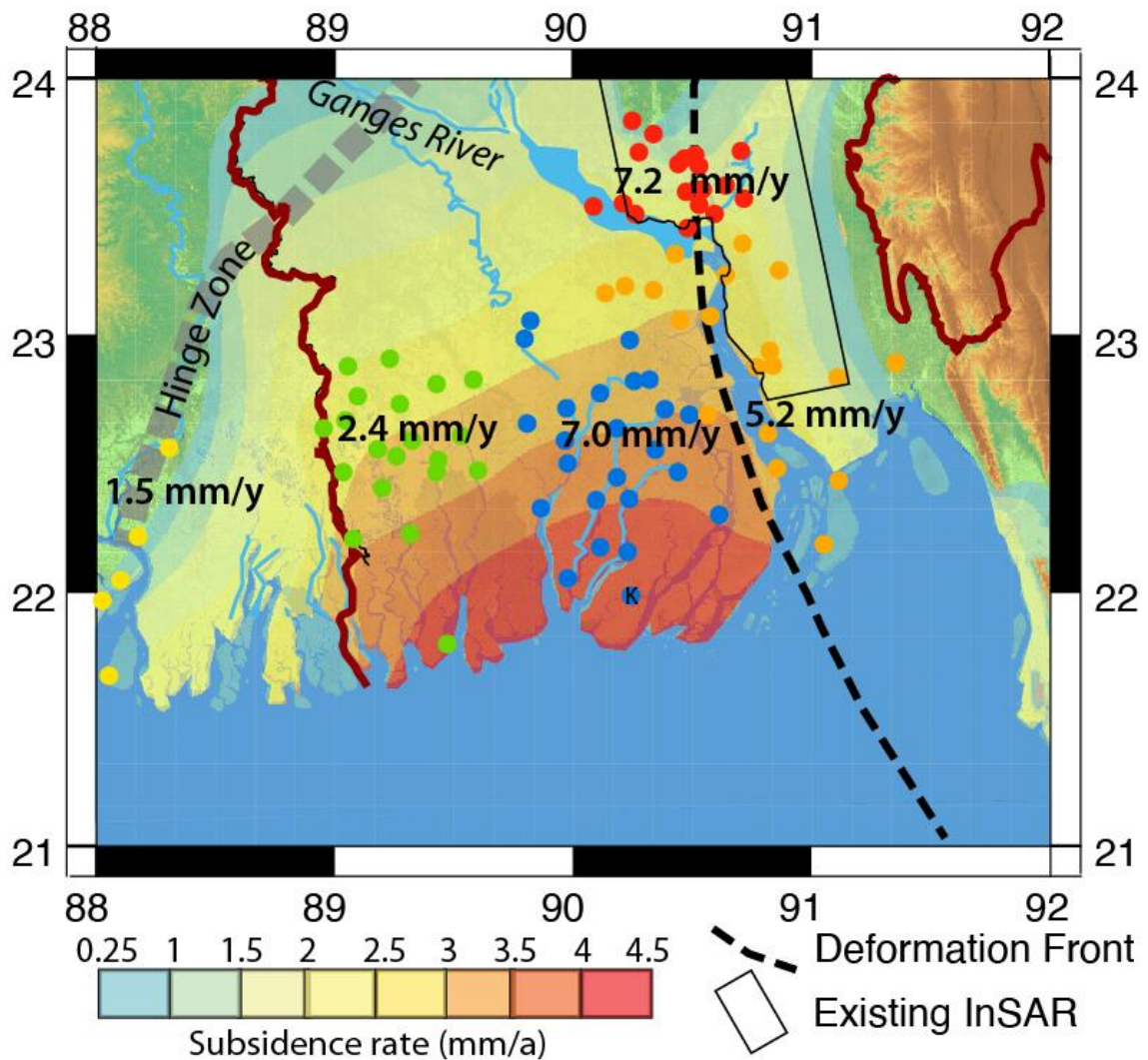


Figure 5. Map of Ganges-Brahmaputra Delta from Grall et al., 2018, showing average subsidence rates over the Holocene (last 10,000 years) derived from radiocarbon dates samples of a suite of over 400 tube wells and a very high resolution seismic line along the Jamuna River (heavy black line). The subsidence rates increase southeast from the Hinge Zone to a maximum of ~4.5 mm/y. The subsidence rates in Sylhet may be underestimated because of the underfilling of the region by sediments. Tectonically induced subsidence is identified between the Dauki and Dapsi Faults near the Shillong Massif. Note the lack of subsidence north of Dhaka corresponding to the Madhupur Tract. The thin black line outlines the area imaged by InSAR in Higgins et al. (2014). Superimposed are the locations of the river gauges (Becker et al., 2020) as colored dots with the corresponding average rates on subsidence over a 20-year period for each set. The K indicates the position of the tide gauge at Khepupara.

flowed past Noakhali (approximately the position of the M in Lower Meghna in Figure 2), but was filled with sediments following the 1950 Assam earthquake (Sarker et al., 2013). These young deposits are clearly undergoing rapid compaction. Dhaka has high rates of subsidence from groundwater withdrawal (Steckler et al., 2010), and the InSAR (Higgins et al., 2014) shows variable rates that correlate with the underlying geology. Further investigations using InSAR from the Sentinel-1 satellite are ongoing (Woods et al., 2019).

DeWolf et al. (2013, in prep.) installed two sets of optical fiber strainmeters in hand-drilled wells in Bangladesh. The site in southwest Bangladesh at Bhanderkote, Khulna (called the Khulna compaction meter or KHLC on map in Fig. 10) contains 6 wells drilled to depths of 20, 40, 60, 80, 100 and 300 m (Fig. 6). Each well contains two pairs of optical fibers grouted into the bottom of the well and attached to a concrete monument at the top. The length of each fiber was measured weekly from 2011 to 2016 by local collaborators. In March 2015, the river adjacent to the site was dredged to improve navigation. Readjustment of the river profile led to bank erosion that destroyed KHLC in

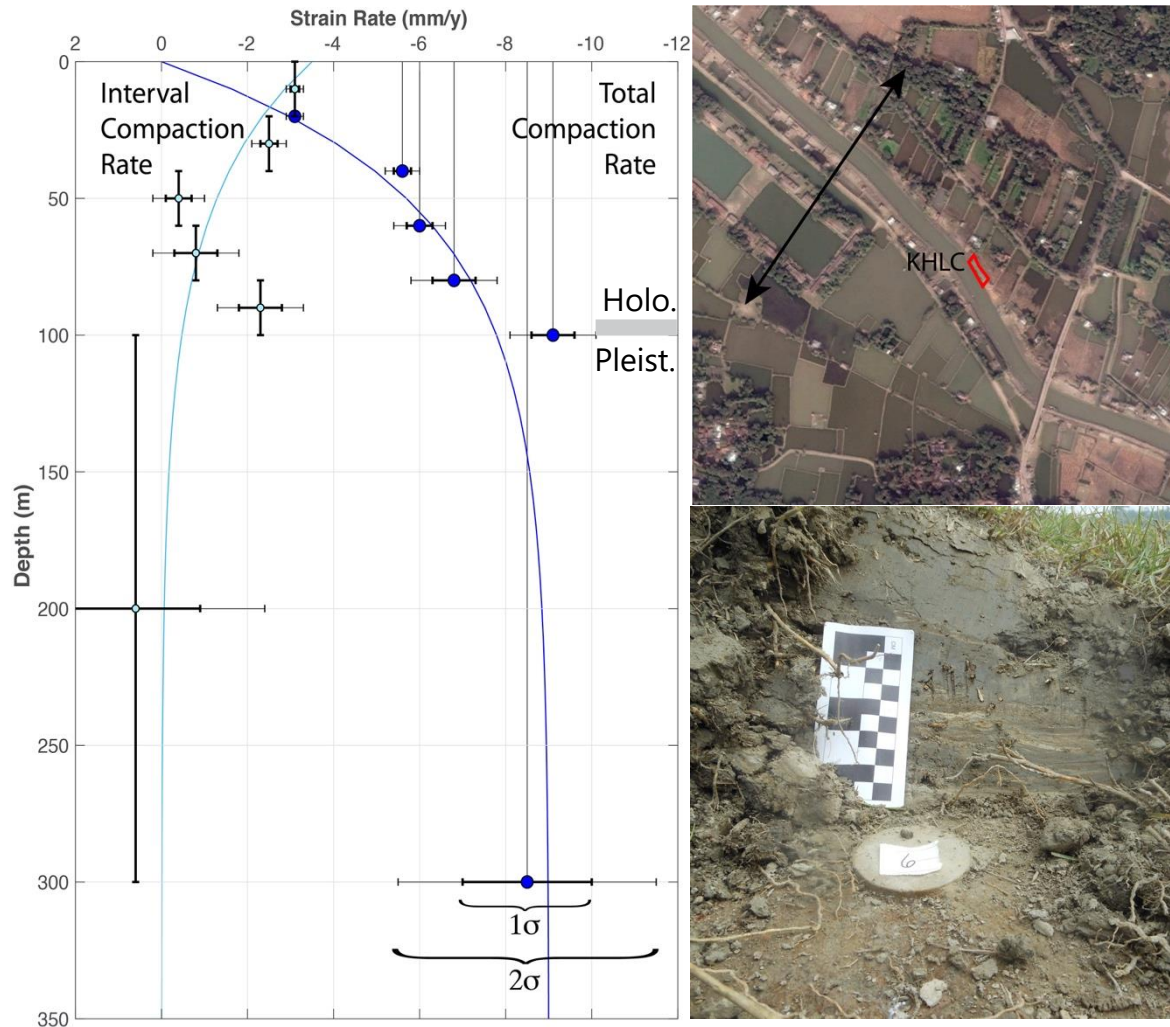


Figure 6. Results from the KHLC compaction meter. A) plot showing the decrease in compaction with depth. The blue dots show the shortening rate of the different length fibers and teal dots show the differential rate between pairs of fibers. Approximate exponential curves to the data for the total compaction and its derivative are shown. Note that all of the compaction is occurring in the Holocene sediments and there is effectively none in the Pleistocene. B) Google Earth image of the KHLC site. The wells were installed on the river bank in the red box. The double arrow shows the width of the river before 1989. Notice the large concrete bridge SE of KHLC over the now small river. C) photo of the marker at the base of one of the monuments taken in 2017 with a cm scale. The lower section shows ~6 cm of tidalites deposited over 4 monsoon seasons. Above are 4-6 cm of muddy deposits in the 2 years since the March 2015 dredging.

2016. Measurements show a seasonal extension of the fibers during the summer monsoon due to clay swelling or poroelasticity with a longer-term subsidence trend. Shortening rates of the fibers generally increase with depth (Figure 6A) and are consistent with an exponential curve for a total compaction rate of ~9 mm/y for the upper 300 m, with most compaction occurring in Holocene strata above 60 m depth and no compaction below 100 m, within errors. Based on nearby tube well transects, the thickness of the Holocene strata here exceeds 90 m (Fig. 2, 6). Thus, KHLC is located in

the broad incised valley excavated by the Brahmaputra River during the last glacial maximum (Fig. 2). The lack of compaction beneath the Holocene is not unexpected, as the sediments below experienced compaction prior to the lowstand incision.

Additional interpretation needs to take into account recent sedimentation on the site. The river at KHLC was previously >300m wide (Fig. 6B), but historical imagery shows it narrowed dramatically between 1989 and 1999 (Wilson et al., 2017) and OSL dating of samples from an auger hole at the site shows 4.44 m of deposition since 1987 ± 3 CE due to the channel filling (Chamberlain et al., 2020). KHLC was installed on the bank of this narrow (<10 m) river in 2011. Boat traffic on the river could only move at high tide leading to the government decision to dredge it. The compaction meter on the river bank was the site of sediment deposition, averaging 10-15 mm/y of tidalites per year until the river was widened (Fig. 6C; Chamberlain et al., 2020). Deposition likely occurred only during high tides during the monsoon when the river level was sufficient to flood the site. Thus, the high subsidence rate measured in the shallower strainmeters is associated with active sediment deposition and consolidation of recently deposited sediments near the surface.

2.2 Estimates of Subsidence in the GBD under this Project

Tube Wells. The Holocene subsidence maps of Grall et al. (2018) was calculated from an extensive set of >400 tubewells with over 200 radiocarbon dates. However, very few wells were drilled in the coastal region, so that there is considerable uncertainty on the rates. As part of this project an additional 57 tube wells were drilled (Figure 7 red circled area). These wells serve several scientific purposes, including estimating subsidence rates. The sediment samples from these wells are on route to Vanderbilt University via ocean freight but have been delayed several times and due to arrive in July 2022. However, radiocarbon samples were sent earlier by courier, and 52 organic-carbon samples have been submitted to a national radiocarbon dating facility (<https://www2.whoi.edu/site/nosams/>) for analysis, with results pending June 2022. When complete, these data will refine the long-term subsidence rates of the Bangladesh coastal zone.

Data from the initial core logs recorded in the field during core collection (Supplement 4) can be used to understand the large-scale structure of Holocene stratigraphy, which influences subsidence through differential compaction. From the core-log data, Figure 8 shows an analysis of the fraction of mud vs. sand across the delta along several core transects. The transects locations are shown in Figure 7. The values represent the fraction of core samples from a given depth that comprise fine-grained muddy sediments across each transect, thus the average frequency of mud across the delta. Results reveal a sharp increase in the fraction of mud in Holocene stratigraphy south of Khulna (Transect G). In the 10-50 m depth interval, mud strata increase from an average of only ~10% of the stratigraphy at Khulna to ~50% of the stratigraphy at Barisal and south. At <10 m depth, mud strata increase more significantly, from 10-40% at Khulna to 70-100%

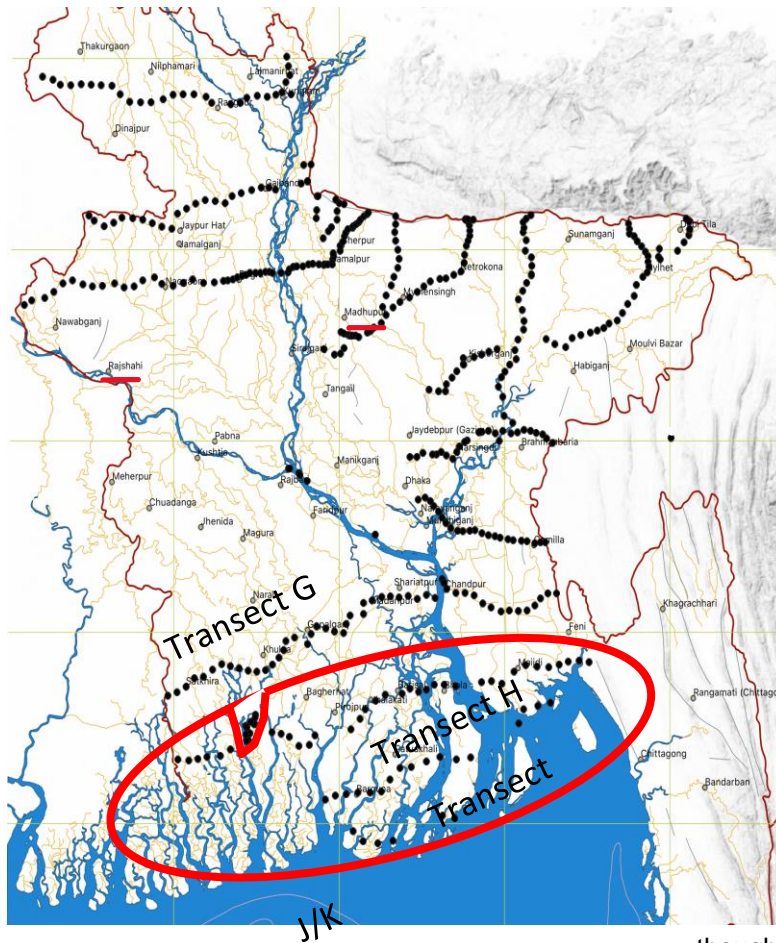


Figure 7. Map of Bangladesh showing the location of tube wells drilled by our team over recent years. The wells circled in red were drilled as part of this project.

in the lower delta. These mud-rich Holocene strata in the lower delta south of Khulna are much more susceptible to compaction-induced subsidence than the sand-dominated stratigraphy found north of the tidal deltaplain as will be seen in the GPS results.

These results show that the modern fluvial-to-tidal transition in the lower delta is associated with an abrupt change in sediment grain size and overall stratigraphic architecture, with important influences on subsidence. However, even

though the transect averages show a clear pattern in mud content, the spatial distribution of those muds are non-uniform across the delta – meaning that the mud fraction varies locally with an effect on local subsidence rates. Another factor affecting local subsidence is the depth to the Pleistocene surface and underlying deposits. These much older units are already largely compacted and do not contribute as significantly to modern subsidence as the less consolidated Holocene units. The non-uniform distribution of mud and Pleistocene deposits is shown in Figure SS3, which summarizes the sand and mud stratigraphy for each core location across the transects labeled in Figure 7 (G, H, J, K). The increase in mud deposits from transect G (through Khulna) to transect H (through Barisal) and south is readily apparent. Any single core location, though, may have significantly sandier or muddier stratigraphy than the regional average, with a presumably corresponding affect on local subsidence rates. Continued mapping of Holocene stratigraphy across the lower delta plain will be important defining the scale of compaction-induced subsidence. Note that all core lithologies are archived in a supplemental table (Supplemental Excel Spreadsheet).

Geodesy. GNSS enables observations using fixed antennas over years to estimate rates of tectonic deformation as well as subsidence or uplift on the order of ± 1 mm/y or better. Generally, it takes >2.5 years to determine reliable horizontal rates and >4.5 years for vertical rates (Blewitt and Lavallée, 2002). The first component of the geodetic subsidence study in this project was to rehabilitate existing continuous GNSS sites and install new ones. GNSS (Global Navigation Satellite Systems) refers to the collection of existing systems, while GPS refers to the U.S. satellite system. As we have processed using only the GPS system, we use the two terms interchangeably. All of our continuous GPS sites include an antenna mounted on a threaded rod imbedded in a reinforced concrete building or on a rod anchored to the ground, a GNSS receiver, solar panels for power, batteries, and a power controller (Fig. 9). Data are recorded every 15 seconds and processed to produce daily estimates of the position of the antenna. Daily positions are accurate to ~ 2 mm in the horizontal and 6 mm in the vertical. These systems capture

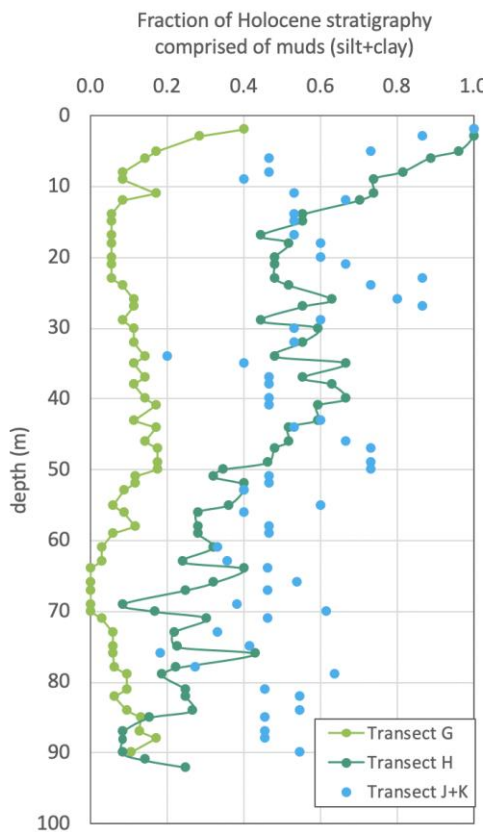


Figure 8. Average lithology across the lower delta along transects labeled in Figure 5.

subsidence where they are coupled to the ground, either the foundation of the building or at the ~2 m depth of the rods. Thus, GNSS, particularly building sites, may not measure the shallowest component of land surface subsidence (Keogh and Törnqvist, 2019). We had already established 5 GPS sites in the field area (Fig. 10) at Patuakhali (PUST), Khepupara (KHEP), Polder 32 (PD32), Khulna (KHUL and KHL2), and Hiron Point (HRNP). PUST and KHUL were established in 2003, but the old instrumentation only provided intermittent data and none over the last decade. KHUL was replaced by KHL2 in 2014, but the receiver was removed from its location after a year. The other stations were installed in 2012. However, the receiver at KHEP was later removed for repairs.

During July-August 2019, 4 new sites were scouted and installed (Fig. 10) at Sonatola (SNT1, SNT2), Jorshing (JRSN) and Baintola (BNTL), and all of the previous sites had system upgrades and/or repairs. All GPS sites were successfully installed/upgraded, and data from existing sites was collected. In addition, cellular modems for data transmittal were upgraded/added to all GPS sites except HRNP. Although a cellular tower has been installed near the site, coverage was only 2G and did not support data communications. The cellular tower was later upgraded and in January 2022 we were able to establish cellular data transmittal for HRNP while servicing all of the stations. Computer hard drives for older PUST and KHUL GPS were located, but still require data download.

At Sonatola, two GPS antennas and receivers were installed. One was installed on the roof of a reinforced concrete column of a primary school (SNT1), similar to other continuous installations in Bangladesh (Fig. 9). The other was installed on a rod identical to the nearby RSET (SNT2). This will enable direct measurement of any subsidence occurring beneath the bottom of the 80' (24 m) long rod used for RSET measurements (see below).

In addition, we were able to install campaign GPS monuments on the Hiron Point and Khepupara tide gauges, and two at Barisal University. These campaign monuments will allow subsequent monitoring of subsidence. Measurements at the two tide gauges will also be able to help assess the stability of the tide gauges. At Khepupara, the tide gauge location has been shifted multiple times and corresponds to changes in rates of apparent relative sea level rise at the tide gauge. At Hiron Point, two occupations of the tide gauge by campaign GNSS systems enabled us to update the offset between the PWD (public works datum) and global mean sea level to 0.996 ± 0.501 m, and significant increase from the current estimate of 0.66 m.

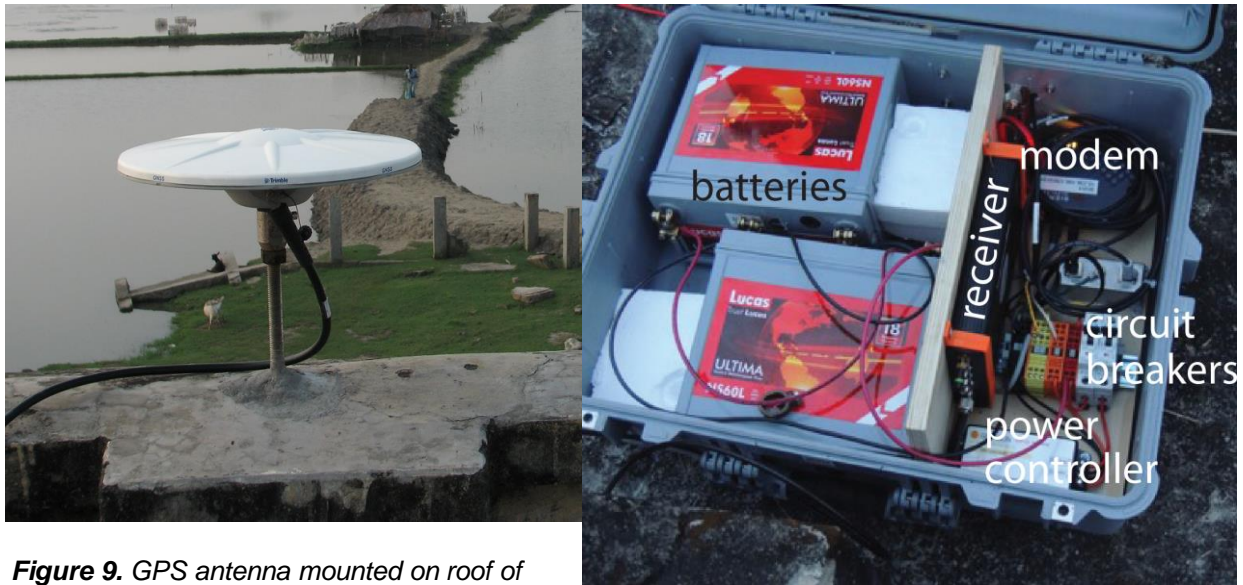


Figure 9. GPS antenna mounted on roof of school at Polder 32 and waterproof case with GPS receiver and other components.

We have processed all available GNSS data in the GBD using GAMIT/GLOBK (Herring et al., 2018) with 16 International GNSS Service (IGS) stations used for stabilization. GAMIT is a comprehensive GPS/GNSS analysis package developed at MIT, the Harvard-Smithsonian Center for Astrophysics (CfA), Scripps Institution of Oceanography (SIO), and Australian National University for estimating GNSS station coordinates and velocities. The vertical rates are given in Table S2 and the vertical time series for each of the sites is shown in Figure S4. Figure 11 shows a summary of the subsidence rates obtained so far, including sites that have been installed by the Earth Observatory of Singapore (Mallick et al., 2019) and the continuous station deployed by the French IRD (Institut de Recherche pour le Développement) through the Belmont Forum BanD-Aid project (Shum et al., 2014), which is maintained by CNRS-INSU (L'institut national des sciences de l'Univers). Elevations from GPS are calculated relative to the ellipsoid and used to determine subsidence velocities. For all sites, the seasonal signal was removed by modeling the vertical deflection from water loading (Steckler et al., 2010). Water level was calculated using >300 daily river gauge and >1200 weekly ground water well measurements of the water table (Steckler et al., 2010; Nooner et al., in prep). The

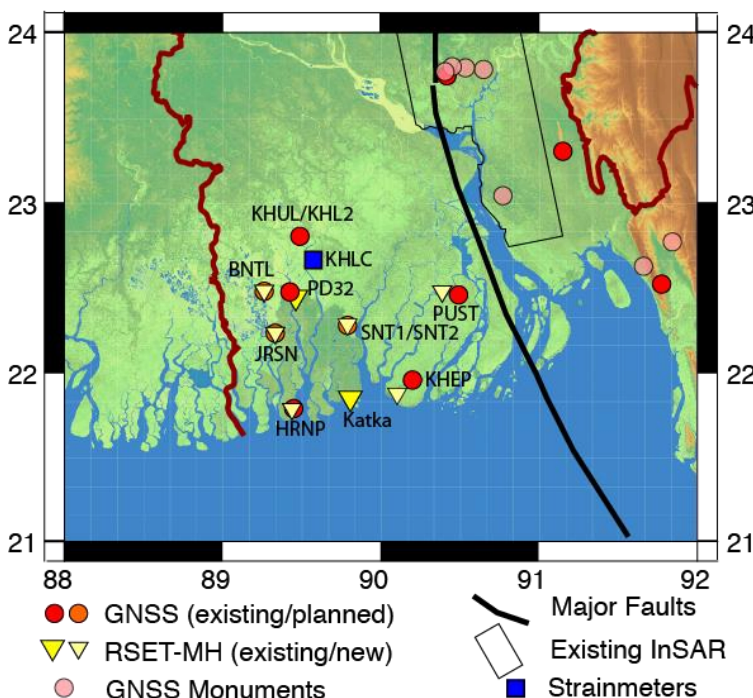


Figure 10. Map of GPS and RSET sites installed, upgraded or serviced in July 2019. All GPS sites now have cellular connections for data downloads. Previously HRNP point data was downloaded by the RSET team when they serviced the RSET.

deflection from the regional water mass was calculated and removed using a best fit estimate of the Young's Modulus at each GNSS station with a best-fit trendline. Elevations have not been adjusted to the PWD datum.

For reference, we note that sites in the northwest of Bangladesh at Rajshahi (RAJS) and Madhupur (MPUR) (location of these cities are on underlined in red in Figure 7) yield low subsidence rates of -1.7 and -0.5 mm/y. These sites are located NW of the hinge zone (Fig. 2, 5) where the total sediment thicknesses are much less than beneath the deep Bengal Basin. Four sites in Dhaka have sufficient data to estimate subsidence rates (Fig. 10). The sites are near the center of the cone of withdrawal from groundwater abstraction in Dhaka, where the water table has been declining by ~3 m/y (Hoque et al., 2007). The Dhaka GNSS sites yield similar subsidence rates ranging from -9.0 to -13.5 mm/y. At the DHAK site recording from 2003-2019, the time series shows a slowing of the subsidence rate from 12.4 to 9.7 mm/y as water withdrawal is shifted to farther from the central city.

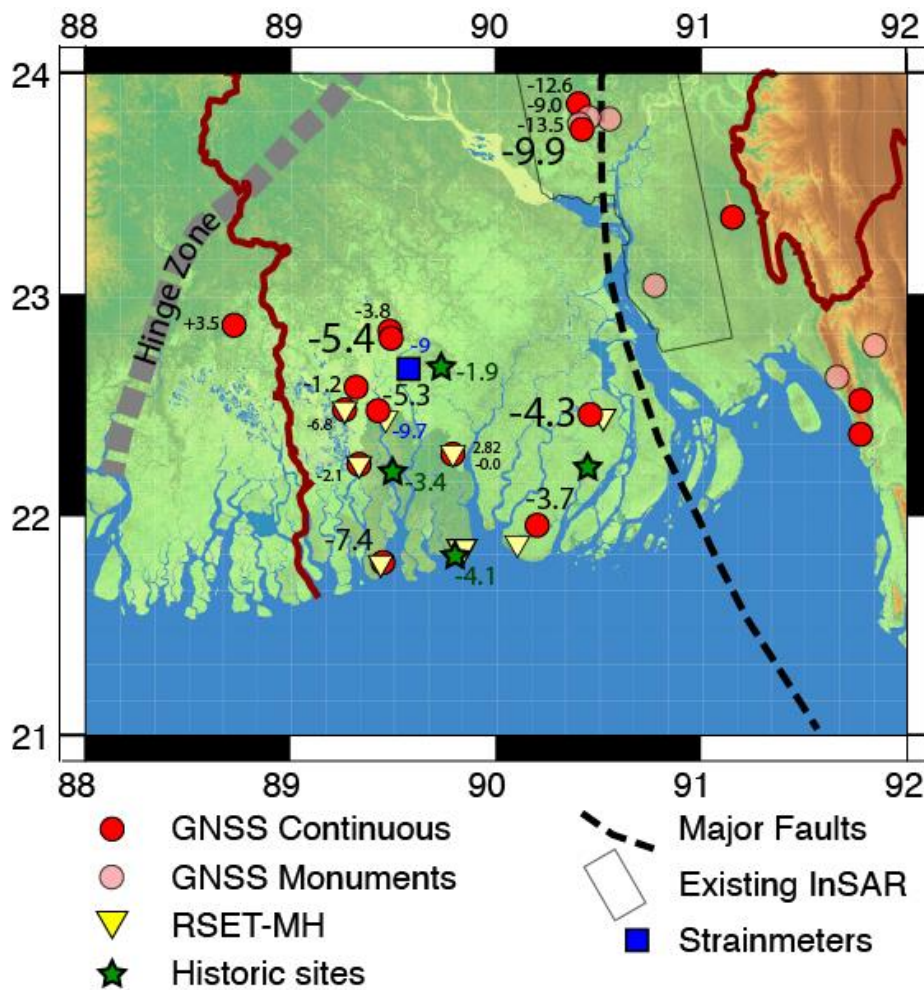


Figure 11. Map of SW Bangladesh showing subsidence rates obtained from GNSS and historic sites. Size of fonts for GNSS sites are proportional to the length of the time series as a proxy for their reliability. Red and pink circles: Active GNSS sites and monuments. Yellow triangles are RSET-MH sites. The blue square is the compaction meter site installed in 2011. The site slumped into the river after dredging of the river in 2015. Green stars: historic sites analysed for subsidence described.

In the SW delta field area, we focus on the sites with the longest record. The font size used in Figure 11 is proportional to the square root of the times series length to reflect the reliability of the rate estimates. The rates for the newest sites, established in 2019, are still too short to be reliable and are not further considered. The larger symbols correspond to sites that have recorded data, sometimes intermittently, for 5-17 years. The eastern sites (PUST -4.3 mm/y and KHEP -3.7 mm/y) yield rates are similar to the long-term rates found by Grall et al., (2018). Subsidence estimates from four historic sites in 3 locations that date from 300-400 years ago also yield subsidence estimates similar to Grall et al. (2018) at 1.9, 3.5 and 4.1 mm/y. However, the GPS sites in the western coastal zone (KHUL/KHL2 -5.4 mm/y, PD32 -5.3 mm/y, HRNP -7.4 mm/y) yield rates 2-3 mm/y greater. We associate these higher rates with muddier settings farther

from the river mouth that may partially reflect additional near-surface consolidation and organic matter oxidation. The first two sites have very similar rates, while the higher rate at HRNP may reflect the very muddy Sundarbans.

The continuous GPS sites, while providing excellent data on the subsidence rates in Bangladesh, are sparse and do not enable us to sufficiently map out the spatial variability of the rates. However, the Survey of Bangladesh, in conjunction with JICA established geodetic monuments throughout Bangladesh (Fig. 12). Sites in southwestern Bangladesh were primarily installed in 2001-2. They were surveyed with a Leica GPS system for 4 hours in 2002. Some of the sites were resurveyed in 2010/2011, although we do not have that data. The sites are 15-30 km apart with a total of 55 sites in southwestern Bangladesh providing excellent coverage of the region for densifying the subsidence map. We surveyed them in 2002, thus the time span between the initial measurements and recent measurements is ~18 years. While sites were occupied only at the start and end of that time span will not yield subsidence rates as accurate as the continuous sites, the density of the sites allows patterns of subsidence to be better discerned.

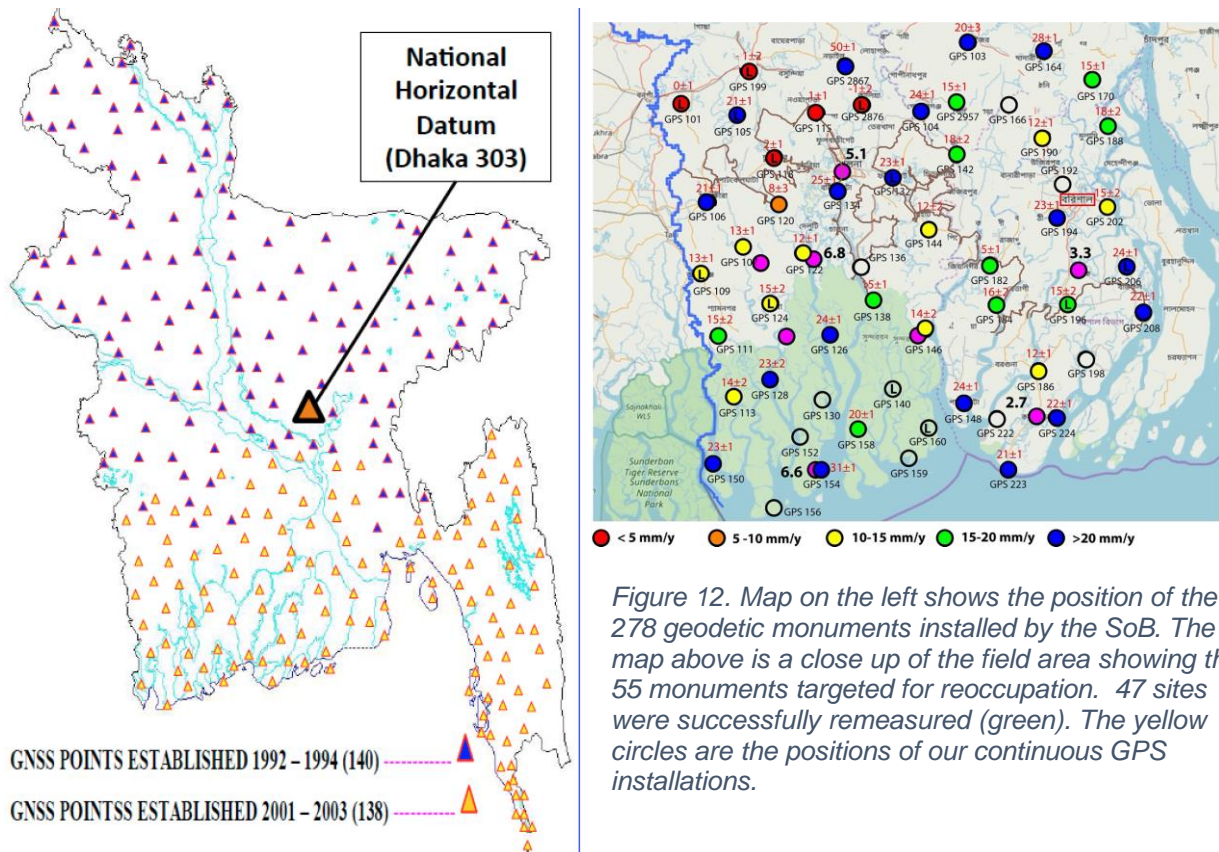


Figure 12. Map on the left shows the position of the 278 geodetic monuments installed by the SoB. The map above is a close up of the field area showing the 55 monuments targeted for reoccupation. 47 sites were successfully re-measured (green). The yellow circles are the positions of our continuous GPS installations.

The field survey took place in several stages from January-March 2020. The team consisted of personnel from Columbia University, IWM, SoB, Dhaka University, the University of Barisal and LaRochelle University. One to two survey teams located sites and set up tripods with tribrachs and campaign GPS receivers, mostly Trimble NetR9s with Zephyr Geodetic antennas. Each team could set up 1-3 systems per day. Sites were generally occupied for ~24 hrs, although some were established for as long as 4 days. For sites where the sky view of the monument was poor due to buildings or trees,

we established a nearby GPS site in an open field and used optical levelling to determine the elevation difference between the monument and the temporary GPS marker. In some sites a tall monument incompatible with our tripods also required levelling. In the Sundarbans, the survey was conducted during a 10-day boat trip. In all, 48 sites were reoccupied while 7 sites were eroded, disturbed or otherwise unusable. Two sites recorded poor data due to heavy tree cover and do not have sufficient resolution.

Processing of the data was done utilizing GAMIT, the same software as used for the continuous GNSS sites. It enabled us to use both global reference sites and our continuous GNSS for the processing. The reoccupied sites had a median uncertainty of 0.94 mm/y in the vertical including uncertainties in the equipment setups. Initial values yielded a mixture of rates from very low to quite high. About ½ the sites had rate >20 mm/y or 360 mm over 18 years (Fig. 12). We strongly suspect that the monuments at these sites are unstable and have undergone local subsidence.

To examine the possibility that the very high rates of subsidence recorded are due to monument instability, Hasnat Jaman reoccupied 4 sites near Barisal in October 2022 during a lull in COVID. He reoccupied 2 sites with lower rates and 2 sites with anomalously high rates. Both sites with lower rates yielded linear trends for the three measurements (Fig. 13 left). In contrast both sites with higher subsidence rates yielded non-linear subsidence. The third measurement showed either no subsidence or uplift relative to the one in January 202 (Fig. 13 right). In the example shown, we suspect that the monument slumped from road level to the field level, creating extra subsidence, and is now shifting vertically with the seasonal movements of the adjacent rice field. Thus, we exclude these high rates from further analysis.

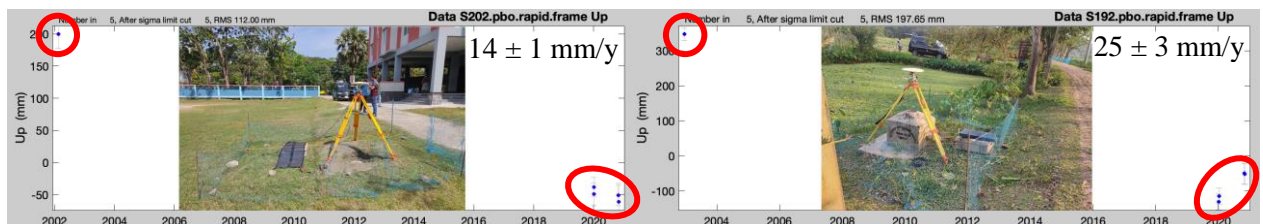


Figure 13. Plots of the time series for two of the reoccupied campaign sites. For the site on the left, the three measurements are colinear. For the site on the right, the third measurements yielded uplift relative to the long-term trend. We suspect that this site has slumped and is now shifting vertically with the rice field. This supports our inference of monument stability.

The remaining sites show an increase in subsidence from the NW to the SE (Fig. 14). The rates increase from near zero in the NW to ~14-15 mm/y (thick gray line in Figure 14). The sites in the northwest that show little to no subsidence are near Tube Well Transect G where the sediments are sandy (Fig. 8) while the remaining sites correspond to the muddier results of Transects H, J, K. The muddier underlying sediments are therefore likely to be contributing to subsidence through sediment compaction. Much of the compaction is occurring in the Holocene sediments. However, these rates are considerably higher than the rates from the continuous GPS (yellow box in Figure 14). Since all of the continuous GPS are installed on reinforced concrete buildings, we interpret that the monuments record shallow subsidence of the sediments that is not observed at the continuous GPS, as described in more detail below. This is supported by the subsidence rates at the KHLIC compaction meter and at the RSET-MH reported by Bomer et al. (2019) for the Sundarbans just south of Polder 32 (blue box in Figure 14). These rates of 8-11 mm/y are less than the more stable campaign GPS sites, but higher

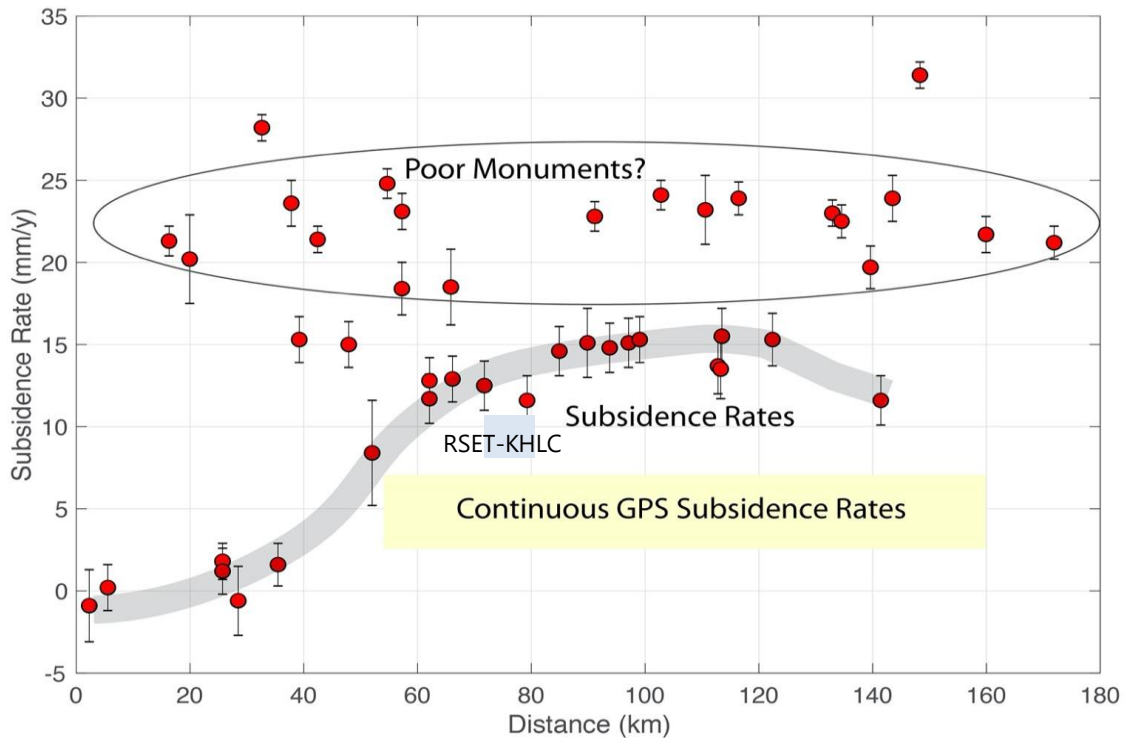


Figure 14. Subsidence rates from the SoB monuments projected along a profile N160°E, perpendicular to the subsidence contours in Grall et al. (2018). Our initial interpretation is that the sites with rate of 18 mm/yr and higher are due to poor monument stability. The remaining rates show systematic trend on increasing from the NW to the SE. However, where there is overlap, the survey rates are about twice as large as the continuous GPS rates. These results require further investigation.

than the continuous GNSS sites. We interpret the differences to be the deep subsidence recorded by the GPS, but not the RSET (described below).

RSET-MH Method. The Rod Surface Elevation Table and Marker Horizon (RSET-MH) method has become a global standard for monitoring elevation gain, sediment deposition, and shallow subsidence in >600 coastal wetlands around the world (Cahoon et al., 1995; Webb et al., 2013). Preliminary work in the southwest region of Bangladesh allowed the installation of 10 RSET-MH stations: 6 within the Sundarbans National Forest, and 4 inside Polder 32 (PD32). One of the goals of this project was to expand this network and include 12 more installations: 2 within the Sundarbans at Hiron Point, and 10 more within polders of the coastal region (see Figure 10 and Supplemental Table S3).

Interannual surface elevation change is recorded using the rod surface elevation table instrument (RSET; Fig. 15). During RSET installation, stainless steel rods (15 mm in diameter) are driven into the substrate until refusal and cemented within a 10-cm diameter PVC pipe for stability. The depth of the benchmark ranges from 30 to 80' (10 to 24 m), depending on the local depth of the incompressible substrate (i.e., consolidated sand). Seasonal measurements of surface elevation relative to the rod are made following the procedures of Cahoon et al. (2002). Nine measurements of surface elevation are taken at eight different positions for a total of 72 measurements at each site (see Figure 15, upper right photo).

Seasonal sediment vertical accretion is directly measured using several methods: sediment tiles, marker horizons, and/or buried plates (Fig. 15). As recommended by Steiger et al. (2003), these techniques are used together to provide quality control in this dynamic depositional setting. Following the approach of Rogers et al. (2013), four ceramic sediment tiles (area=100 cm²) are placed on the ground surface in the vicinity of each RSET station. Following a deployment period of ~6 months, tiles are excavated and vertical accretion measured at several points on each tile for a total of eight measurements per tile (Fig. 15). The average of all measurements is calculated to obtain the amount of seasonal accretion. Artificial marker horizons such as brick dust or glitter can also be used to measure vertical accretion. This material is dispersed on the ground surface in two plots (area ≈ 1m²) situated on different sides of the RSET receiver (Fig. 15). During subsequent field excursions, small cubic cores (~4 cm²) are excavated in undisturbed locations to locate marker horizons and quantify sediment accretion. The distance from the ground surface to the marker horizon is calculated as the amount of vertical accretion that had occurred during the deployment period. In regions of human occupation where soil disturbance is expected, aluminium plates (~15 cm x 30 cm) are buried at a known depth (~30 cm) on difference sides of the RSET receiver, and a sounding rod is used to measure depth to the plate during subsequent field occupations.

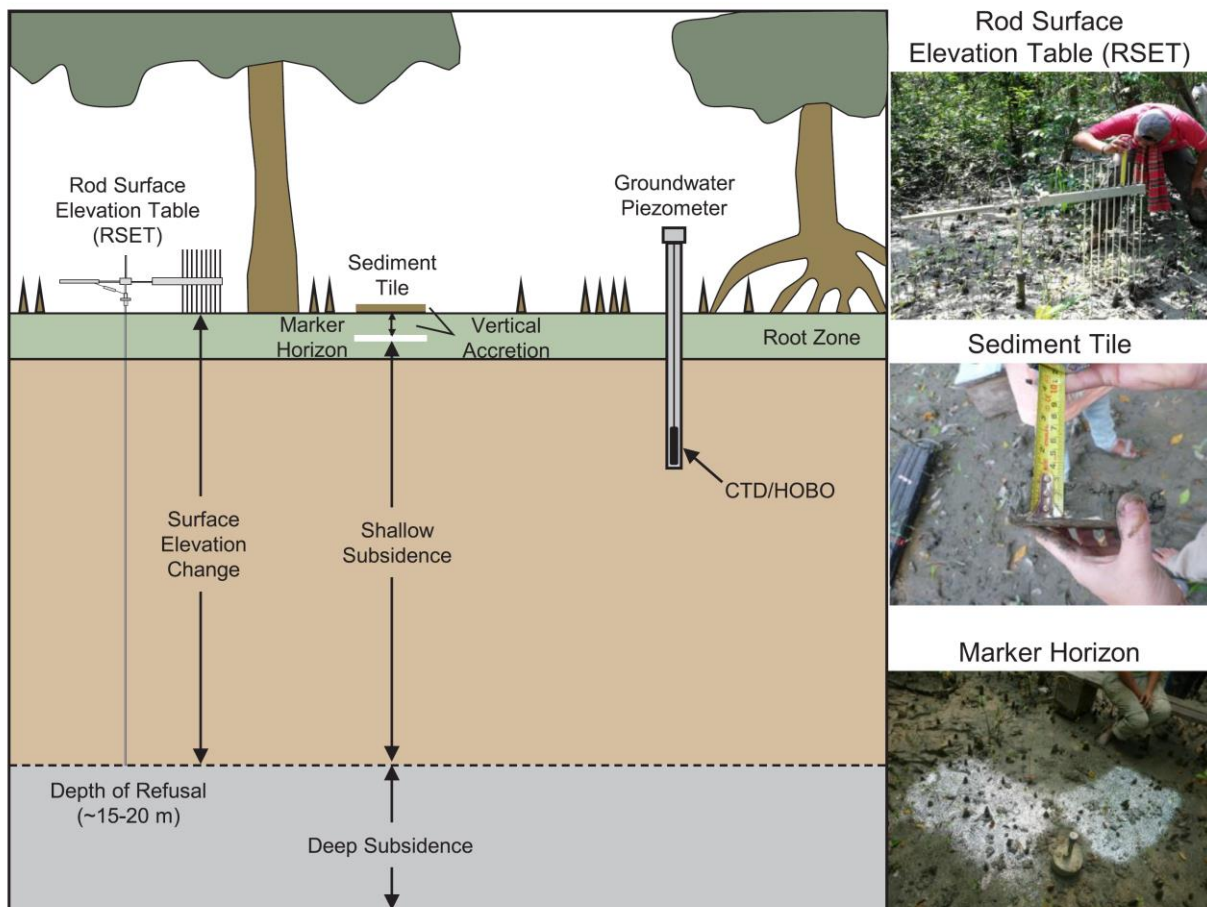


Figure 15. Schematic diagram (not to scale) of the RSET-MH method that is used to quantify shallow subsidence in wetland settings (from Bomer et al., 2019). The RSET measures interannual elevation change, and vertical accretion is measured using either marker horizons (brick dust or glitter) or sediment tiles. This method is modified in polder settings by burying aluminium plates at depth to measure vertical accretion. Shallow subsidence is measured from the difference in vertical accretion and surface elevation change. The bottom photo shows an installed RSET with glitter marker horizon. Above, the sediments accumulated on a tile are measured. At the top, the measurement rods are attached to the RSET and the surface elevation is being measured.

Comparisons of surface elevation change (SEC) and vertical accretion (VA) are used to quantify shallow subsidence (SS), whereby:

$$SS = VA - SEC \quad (2)$$

(from Cahoon et al., 1995). Positive values of SS indicate that shallow subsidence has occurred at depth between the ground surface and the depth of refusal for the RSET rods (see Fig. 15), and negative values indicate shallow subsurface expansion has occurred. SS values close to zero indicate that surface elevation change is occurring primarily as a function of sediment accretion, with negligible shallow subsidence or expansion (see Cahoon et al., 2015).

Earlier work from Bomer et al. (2019) showed shallow subsidence on the order of 7 to 18.4 mm/y occurs in the Sundarbans mangrove forest, with greater shallow subsidence during the dry season than during the monsoon season (see Fig. 16 and Table 1). There were a few instances during the monsoon season when surface elevation gain exceeded vertical accretion, indicating shallow subsurface expansion, likely from below ground biomass production and clay swelling from higher groundwater tables (Fig. 16). Interestingly, rates of shallow subsidence at streambank sites (11.3 ± 5.0 mm/y) were ~34% higher than those of interior sites (8.0 ± 3.7 mm/y), likely due to greater sedimentation (VA) measured at those sites (Fig. 16 and Table 1; Bomer et al., 2019).

During July-August 2019, 12 new RSETs were scouted and installed (Fig. 10) at Sonatola (SNT1), Jorshing (JRSN), Baintola (BNTL), Patuakhali (PUST), Khepupara (KHEP), and Hiron Point (HRNP). At each site, 2 RSET-MH were installed so that one was located inside the embankment perimeter wall, and another was located outside the embankment on the riverbank terrace. In these locations, RSET rods were installed to depths averaging 55-80 ft (16-24 m), and the buried aluminium plate MH method was employed. The expansion of the RSET-MH network for this project allows not only the investigation of sedimentation, elevation, and shallow subsidence spatially across the lower tidal deltaplain, but also inside vs outside polder embankments where land use practices differ. The baseline measurement of the new arrays was accomplished in December 2019.

For this project, the existing and new RSET-MH were measured seasonally until the COVID pandemic, then only measured annually when possible. The longest running datasets analyzed for this report include 8 years of measurements in the Sundarbans mangrove forest at Shorbothkhali and Polder 32 at the village of Shrinagar (PD32 in Fig.

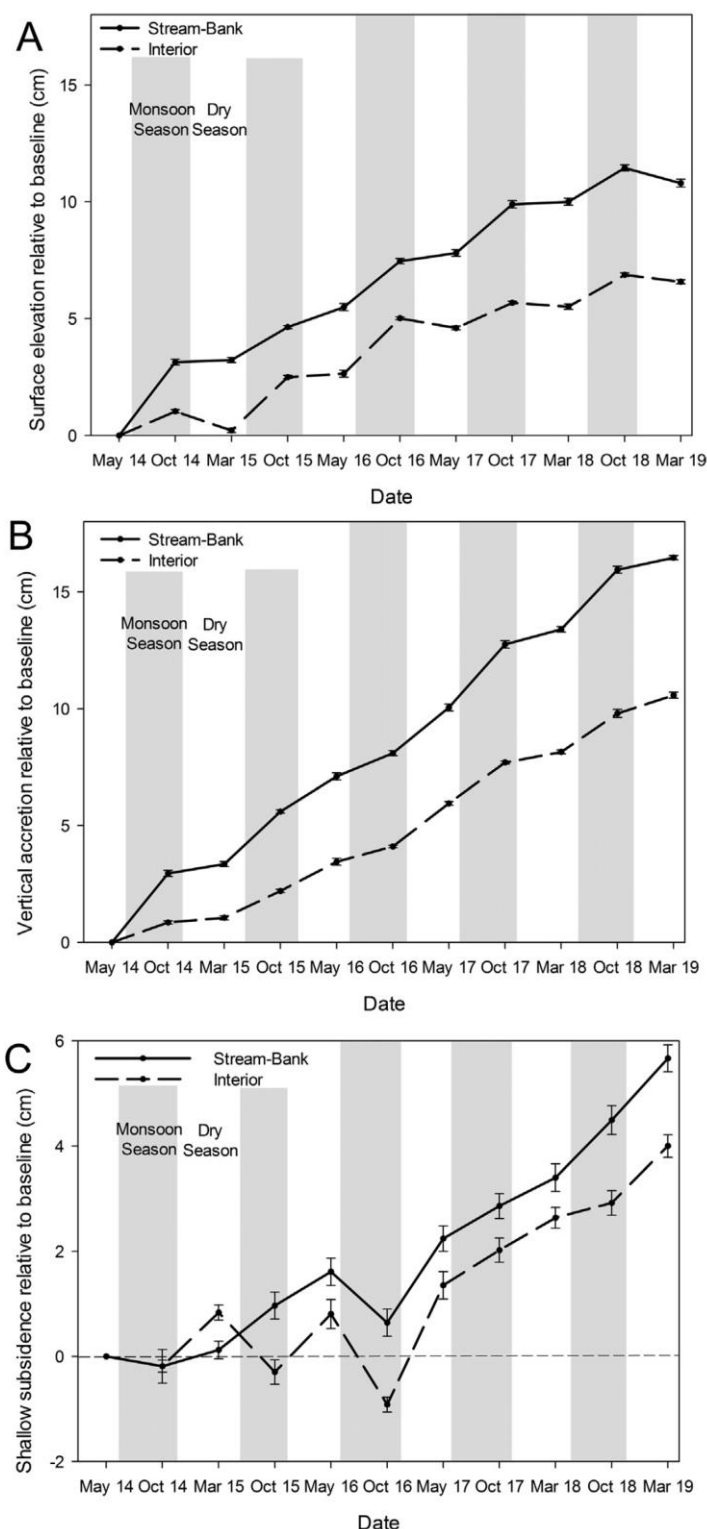


Figure 16. Inter-annual change in (A) surface elevation, (B) vertical accretion, and (C) shallow subsidence in the Sundarbans mangrove forest near Polder 32 (PD32, location shown in Fig 4) from Bomer et al. (2019). Positive values of shallow subsidence occur from compaction and dewatering of the shallow subsurface, and negative values represent expansion in the subsurface (i.e., clay shrink-swell, belowground biomass production-decay, etc.). Error bars are the standard error for all measurements.

10). Results are compiled in Table 1 and in Supplemental Figures S5 and S6. Results in the Sundarbans mangrove forest follow similar seasonal trends previously outlined by Bomer et al., 2019, and shallow subsidence averaged from all sites remains large but highly variable (9.7 ± 5.2 mm/yr). Creekbank sites continue to display slightly greater shallow subsidence values than interior sites (12.0 ± 5.5 mm/yr, compared to 7.4 ± 5.5 mm/yr; Table 1), likely due to greater sedimentation rates (VA). Within the polder, surface elevation change appears to be tracking vertical accretion closely, and shallow subsidence averaged from all sites is smaller than the Sundarbans but also highly variable (4.3 ± 4.4 mm/yr). Some of this variability is due to extensive seasonal soil

Station	Landscape	Record Duration (yr)	Surface Elevation Change (cm yr ⁻¹)	Vertical Accretion – ST (cm yr ⁻¹)	Vertical Accretion – MH (cm yr ⁻¹)	Shallow Subsidence (cm yr ⁻¹)
RSET-S1	Stream-Bank	5.0	2.59 ± 0.17	3.29 ± 0.29	3.64 ± 1.18	0.70 ± 0.46
RSET-I1	Interior	5.0	1.40 ± 0.14	2.62 ± 0.28	2.78 ± 1.01	1.22 ± 0.42
RSET-I2	Interior	3.5	1.05 ± 0.22	1.76 ± 0.29	2.32 ± 0.73	0.71 ± 0.51
RSET-S2	Stream-Bank	3.5	1.16 ± 0.37	3.00 ± 0.31	3.00 ± 0.57	1.84 ± 0.68
Average	Stream-Bank	5.0	2.16 ± 0.26	3.29 ± 0.24	3.32 ± 0.88	1.13 ± 0.50
Average	Interior	5.0	1.32 ± 0.17	2.12 ± 0.20	2.55 ± 0.87	0.80 ± 0.37

Table 1: Mean annual rates (\pm standard error) of surface elevation, vertical accretion measured by sediment tiles (ST) and marker horizons (MH), and shallow subsidence among study sites in the Sundarbans mangrove forest near Polder 32 (from Bomer et al., 2019). Shallow subsidence values are based on the difference between surface elevation change and vertical accretion from the sediment tile method, as Bomer et al., (2019) observed crab bioturbation led to slightly greater MH measurements.

expansion that is occurring at one of the sites (RSET-08; see Fig. S5). Similar to the Sundarbans, shallow subsidence at creek bank sites within the polder is slightly greater than interior sites as soil expansion was less pronounced at those sites (6.2 ± 0.2 mm/yr, compared to 2.3 ± 6.5 mm/yr, Table 1).

For the new RSET-MH installed for this project, plots of surface elevation and vertical accretion are shown in Supplemental (Figures S7 & S8), but the datasets are too short (3 years) for any meaningful analysis and calculation of shallow subsidence.

2.3 Discussion

Temporal and methodological controls on subsidence rates. The subsidence measurements presented here using different methodologies exhibit variations that show systematic patterns spatially—both in the horizontal and with depth—and temporally, (Fig. 11, 17). Overall, subsidence rates are inversely time-dependent, with younger deposits consolidating at greater rates commensurate with their age (i.e., Sadler effect). We find this fundamental temporal control also holds true in the GBD. Holocene averaged subsidence rates (Grall et al., 2018) (Fig. 5) are lower than contemporary rates from tide gauges, GNSS, RSET and the vertical strainmeter. The rates from the 300-600 year old historic sites (Fig. 8; Sarker et al., 2012; Hanebuth et al., 2013; Chamberlain et al., 2020) are similar to the Holocene rates (Grall et al., 2018), providing a timescale for shallow sediment compaction similar to the Mississippi Delta (Jankowski et al., 2017; Keogh and Törnqvist, 2019). The Nile Delta also shows higher contemporary rates from GNSS and InSAR (6-10 mm/y; Gebremichael et al., 2018; Saleh and Becker, 2019) relative to Holocene rates (0-4.5 mm/y; Marriner et al., 2012).

GNSS subsidence rates from the past two decades (i.e., modern rates) generally show slightly higher values than the longer-term Holocene average rates (Figs. 5, 11, 17). In the east, near the Lower Meghna River, rates are within about a millimeter/year of the Holocene rates. However, farther west, GNSS subsidence rates are consistently a few mm/y higher than the longer-term rates. The rates at KHUL/KHL2 and PD32 are 5.3-5.4 mm/y (Fig. 10, 11) while the longer term rates are 2.5-3 mm/y (Fig. 5). The rate at HRNP in the Sundarbans is even larger at 7.4 mm/y. We tentatively ascribe this difference to greater sediment compaction in the muddier sediments as described in the next section. The modern rates from tide and river gauges (Fig. 5; Becker et al., 2020) show an overall similarity to the GNSS rates in being slightly higher than the Holocene average values. However, the rates to the west are lower while the rates farther east are higher, inconsistent with attributing the GNSS rate differences to lithology.

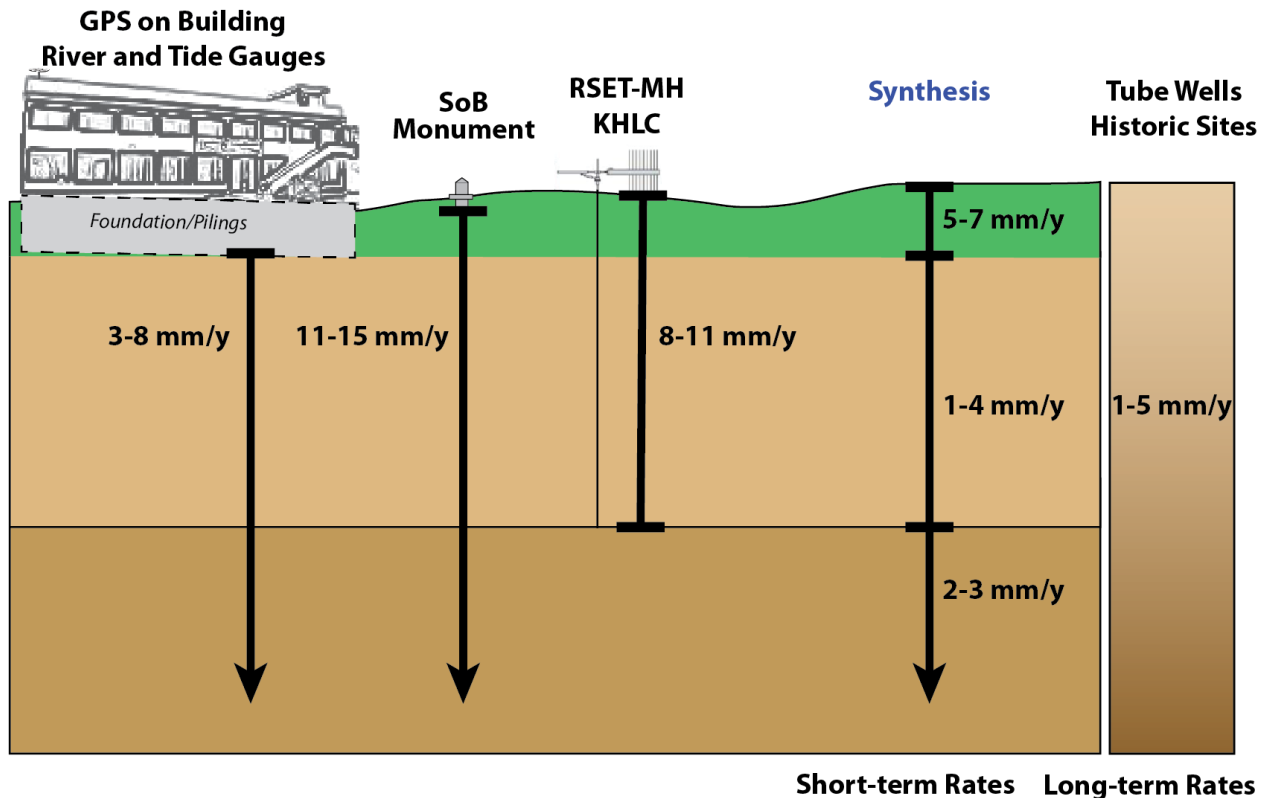


Figure 17. Cartoon presenting a synthesis of subsidence versus depth based on combining measurements from multiple instruments, each of which measure compaction or subsidence over a different depth range. GPS on building and tide gauges measure subsidence below the building or gauge foundations and miss shallow compaction. The RSET-MH and KHLC compaction meter measure compaction above the base of their instruments. The campaign GPS on SoB monuments measures both shallow and deep subsidence. Combining the results, the synthesis column shows a preliminary estimate of subsidence in each depth range. The long-term rates correspond to the sum of the two deeper brown layers.

Farther east, the river gauges show substantial subsidence (5.2 mm/y) along and east of the Meghna River where the Holocene rates rapidly taper to zero (Fig. 5). We interpret this to reflect short-term subsidence associated with ongoing deformation above the locked subduction megathrust (Steckler et al., 2016; Mallick et al., 2019; Fig. 1), which may reach 2-3 mm/y (Oryan, 2022). Megathrust earthquakes would likely uplift this region. The 1762 M8.5 earthquake farther south along the Arakan coast resulted in 2-7 m of coastal uplift (Aung et al., 2008; Wang et al., 2013; Mondal et al., 2018). Over the longer term, we expect that the net effect of the current interseismic subsidence, and infrequent coseismic and postseismic uplift would be a slight net uplift related to shortening on the blind detachment folds in the frontal foldbelt (Betka et al., 2018; Mondal et al., 2018, Mallick et al., 2021). Thus, we interpret the difference between the shorter-term and longer-term rates to reflect the seismic cycle in this region.

The highest rates of subsidence are located north of the coastal zone near Dhaka (Fig. 5, 8) due to groundwater extraction. At Dhaka, there is a significant cone of withdrawal from water pumping such that the water table is currently >70 m below sea level and had been dropping by ~3 m/y since the 1980s (Akhter et al., 2009; Shamsudduha et al., 2009, 2011). GNSS sites at the center of the cone show subsidence rates of 9-13 mm/y (Fig. 8). The river gauges, covering a large area from the center of the cone out beyond the cone edge, yield 7.2 mm/y.

The devices measuring shallow subsidence, the RSET-MH and KHLC, show higher rates of 9-10 mm/y (Fig. 11, 16). These instruments, located in sites of active sedimentation, include shallow subsidence not recorded by either the river gauges or GNSS. The anchor depth of the river gauges in Bangladesh is unknown; they average 20 m in the Mississippi Delta (Keogh and Törnqvist, 2019). The GNSS sites in Bangladesh are mainly installed on reinforced concrete buildings. The depth of pilings for the foundations are unknown, however, the ground is compacted before construction and there is no young sedimentation. Thus, shallow subsidence above some significant depth is not measured by either river gauges or GNSS. RSET-MH in the Mississippi Delta (Jankowski et al., 2017) show that shallow subsidence is primarily focused in the upper 5-10 m of sediment, averaging 6.4 ± 5.4 mm/year (Jankowski et al., 2017). GNSS-IR (interferometric reflectometry; Karegar et al., 2020) measures subsidence of the ground surface relative to anchored GNSS and found rates of 3-6 mm/y. Our results suggest similar amounts of shallow subsidence recorded by the RSET-MH and KHLC that are missed by the river gauges and continuous GNSS sites because this subsidence occurs shallower than the depth at which the instruments are rooted. The GNSS do include deep subsidence that occurs below the base of the RSET or strainmeters. Thus, the total subsidence at a site with active sedimentation may be equal to the values obtained by the campaign GNSS and may therefore reach values of 14-15 mm/y.

Parsing the subsidence rates, we estimate that the deep subsidence from below the Holocene strata is 2-3 mm/y (Fig. 17). In delta systems, it is recognized that thick sedimentary deposits isostatically loading the lithospheric plate creates subsidence. Karpytchev et al. (2018) and Krien et al. (2019) modeled the subsidence induced by Holocene sedimentation and estimate 1-3 mm/y, similar to our observations. This indicates that there is little contribution from sediment compaction at great depths. This is expected because of the incision of the river valleys during the last ice age. The river valleys were incised by up to 100 m or more (Fig. 2). Since sediment does not significantly decompact when material is eroded, it will not start to compact again until the weight of the sediments above exceed the maximum reached before the incision. As a result, for most of the incised valleys, there is no compaction of the sediment below the Holocene. At intermediate depths, perhaps corresponding to the Holocene sediment thickness of up to ~100 m (Fig. 2), we estimate only 1-4 mm/y. However, we note that the KHLC compaction meter (Fig. 6) shows subsidence that is spread through the entire Holocene section and less focused on the shallow sediment as discussed below.

The role of lithology with subsidence. Differences in subsidence rates indicate that there is a considerable amount of ongoing shallow subsidence in the GBD due to sediment compaction, consolidation and organic matter degradation. GNSS subsidence rates are consistently a few mm/y higher than the longer-term rates in southwestern Bangladesh farther from the sandy main mouths of the Ganges River: the Hooghly River in India prior to the mid 1600s, the Arial Khan/Tetulia Channel from then until the mid 1900s and the Lower Meghna River since then (Fig. 1). Thus, the recent sediments are expected to be muddier in this region between the major rivers. Thicker total Holocene sediments upstream of the Swatch of No Ground canyon in SW Bangladesh (Fig. 2) may also play a role in contributing to subsidence from compaction here.

This lithologic control is reinforced by the minimal compaction of the northwestern campaign GPS subsidence values near Jessore (Fig. 12, 14). Five sites show minimal subsidence (Fig. 12, 14). These sites are north of Transect H where the sediments average only 10% mud (Fig. 8) despite being in the Ganges incised valley. These sites are also the closest to the Hinge Zone (Fig. 2, 5), the total sediment thickness there may be $\frac{1}{2}$ of the values farther to the SE. Together they indicate little subsidence as a result of the lithology and tectonic setting of these sites.

More local lithologic differences may also contribute to variations in compaction. For example, while the GNSS on Polder 32 measures 5.3 mm/y subsidence (Fig. 12), the RSET-MHs 6-9 km away in the Sundarbans record 8-11 mm/y of shallow subsidence (Fig. 16; Table 1). RSET-MH subsidence values only include compaction above the base of the rods (in this case, 24.4 m). Meanwhile, KHLC to the NE shows the shallow subsidence is distributed over a greater depth range (Fig. 9). While the total compaction of 9 mm/y is similar between KHLC and the RSET-MH, KHLC only records 3.1 and 5.6 mm/y at the shallowest 20 and 40 m depth wells. This indicates significant variability in the shallow subsidence between sites, with the natural Sundarbans mangrove forest having more compaction occurring at very shallow depths (Bomer et al., 2020). This may be due to the muddier nature of the deposits in the Sundarbans and the greater root density in the mangroves (Bomer et al., 2020) since muddy sediments undergo more shallow compaction than sands (Kominz et al., 2011). At the compaction meter site, in contrast, the deposits beneath the recent channel fill were mainly very fine sand (Wilson et al., 2015; Chamberlain et al., 2020). Furthermore, shallow subsidence in natural areas such as the Sundarbans mangrove forest is driven by seasonal dewatering of the shallow subsurface (<2m) with lowering of the groundwater table during the dry season (Bomer et al., 2020).

3 Subsidence Maps

We have used our results to construct subsidence maps of the Bangladesh coastal Zone. For the rates, we construct two maps (Fig. 18, 19). The first (Fig. 18) corresponds to the rates based primarily on the continuous GPS measurement (Steckler et al., 2022) with additional input from tide gauges (Becker et al., 2020) and historic sites (Sarker et al., 2012; Hanebuth et al., 2013; Steckler et al., 2022). This the rate that is appropriate for buildings, embankments and other prepared surfaces. It does not include the near-surface compaction that is seen in actively sedimenting fields. The number of reliable measurements is limited and thus caution must be exercised for interpolating and extrapolating values before there is a better understanding of the controls on the variability that are observed.

The second (Fig. 19) corresponds to the rates based primarily on the campaign GPS measurement. This the rate that is appropriate for open fields and rice paddies that are actively sedimenting. It included the shallow compaction that is driven by sedimentation. There is a larger number of values and less variability, which increases the coherent of the rates in the figure. Although the results show high rates of subsidence, these rates are only present in fields with active sedimentation. These sedimentation rates are necessarily larger than the shallow compaction that they drive. Therefore, the elevation change is either much lower or in many cases still positive. This is the case for the RSET-MH at Polder 32 (Fig. 14, Table 1), which shows a net elevation gain of 13-22 mm/y, far larger than the 2-3 mm/y of deep subsidence beneath the area. Thus, for the subsidence maps for 25, 50 and 100 years in the future (Fig. 20), we restrict our maps to the subsidence rates based on the continuous GPS, as maps based on the other rates could be misleading.

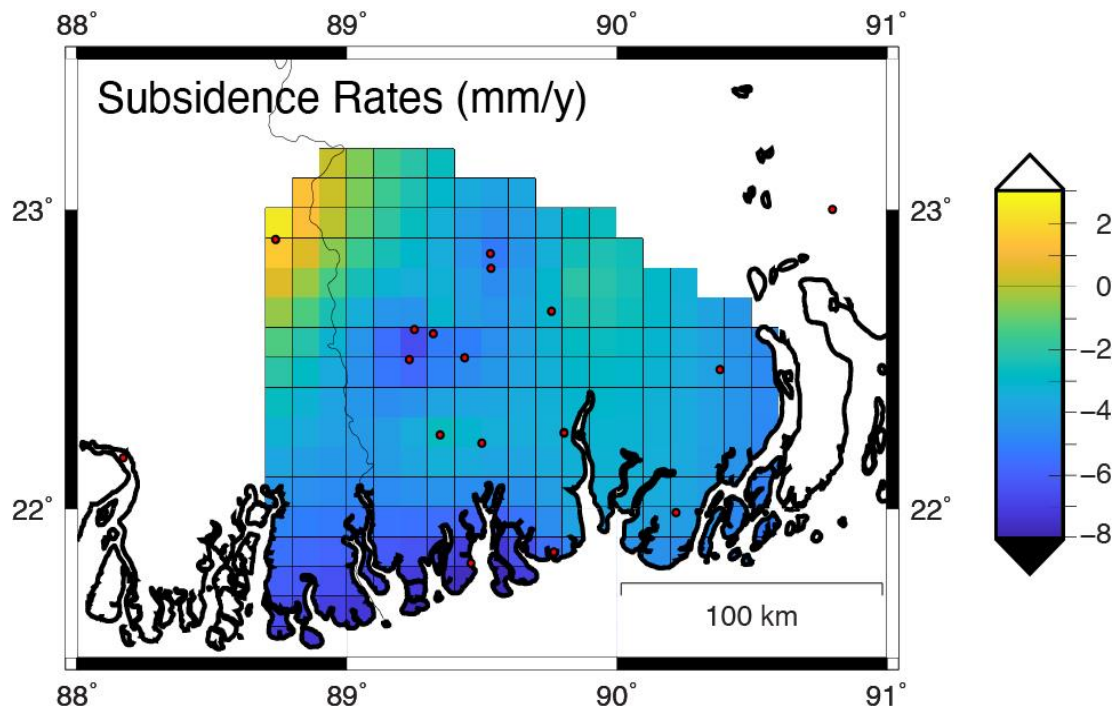


Figure 18. Map of subsidence rates for the Bangladesh coastal zone based on continuous GPS measurements, tide gauges and historic sites. The red dots are the locations of the sites used to construct the maps.

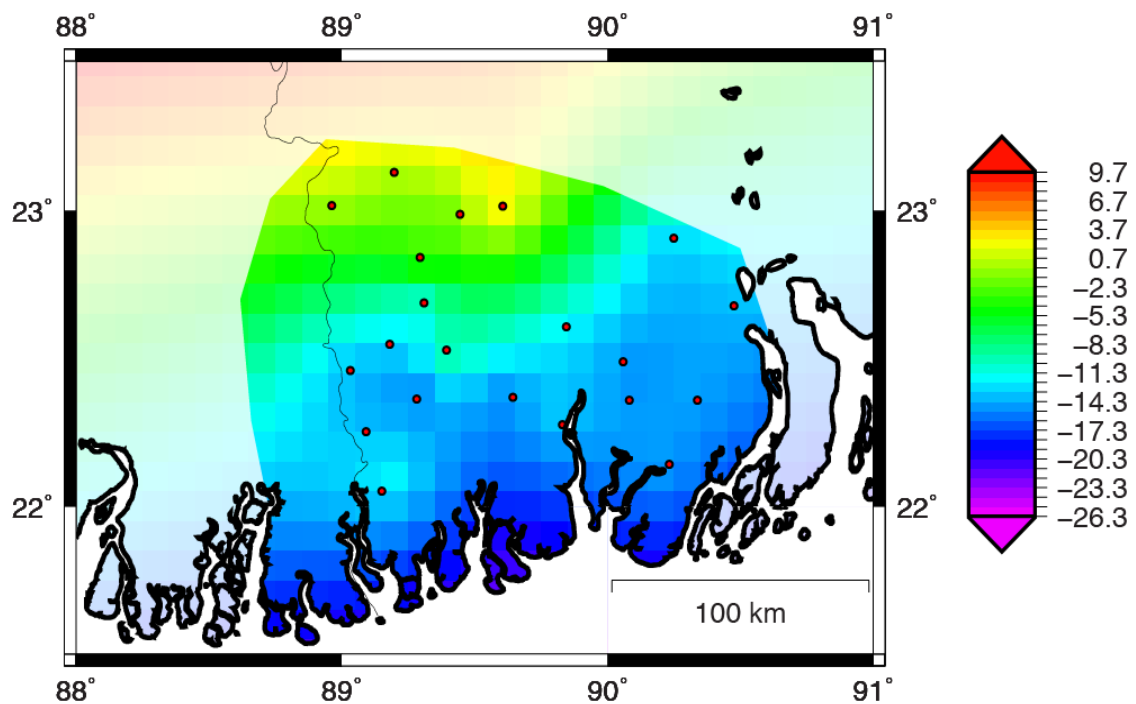
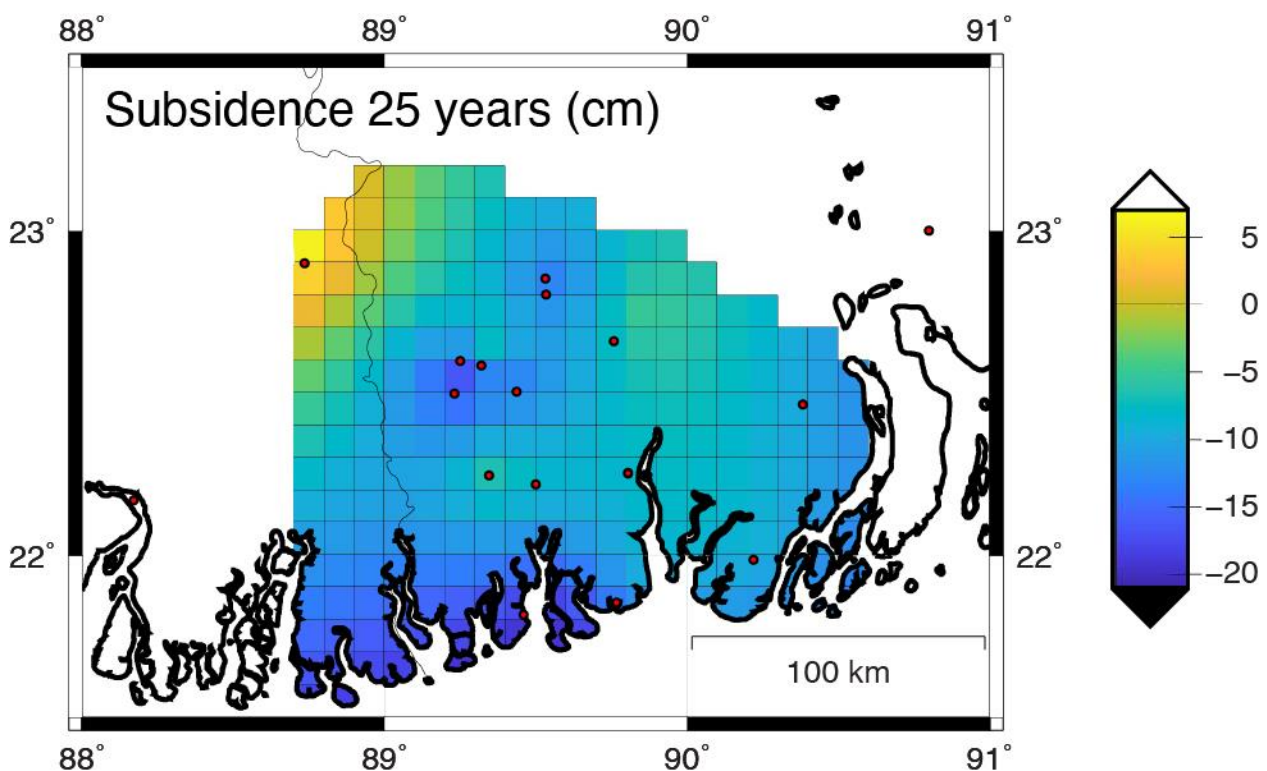


Figure 19. Map of subsidence rates for the Bangladesh coastal zone based on campaign GPS measurements. The red dots are the locations of the sites used to construct the maps.

4 Implications for Coastal Change

Landscape and coastline changes depend upon the combined effects of land subsidence, sea level rise and sedimentation. In order to investigate the influence of land subsidence, we examine landscape changes derived from satellite observations. The same methodology used to produce the 2022 continuous land cover map from Sentinel 2 was used to map changes from 1989 to 2020 using Landsat 5/8 imagery. Briefly, land cover is represented using a three endmember linear spectral mixture model (Adams et al., 1986; Adams & Gillespie, 2006) spanned by soil/sediment substrate (S), green vegetation (V) and dark shadow and water (D) (Fig. 21A). Spectrally diverse global compilations of Landsat (Small, 2004; Small and Milesi, 2013; Sousa and Small, 2017), MODIS (Sousa and Small, 2019) and Sentinel 2 (Small, 2018) consistently show a continuous spectral feature space spanned by substrates, vegetation, water/shadow, ice/snow and evaporites. As most landscapes do not contain ice/snow or evaporites, the three endmember SVD mixture model is generally applicable and able to represent subpixel fractions of the three most spectrally and biophysically distinct materials observed over most of Earth's non-polar landmasses.

Landsat 5 TM and Landsat 8 OLI imagery was used to produce SVD fraction maps for 1989 (earliest TM available) and 2020. As two swaths are required to cover the study area, four scenes from two acquisition dates are mosaiced for each year. Scene selection was based on comparison of overpass times with water level data from BIWTA



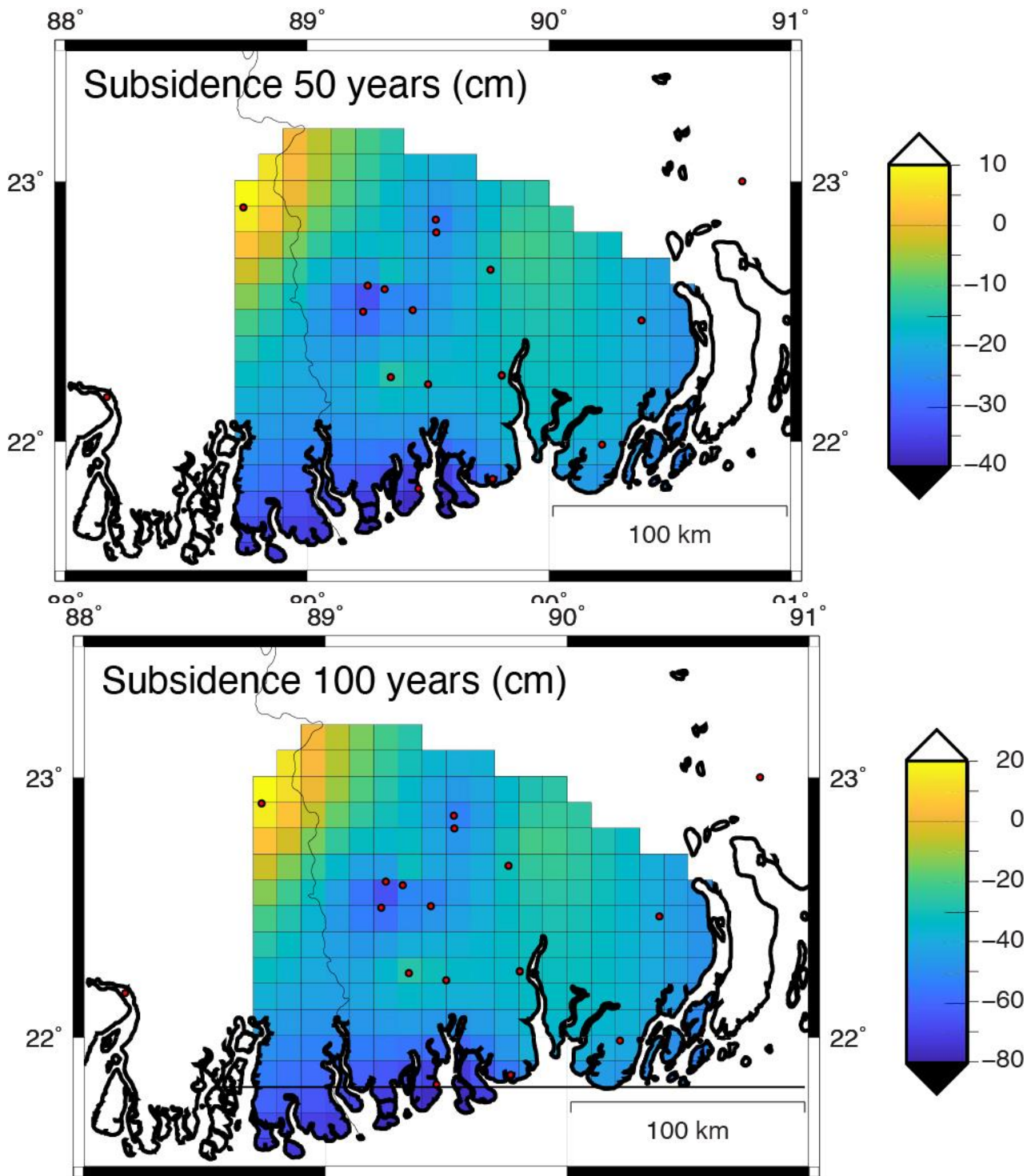
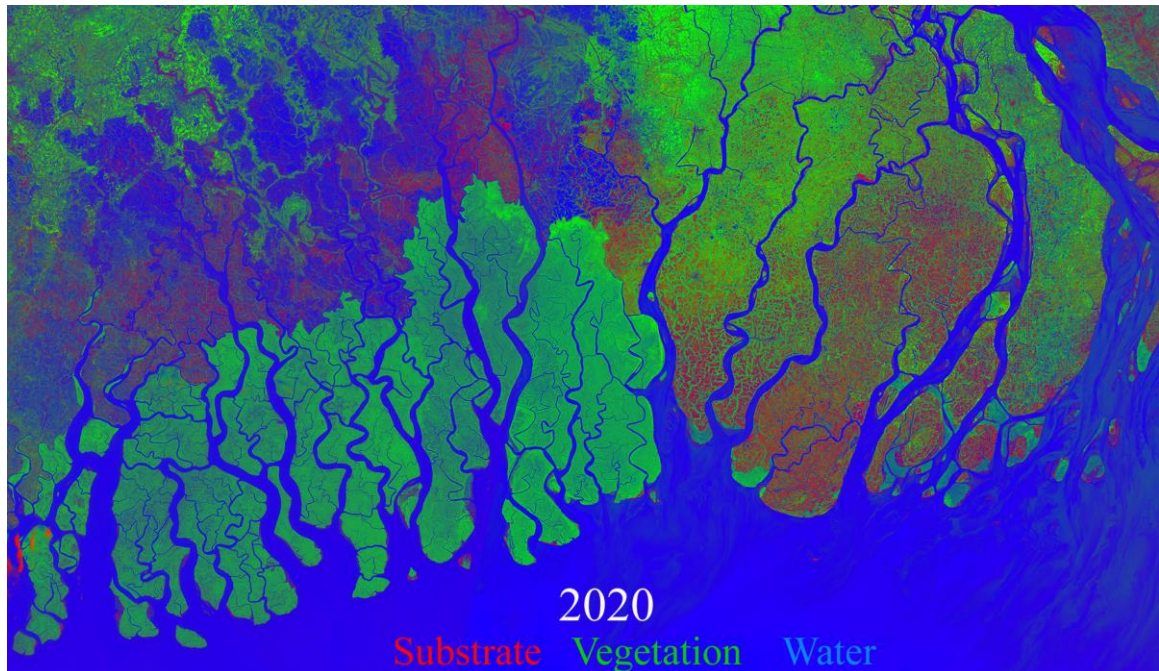


Figure 20. Total cumulative subsidence estimated for 25, 50 and 100 years in the future based upon the subsidence rate map in Figure 18.

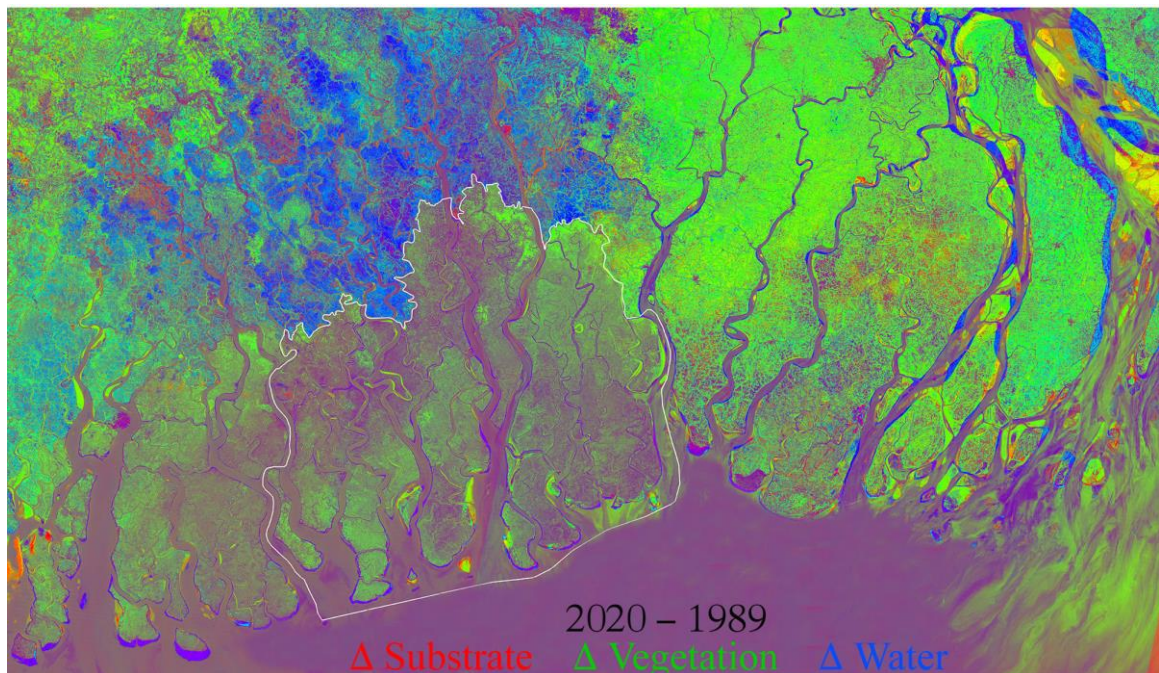
tide gauges in and around the Sundarbans to assure that all scenes were acquired at comparable low water levels to assure similar exposure of tidal flats. We intentionally focus on early year acquisitions to benefit from low discharge water levels and maximum likelihood of cloud-free conditions. Landsat data were obtained from the USGS archive, calibrated to Top of Atmosphere reflectance, mosaiced, unmixed by least squares inversion of the three endmember SVD mixture model and differenced to produce a map of SVD fraction changes between 1989 and 2020. The 2020 land cover fraction map and the 2020-1989 fraction change map are shown in Figure 21.

Changes in land cover and shoreline movement are inferred from the fraction change map (Fig. 21C). Comparisons of near-simultaneous 30 m Landsat fraction estimates and aggregated 2.6 m WorldView2 fraction estimates indicate that Landsat fraction estimates scale linearly with WorldView2 for fractions > 0.15 with greater dispersion at lower fractions. For this reason, we use a fraction threshold of 0.2 as a conservative indication of substantive change in land cover. To assist with interpretation and quantification of the continuous fraction change map, we harden it using a decision tree classification to identify areas of fraction change > 0.2. The fraction change classification is shown in Figure 21C.

A



B



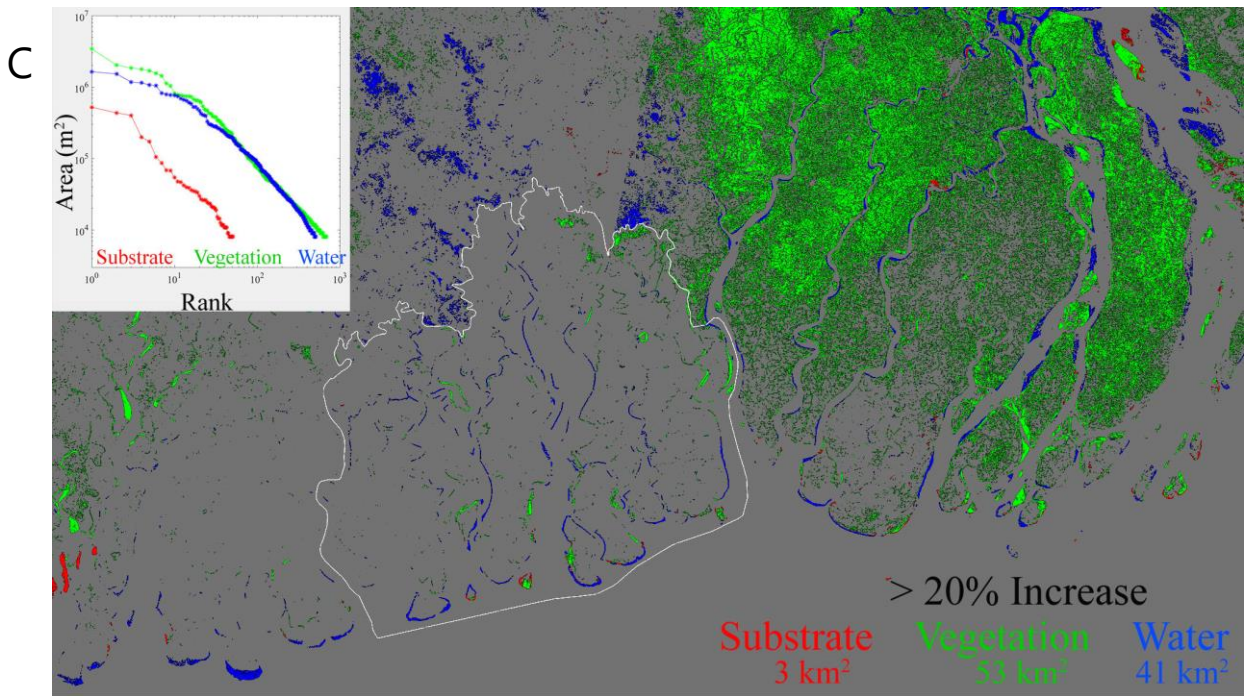


Figure 21. Land cover change 1989 - 2020. Landsat-derived continuous land cover fraction map (A) shows areal percent of soil/sediment substrate, vegetation (trees & crops) and water at 30 m resolution for February/March 2020. Continuous land cover fraction change map (B) shows increase in areal percent of each land cover type between 1989 and 2020. Discrete land cover change classification (C, on following page) shows increases in land cover fraction > 20% between 1989 and 2020. Shoreline movement from erosion and deposition within the Bangladesh Sundarbans appear as elongate bands of increased tree cover (green) and water (blue) along channels and on island peripheries. Rank-size distributions (C inset) of spatially contiguous areas of > 20% increase observed within the Sundarban show more and larger changes related to bank erosion (water increase) and forest expansion (trees increase). Growth of tidal flats (substrate increase) is underrepresented because intertidal mud flats are much darker than dry soil and generally fall below the 20% increase threshold. The large increase in forest area is an indication of the rapid colonization of stable tidal flats by vegetation. Increases in vegetation and water outside the Sundarbans reflect increases in aquaculture and dry season agriculture, as well as significant expansion of tree cover on polder embankments north and east of the Sundarbans.

To highlight the potential effects of subsidence, erosion and deposition, we quantify the size distribution of spatially contiguous changes in shoreline location within the Bangladesh Sundarbans. With the exception of some south-facing shorelines on the Bay of Bengal (e.g., Kuakata), the largest and most pervasive shoreline movements have occurred in the Sundarbans. This are primarily related to channel migration (symmetric erosion and deposition on opposite banks), channel widening (erosion on both banks) and extension & colonization of tidal mud flats. We have field validated the observed changes on multi-day transits through the

Sundarban in 2017, 2019 and 2022. We quantify these changes in the Bangladesh Sundarban using rank-size distributions (Figure 21C inset) of the size and frequency of spatially contiguous changes resulting from shoreline movements. As the distributions show, the processes of erosion and deposition appear to be approximately balanced with similar rank-size distributions for vegetation (deposition & colonization) and water (erosion) with somewhat more area being deposited/colonized as a result of channel narrowing and closing.

In the discrete land cover change distribution (Fig. 21C), the differences east and west of the Baleshwar River are very striking. To the east, there is primarily an increase in

vegetation between 1989 and 2020, while to the west, most of the changes that exceed the 20% threshold are increases in water. In the east, we observe lower rates of subsidence (Fig. 11), which are similar to the long-term rates (Fig. 5) and we presume that there is also greater sediment supply from the Meghna River. In contrast, farther west, we see increases in water in the poldered region and widening of the major channels in the Sundarbans. In this region, we see greater subsidence (5.3-5.4 mm/y) in the poldered region and 7.4 mm/y in the Sundarbans (Fig. 11). This area has also had a decrease in riverine sediment input since the eastward avulsion of the Ganges River in the 15-1600s. Along the coast, there is a change from accretion in the Meghna River to erosion farther west (Allison, 1998; Brammer, 2014). While the dramatic difference in landscape change is due to the combined effects of land subsidence and sediment supply, in conjunction with sea level rise, we note that the landscape changes are congruent with the subsidence differences.

5 Summary

The CEIP-1 Design phase in 2011-2012 assumed a uniform subsidence rate of 10 mm/y over the entire coastal area for designing embankments and the drainage systems for a design period of 30 years. While this value is consistent with the published estimate at the times (Ericson et al., 2006; Syvitski et al., 2009; Ostanciaux et al., 2012), newer published results and our newer data is starting to be able to refine rates of subsidence in the GBD. The different tools for measuring the subsidence occurring in different depth ranges (Fig. 17). GPS on building measure the total deeper subsidence, but miss shallowest subsidence above the depth of foundation/pilings of the building. We note that the subsidence rates from the continuous GPS (Fig. 11; 3-8 mm/y) are similar to both the rates estimate for the region by tide gauge analysis (Fig. 5; Becker et al., 2020), and average Holocene subsidence (Fig. 5; Grall et al., 2018). Although the distribution has some differences. In addition, the continuous GPS rates are a few millimeters/year higher in the SW coastal zone due to greater compaction of muddy sediments there. The similarity of rates for these methods indicates that the anchoring of the tide gauges also excludes the shallowest component of subsidence. We also note that the lateral differences in subsidence between the western and central coastal zone (Fig. 11) are consistent with the landscape changes observed through satellite remote sensing (Fig. 21)

In contrast, methods that include very shallow subsidence, such as the RSET-MH, KHLC compaction meter, and the campaign GPS survey yield much higher rates (Fig. 7, 12, 14, 16). The RSET-MH measure all of the subsidence above the base of the rods (≤ 24 m). The campaign GPS at Survey of Bangladesh (SoB) monuments measure the total subsidence, but some sites include local subsidence of the monuments and were excluded (Fig. 13, 14). Using the combination of these tools, we can create a preliminary estimate of subsidence in three depth zones.

For the deepest zone, we estimate 2-3 mm/y of subsidence (Fig. 17). This includes both isostasy and deeper sediment compaction. These values are similar to isostatic loading models (Karpytchev et al., 2018, Krien et al., 2019) that estimate 1-3 mm/y. In the intermediate zone above the base of the RSETs at ~ 24 m but below the foundations of building at a few meters, we find 1-4 mm/y of subsidence. Values of 1 mm/y correspond to regions with a sandier lithology, while compaction for muddier regions is likely 3-4 mm/y. The shallowest region of the upper few meters may have subsidence rates as large as 5-7 mm/y corresponding to the dewatering of very loose muds at the surface and decay of organic matter. These estimates are very preliminary and will almost certainly change as we obtain newer data from the measurement systems. Additional measurements of lithology and porosity near the RSET and SoB monuments will further help refine estimates of the shallowest subsidence.

We note that in the NW part of the field area, there are 5 campaign GPS sites (GPS 101, GPS 115, GPS 118, GPS 199 and 2876) that display virtually no subsidence (Fig. 11). These are located in the moribund fluvial delta (Wilson and Goodbred, 2015) near the Hinge Zone separating the Indian craton from the deep Bengal Basin (Steckler et al., 2008). Sediment thicknesses there are lower, likely 9-10 km rather than 16-20 km (Singh et al, 2016). The tube wells also indicate sandier sediments (Fig. 6). Together, these are consistent with limited subsidence in this region.

The highest rates of subsidence are 11-15 mm/y, but that includes compaction of the shallowest muddy sediments. Depending on the site preparation of the polder embankments, such as excavation of the base of the polder, mechanical compaction of the underlying material and filling of the interior of the embankment with sand, a considerable amount of the shallowest subsidence should be eliminated. As a result, at this time it appears that the design allowance of 10 mm/y subsidence over the design period of the polders should be sufficient for their stability. As the data is refined, it is possible that some of the shallowest subsidence may shift to the next zone below.

However, there is still considerable uncertainty. Thus, it is possible that local areas may have subsidence exceeding 10 mm/y. These results are averaged regional values; only one of the sets of RSETs has been in place sufficiently to provide a subsidence estimate. There are 7 set of pairs of RSETs that need additional measurement time to obtain a shallow subsidence rate. Similarly, the 4 new GPS also need additional years to obtain an accurate subsidence rate. The continuation of the RSET and GPS measurements beyond the end of this program is necessary. Since the GPS and RSET are co-located, when the data are mature we can better determine shallow and deep subsidence rates across the region, rather than an average. We also need further investigation of the sediments and monument stability around the observation sites. These measurements are critical for improving and refining these preliminary estimates.

While IWM participated in both the GPS and RSET installations and subsidence measurements, only two students from Dhaka University are fully trained in making the RSET measurements, and both of them have graduated. Only one professor each from Barisal University and Dhaka University are fully trained in the GPS measurements and GPS data processing. However, the Barisal University professor is starting graduate school in the U.S. in 2023 and the Dhaka University professor is now the VC of Bangladesh Open University and has significantly less time available for research. Thus, additional capacity building is required for this technology to be fully transferred to Bangladesh.

6 References

- Adams, J. B., & Gillespie, A. R. (2006). *Remote sensing of landscapes with spectral images: A physical modeling approach*. Cambridge University Press.
- Adams, J. B., Smith, M. O., & Johnson, P. E. (1986). Spectral mixture modeling: A new analysis of rock and soil types at the viking lander 1 site. *Journal of Geophysical Research: Solid Earth*, 91(B8), 8098–8112. <https://doi.org/10.1029/JB091iB08p08098>
- Akhter, H., M.S. Ahmed and K.B.S. Rasheed (2009). Spatial and temporal analysis of groundwater level fluctuations in Dhaka City, Bangladesh, *Asian J. Earth Sciences*, 2,49-57.
- Akhter, S.H. (2010), Earthquakes of Dhaka, in Environment of Capital Dhaka—Plants Wildlife Gardens Parks Air Water and Earthquake, edited by M. A. Islam, pp. 401–426, Asiatic society of Bangladesh, Bangladesh.
- Alam, M., 1996. Subsidence of the Ganges–Brahmaputra delta of Bangladesh and associated drainage, sedimentation and salinity problems. In: Milliman, J.D., Haq, B.U. (Eds.), *Sea-level Rise and Coastal Subsidence*. Kluwer Academic Publishers, Dordrecht, pp. 169–192.
- Alauddin, M. and Hamid, M. A. (1999). Shrimp culture in Bangladesh with emphasis on social and economic aspects. Towards sustainable shrimp culture in Thailand and the region. Edited by P.T. Smith. Canberra: Australian Centre for International Agricultural Research. 53-62
- Allison, M.A. (1998). Historical changes in the Ganges-Brahmaputra Delta front. *Journal of Coastal Research*, 14(4), 1269–1275.
- Allison, M. A., Khan, S. R., Goodbred, S. L., & Kuehl, S. A. (2003). Stratigraphic evolution of the late Holocene Ganges-Brahmaputra lower delta plain. *Sedimentary Geology*, 155(3), 317–342. [https://doi.org/10.1016/S0037-0738\(02\)00185-9](https://doi.org/10.1016/S0037-0738(02)00185-9).
- Allison, M., B. Yuill, T. Törnqvist, F. Amelung, T. Dixon, G. Erkens, R. Stuurman, M. Steckler, J.P.M. Syvitski, and P. Teatini. Coastal Subsidence: Global Risks and Research Priorities, *EOS*, 97, doi:10.1029/2016EO055013, 2016.
- Athy, L.F., 1930. Density, porosity, and compaction of sedimentary rocks. *Bull. Am. Ass. Petrol. Geol.*, 14: 1-24.
- Auerbach, L., Goodbred, S., Mondal, D., Wilson, C., Ahmed, K.R., Roy, K., Steckler, M., Gilligan, J., Ackerly, B. (2015). In the Balance: Natural v. Embanked Landscapes in the Ganges-Brahmaputra Tidal Delta Plain, *Nature Climate Change*. 5, 153-157, doi: 10.1038/nclimate2472.
- Aung T.T., K. Satake, Y. Okamura, M. Shishikura, W. Swe, H. Saw, T.L. Swe, S.T. Tun, T. Aung (2008). Geologic evidence for three great earthquakes in the past 3400 years off Myanmar, *Journal of Earthquake and Tsunami*, 2, 259–265.
- Bahr, D.B., Hutton, E.W.H., Syvitski, J.P.M., Pratson, L.F., 2001. Exponential approximations to compacted sediment porosity profiles. *Computers & Geosciences* 27, 691–700.
- Becker, M., F. Papa, M. Karpytchev, C. Delebecque, Y. Krien, J.U. Khan, V. Ballu, F. Durand, G. Le Cozannet, A.K.M.S. Islam, S. Calmant, C.K. Shum (2020) Water level changes, subsidence, and sea level rise in the Ganges–Brahmaputra–Meghna delta, *Proceedings of the National Academy of Sciences*, 117 (4) 1867-1876; doi:10.1073/pnas.1912921117.
- Best, J.L., Ashworth, P.J., Sarker, M.H., Roden, J.E., 2007. The Brahmaputra-Jamuna River. In: Gupta, A. (Ed.), *Bangladesh. In Large Rivers: Geomorphology and Management*, pp. 395–433.
- Betka, P.M., L. Seeber, S. Thomson, M.S. Steckler, R. Sincavage, C. Zoramthara (2018). Slip partitioning above a shallow, weak décollement beneath the Indo-Burman accretionary prism, *Earth and Planetary Science Letters* 503, 17–28, 10.1016/j.epsl.2018.09.003.
- Blewitt, G. and D. Lavallée (2002) Effect of annual signals on geodetic velocity. *Journal of Geophysical Research*, 107, 2145-2156, doi: 10.1029/2001JB000570.
- Blum M.D., Roberts, H.H. (2009) Drowning of the Mississippi Delta due to insufficient sediment supply and global sea-level rise. *Nat. Geosci.* 2: 488–491. doi:10.1038/NGEO553
- Bomer, E.J., C.A. Wilson and D.K. Datta, 2019. An Integrated Approach for Constraining Depositional Zones in a Tide-Influenced River: Insights from the Gorai River, Southwest Bangladesh, *Water* 11, 2047; doi:10.3390/w11102047
- Bomer, E.J., Wilson, C.A., Hale, R.P., Hossain, A.N.M., and Rahman, F.M.A. (2020). Surface elevation and sedimentation dynamics in the Ganges-Brahmaputra tidal delta plain, Bangladesh: implications for the sustainability of natural and human-impacted coastal systems. *Catena*.187:104312.
- Brammer, H. (1990). Floods in Bangladesh: Geographical background to the 1987 and 1988 floods. *Geographical Journal*, 156, 12–22. <https://doi.org/10.2307/635431>
- Brammer, H. (2014). Bangladesh's dynamic coastal regions and sea-level rise. *Climate Risk Management*, 1, 51-62.

- Brown, S., R. J. Nicholls, Subsidence and human influences in mega deltas: The case of the Ganges-Brahmaputra-Meghna. *Sci. Total Environ.* 527–528, 362–374 (2015).
- Cahoon, D.R., D.J. Reed, and J.W. Day. 1995. Estimating shallow subsidence in microtidal salt marshes of the southeastern United States: Kaye and Barghoorn revisited. *Mar. Geol.* 128:1–9. doi:10.1016/0025-3227(95)00087-F
- Cahoon, D.R., J.C. Lynch, B.C. Perez, B. Segura, R.D. Holland, C. Stelly, et al. 2002. High precision measurements of wetland sediment elevation: II. The rod surface elevation table. *J. Sediment. Res.* 72:734–739. doi:10.1306/020702720734
- Cahoon, D. R. 2015. Estimating relative sea-level rise and submergence potential at a coastal wetland. *Estuaries and Coasts* 38(3):1077-1084. doi:10.1007/s12237-014-9872-8
- Chamberlain, E.L., S.L. Goodbred, R. Hale, M.S. Steckler, J. Wallinga, C. Wilson (2020). Integrating geochronologic and instrumental approaches across the Bengal Basin, *Earth Surface Processes and Landforms*, 45, 56-74., <https://doi.org/10.1002/esp.4687>.
- Chapman, R.E., 1983. Chapter 3: Compaction of sediment and sedimentary rocks, and its consequences. In: Chapman, R.E. (Ed.), *Petroleum Geology, Developments in Petroleum Science* 16. Elsevier, Amsterdam, pp. 41–65.
- DeWolf; S., S.L. Nooner; M.S. Steckler; M.A. Zumberge; S.H. Akhter, Optical Fiber Borehole Strainmeter Arrays for Measuring Sediment Compaction in Bangladesh, Abstract EP31A-0831 presented at 2013 Fall Meeting, AGU, San Francisco, Calif., 9-13 Dec. 2013.
- Dixon, T. H., Amelung, F., Ferretti, A., Novali, F., Rocca, F., Dokka, R., et al. (2006). Space geodesy: Subsidence and flooding in New Orleans. *Nature*, 441(7093), 587–588. <https://doi.org/10.1038/441587a>.
- Dunn F.E., S.E. Darby, R.J. Nicholls, S. Cohen, C. Zarfl and B.M. Fekete (2019). Projections of declining fluvial sediment delivery to major deltas worldwide in response to climate change and anthropogenic stress, *Environ. Res. Lett.* 14, 084034, doi: 10.1088/1748-9326/ab304e.
- Eaton, Richard M. *The Rise of Islam and the Bengal Frontier, 1204-1760*. Berkeley: University of California Press, 192pp.
- Ericson, J.P., Vörösmarty, C.J., Dingman, S.L., Ward, L.G., Meybeck, M., 2006. Effective sealevel rise and deltas: causes of change and human dimension implications. *Glob. Planet. Chang.* 50, 63–82. <http://dx.doi.org/10.1016/j.gloplacha.2005.07.004>.
- Erkens, G., M.J. van der Meulen, H. Middelkoop (2016). Double trouble: subsidence and CO2 respiration due to 1,000 years of Dutch coastal peatlands cultivation, *Hydrogeol. J.* 24, 551–568, doi: 10.1007/s10040-016-1380-4.
- Gebremichael, E., Sultan, M., Becker, R., El Bastawesy, M., Cherif, O., & Emil, M. (2018). Assessing land deformation and sea encroachment in the Nile Delta: A radar interferometric and inundation modeling approach. *Journal of Geophysical Research: Solid Earth*, 123, 3208–3224. <https://doi.org/10.1002/2017JB015084>
- Giosan, L, J. Syvitski, S. Constantinescu and J. Day (2014). Protect the world's deltas. *Nature* 516, 31–33.
- Gluyas, J., C.A. Cade, (1997). Prediction of porosity in compacted sands, AAPG Memoir 69: Reservoir Quality Prediction in Sandstones and Carbonates, Edited by J.A. Kupecz, J. Gluyas, and S. Bloch, 19-27.
- Goodbred SL, Kuehl SA, Steckler M, Sarker MH. 2003. Controls on facies distribution and stratigraphic preservation in the Ganges-Brahmaputra delta sequence. *Sediment. Geol.* 155:301–16
- Goodbred, S.L., P.M. Paolo, M.S. Ullah, R.D. Pate, S.R. Khan, S.A. Kuehl, S.K. Singh, W. Rahaman (2014). Piecing together the Ganges-Brahmaputra-Meghna River delta: Use of sediment provenance to reconstruct the history and interaction of multiple fluvial systems during Holocene delta evolution. *GSA Bulletin* 126, 1495–1510. doi: 10.1130/B30965.1.
- Gordon, D.S., Flemings, P.B. (1998). Generation of overpressure and compaction-driven fluid flow in a Plio-Pleistocene growth-faulted basin, Eugene Island 330, offshore Louisiana. *Basin Res.* 10, 177–196.
- Goswami, D.C., 1985. Brahmaputra River, Assam, India: basin denudation and channel aggradation. *Water Resources Research* 21, 959–978.
- Grall, C., M.S. Steckler, J.L. Pickering, S. Goodbred, R. Sincavage, C. Paola, S.H. Akhter, V. Spiess (2018) A base-level stratigraphic approach to determining Holocene subsidence of the Ganges–Meghna–Brahmaputra Delta plain. *Earth and Planetary Science Letters*, *Earth and Planetary Science Letters* 499, 23–36, 10.1016/j.epsl.2018.07.008.
- Grimaud, J.-L., Grall, C., Goodbred, S., Steckler, M. S., Sincavage, R., Pickering, J. L., Paola, C., Seeber, L., Hossain, M. S. (2020). Flexural deformation controls on Late Quaternary sediment

- dispersal in the Garo-Rajmahal Gap, NW Bengal Basin. *Basin Research*, 32, 1242–1260. <https://doi.org/10.1111/bre.12425>
- Hanebuth, T.J.J., Kudrass, H.R., Linstaedter, J., Islam, B., Zander, A.M., 2013. Rapid coastal subsidence in the central Ganges–Brahmaputra Delta (Bangladesh) since the 17th century deduced from submerged salt-producing kilns. *Geology* 41 (9), 987–990. <http://dx.doi.org/10.1130/G34646.1>.
- Hanebuth, T.J.J., Kudrass, H.R., Zander, A.M., Akhter, H.S., Neumann-Denzau, G., Zahid, A., 2021. Stepwise, earthquake-driven coastal subsidence in the Ganges–Brahmaputra Delta (Sundarbans) since the eighth century deduced from submerged in situ kiln and mangrove remnants. *Nat. Hazards*. <https://doi.org/10.1007/s11069-021-05048-2>
- Hedberg, H.D. (1936). Gravitational compaction of clays and shales. *Am. J. Sci.*, 31, 241-287.
- Herring, T.A., R.W. King, M.A. Floyd, S.C. McClusky, 2018. Introduction to GAMIT/GLOBK Release 10.7, 54p.
- Higgins, S.A., Overeem, I., Steckler, M.S., Syvitski, J.P.M., Seeber, L., Akhter, S.H., 2014. InSAR measurements of compaction and subsidence in the Ganges–Brahmaputra Delta, Bangladesh. *J. Geophys. Res. Earth Surf.* 119 (8). <http://dx.doi.org/10.1002/2014JF003117> (2014JF003117).
- Hoque, M., Alam, M., 1997. Subsidence in the lower deltaic areas of Bangladesh. *Mar. Geod.* 20 (1), 105–120. <http://dx.doi.org/10.1080/01490419709388098>.
- Hoque MA, Hoque MM, Ahmed KM (2007) Declining groundwater level and aquifer dewatering in Dhaka metropolitan area, Bangladesh: causes and quantification. *Hydrogeol J* 15:1523–1534. doi:10.1007/s10040-007-0226-5
- Ismail, M., K.S. Krishna, K. Srinivas, J. Mishra and D. Saha (2019) Crustal architecture and Moho topography beneath the eastern Indian and Bangladesh margins – new insights on rift evolution and the continent–ocean boundary. *Journal of the Geological Society*, 176, 553-573, doi:10.1144/jgs2018-131
- Jankowski, K.L., Törnqvist, T.E., Fernandes, A.M., 2017. Vulnerability of Louisiana’s coastal wetlands to present-day rates of relative sea-level rise. *Nat. Commun.* 8, 14792. <https://doi.org/10.1038/ncomms14792>.
- Karegar, M. A., Larson, K. M., Kusche, J., & Dixon, T. H. (2020). Novel quantification of shallow sediment compaction by GPS interferometric reflectometry and implications for flood susceptibility. *Geophysical Research Letters*, 47, e2020GL087807. <https://doi.org/10.1029/2020GL087807>
- Karpytchev, M., Ballu, V., Krien, Y., Becker, M., Goodbred, S., Spada, G., Calmant, S., Shum, C., and Z. Khan (2018). Contributions of a strengthened early Holocene monsoon and sediment loading to present-day subsidence of the Ganges-Brahmaputra Delta. *Geophysical Research Letters*, 45, 1433–1442. doi.: 10.1002/2017GL076388.
- Keogh, M.E., and T.E. Törnqvist (2019). Measuring rates of present-day relative sea-level rise in low-elevation coastal zones: a critical evaluation. *Ocean Sci.*, 15, 61–73, <https://doi.org/10.5194/os-15-61-2019>.
- Kesel, R.H. (1988). The decline in the suspended load of the Lower Mississippi River and its influence on adjacent wetlands. *Environ. Geol. Water Sci* 11, 271–281. <https://doi.org/10.1007/BF02574816>
- Kominz M.A., K. Patterson, and D. Odette (2011). Lithology dependence of porosity in slope and deep marine sediments, *Journal of Sedimentary Research*, 2011, 81, 730–742, doi: 10.2110/jsr.2011.60.
- Kondolf G.M., Z.K. Rubin and J.T. Minear (2014). Dams on the Mekong: cumulative sediment starvation *Water Resour. Res.* 50, 5158–69
- Kooi, H., DeVries, J.J., 1998. Land subsidence and hydrodynamic compaction of sedimentary basins. *Hydrology and Earth System Sciences* 2, 159–171.
- Krien, Y., M. Karpytchev, V. Ballu, M. Becker, C. Grall, S. Goodbred, S. Calmant, C.K. Shum, and Z. Khan (2019) Present-day subsidence in the Ganges-Brahmaputra-Meghna delta: Eastern amplification of the Holocene sediment loading contribution. *Geophys. Res. Lett.* 49, 10764–10772.
- Mallick, R., Bürgmann, R., Johnson, K., & Hubbard, J. (2021). A unified framework for earthquake sequences and the growth of geological structure in fold-thrust belts. *Journal of Geophysical Research: Solid Earth*, 126, e2021JB022045, doi: 10.1029/2021JB022045
- Mallick, R., E.O. Lindsey, L. Feng, J. Hubbard, P. Banerjee, and E.M. Hill (2019). Active Convergence of the India-Burma-Sunda Plates Revealed by a New Continuous GPS Network, *Journal of Geophysical Research: Solid Earth*, 124. doi: 10.1029/2018JB016480
- Marriner, N., Flaux, C., Morhange, C., Kaniewski, D., 2012. Nile Delta’s sinking past: Quantifiable links with Holocene compaction and climate-driven changes in sediment supply? *Geology* 40 (12), 1083–1086. <https://doi.org/10.1130/G33209.1>.

- Meckel, T.A., ten Brink, U.S., Williams, S.J., 2007. Sediment compaction rates and subsidence in deltaic plains: numerical constraints and stratigraphic influences. *Basin Res* 19, 19–31.
- Milliman, J.D., and K.L. Farnsworth (2011). *River Discharge to the Coastal Ocean: A Global Synthesis*. Cambridge University Press, 384 pp.
- Milliman J.D., J.M. Broadus and F. Gable, (1989). Environmental and Economic Implications of Rising Sea Level and Subsiding Deltas: The Nile and Bengal Examples. *Ambio*, 18, 340-345.
- Minderhoud, P.S.J., G. Erkens, V.H. Pham, V.T. Bui, L. Erban, H. Kooi and E. Stouthamer (2017) Impacts of 25 years of groundwater extraction on subsidence in the Mekong delta, Vietnam, *Environ. Res. Lett.* 12, 064006, doi:10.1088/1748-9326/aa7146.
- Mirza, M.M.Q. (2003). Three Recent Extreme Floods in Bangladesh: A Hydro-Meteorological Analysis, *Natural Hazards* 28, 35–64.
- Mitra, S., Priestley, K. F., Borah, K., & Gaur, V. K. (2018). Crustal structure and evolution of the Eastern Himalayan plate boundary system, Northeast India. *Journal of Geophysical Research: Solid Earth*, 123, 621–640. doi: 10.1002/2017JB014714
- Mondal, D., C.M. McHugh, R.M. Mortlock, M.S. Steckler, S. Mustaque (2018). Microatolls document the 1762 and prior earthquakes along the southeast coast of Bangladesh, *Tectonophysics*, 745, 196–213, doi: 10.1016/j.tecto.2018.07.020.
- Nienhuis, J.H., A.D. Ashton, D.A. Edmonds, A.J.F. Hoitink, A.J. Kettner, J.C. Rowland & T.E. Törnqvist (2020). Global-scale human impact on delta morphology has led to net land area gain. *Nature*, 577, 514-518, doi: 10.1038/s41586-019-1905-9.
- Oryan, B. (2022) Long-term and short-term processes affecting inelastic deformation above subduction zone interfaces, Ph.D. Thesis, Columbia University, 202p.
- Ostanciaux, É., Husson, L., Choblet, G., Robin, C., Pedoja, K., 2012. Present-day trends of vertical ground motions along the coast lines. *Earth Sci. Rev.* 110, 74–92. <http://dx.doi.org/10.1016/j.earscirev.2011.10.004>.
- Palamenghi, L. (2012) Tectonic and Sea Level Control on the Transport and Depositional Processes in a Siliciclastic Sedimentary Basin. Insights from the Ganges-Brahmaputra Delta, Bengal Basin, Bangladesh. Ph.D. Thesis, University of Bremen, 166pp.
- Parua, P.K. (2010). *The Ganga: Water Use in the Indian Subcontinent*. Water Science and Technology Library 64, Springer, 404 pp. doi: 10.1007/978-90-481-3103-7
- Paszowski, A., Goodbred, S., Borgomeo, E., Khan, M. S. A., and Hall, J. W. (2021). Geomorphic change in the Ganges–Brahmaputra–Meghna delta. *Nature Reviews Earth & Environment*, 2, 763–780. doi: 10.1038/s43017-021-00213-4.
- Pawlowicz, R., B. Beardsley and S. Lentz (2002). Classical tidal harmonic analysis including error estimates in MATLAB using T_TIDE, *Computers & Geosciences* 28, 929–937.
- Pethick, J. and Orford, J.D. (2013). Rapid rise in effective sea-level in southwest Bangladesh: Its causes and contemporary rates. *Global Planetary Change* 111: 237–245. doi: 10.1016/j.gloplacha.2013.09.019
- Pickering, J.L., S.L. Goodbred Jr., M.D. Reitz, T.R. Hartzog, D.R. Mondal, and M.S. Hossain (2014), Late Quaternary sedimentary record and Holocene channel avulsions of the Jamuna and Old Brahmaputra River valleys in the upper Bengal delta plain, *Geomorphology* 227: 123-136, doi: 10.1016/j.geomorph.2013.09.021
- Reitz, M.D., Pickering, J.L., Goodbred, S.L., Paola, C., Steckler, M.S., Seeber, L., Akhter, S.H., 2015. Effects of tectonic deformation and sea level on river path selection: theory and application to the Ganges–Brahmaputra–Meghna River Delta. *J. Geophys. Res. Earth Surf.* <http://dx.doi.org/10.1002/2014JF003202>.
- Rogers, K.G., S.L. Goodbred, D.R. Mondal, 2013. Monsoon sedimentation on the ‘abandoned’ tide-influenced Ganges-Brahmaputra delta plain, *Estuarine, Coastal and Shelf Science* 131, 297-309, <http://dx.doi.org/10.1016/j.ecss.2013.07.014>
- Rogers, K., & Overeem, I. (2017). Doomed to drown? Sediment dynamics in the human-controlled floodplains of the active Bengal Delta. *Elementa Science of the Anthropocene*, 5, 66. Doi: 10.1525/elementa.250
- Sadler, P.M., 1981. Sediment accumulation rates and the completeness of stratigraphic sections. *J. Geol.* 89, 569–584.
- Saleh, M., Becker, M., 2019. New estimation of Nile Delta subsidence rates from InSAR and GPS analysis. *Environ. Earth Sci.* 78 <https://doi.org/10.1007/s12665-018-8001-6>.
- Sarker, M.H., Choudhury, G.A., Akter, J., Hore, S.K., 2012. Bengal Delta Not Sinking at a Very High Rate. *Daily Star* (23rd December 2012).

- Sarker, M.H., J. Akter and Md.M. Rahman, 2013. Century-scale dynamics of the Bengal Delta and future development, 4th International Conference on Water & Flood Management (ICWFM-2013), 91-104.
- Shamsudduha, M., Chandler, R.E., Taylor, R.G., and Ahmed, K.M. (2009). Recent trends in groundwater levels in a highly seasonal hydrological system: the Ganges-Brahmaputra-Meghna Delta. *Hydrology and Earth System Sciences* 13, 2373–2385.
- Shamsudduha, M., Taylor, R.G., Ahmed, K.M., Zahid, A., 2011. The impact of intensive groundwater abstraction on recharge to a shallow regional aquifer system: evidence from Bangladesh. *Hydrogeology Journal* 19, 901–916.
- Sharma, S., Deshpande, S., 2017. Architectural strategies used in Hindu temples to emphasize sacredness. *J. Architect. Plann. Res.* 34 (4), 309–319.
- Sheldon, N.D. and G.J. Retallack (2001). Equation for compaction of paleosols due to burial. *Geology*, 29, 247–250.
- Shum, C., A. Liibus, R. Ahmed, B. Braun, V. Ballu, S. Calmant, J. Chen, J. Guo, F. Hossain, M. Hossain, C. Jenkins, Z. Khan, M. Kuhn, J. Kusche, F. Papa; M. Becker, A. Bernzen, C. Brachet, M. Calzas, C. Dai, O. Francis, Y. Jia, J. Kim, C. Kuo, D. Maillard, C. Mayet, R. Rietbroek, K. Shang, L. Testut, K. Tseng, B. Uebbing, P. Valtý, J. Wan, K. Zhu (2014). Quantifying and projecting relative sea-level rise at the regional scale: The Bangladesh Sea-Level Project (BanD-AID), Abstract G21B-0439, EOS Trans., Fall American Geophysical Union Meeting, San Francisco, December 15–19.
- Sincavage R., Goodbred, S., and Pickering, J., (2017) Holocene Brahmaputra River path selection and variable sediment bypass as indicators of fluctuating hydrologic and climate conditions in Sylhet Basin, Bangladesh: *Basin Research*, 30, 302–320, doi:10.1111/bre.12254. 2017
- Singh, A., K. Bhushan, C. Singh, M.S. Steckler, S.H. Akhter, L. Seeber, W.-Y. Kim, A.K. Tiwari, R. Biswas, Crustal structure and tectonics of Bangladesh: New constraints from inversion of receiver functions, *Tectonophysics*, 680, 99–112, doi: 10.1016/j.tecto.2016.04.046, 2016.
- Slingerland, R. and Smith, N. D. (2004). River Avulsions and Their Deposits, *Ann. Rev. of Earth and Planetary Sci.*, 32, 255-283.
- Sarker, M. H. & Thorne, C. R., (2006). "Morphological response of the Brahmaputra-Padma-Lower Meghna river system to the Assam Earthquake of 1950, In: Braided Rivers: Process, Deposits, Ecology and Management (ed. by G. H. S. Smith, J. L. Best, C. S. Bristow, & G. E. Petts)." 289–310. Special Publication 36 of the IAS, Blackwell Publishing, UK.
- Sarma, J.N., 2005. Fluvial process and morphology of the Brahmaputra River in Assam, India. *Geomorphology* 70, 226–256.
- Sclater, J. G., and Christie, P. A. (1980), Continental stretching; An explanation of the post Mid-Cretaceous subsidence of the central North Sea basin: *Journal of Geophysical Research*, 85, 3711-3739.
- Small, C. (2004). The Landsat ETM+ spectral mixing space. *Remote Sensing of Environment*, 93(1), 1–17. <https://doi.org/10.1016/j.rse.2004.06.007>
- Small, C. (2018). Multisource imaging of urban growth and infrastructure using Landsat, Sentinel and SRTM. In *NASA landsat-sentinel science team meeting*.
- Small, C., & Milesi, C. (2013). Multi-scale standardized spectral mixture models. *Remote Sensing of Environment*, 136, 442–454. <https://doi.org/10.1016/j.rse.2013.05.024>
- Sousa, D., & Small, C. (2017). Global cross-calibration of Landsat spectral mixture models. *Remote Sensing of Environment*, 192, 139–149. <https://doi.org/10.1016/j.rse.2017.01.033>
- Steckler, M.S., Akhter, S.H., and L. Seeber (2008). Collision of the Ganges-Brahmaputra Delta with the Burma Arc: Implications for earthquake hazard. *Earth and Planetary Science Letters*, 273, 367-378.
- Steckler, M.S., Mondal, D., Akhter, S.H. Seeber, L., L. Feng, J. Gale, E.M. Hill, M. Howe (2016) Locked and loading megathrust linked to active subduction beneath the Indo-Burman Ranges, *Nature Geosciences*, *Nature Geosciences*, 9, 615–618, doi: 10.1038/ngeo2760.
- Steckler, M.S., Nooner, S.L., Akhter, S.H., Chowdhury, S.K., Bettadpur, S., Seeber, L., Kogan, M.G., 2010. Modeling Earth deformation from monsoonal flooding in Bangladesh using hydrographic, GPS, and Gravity Recovery and Climate Experiment (GRACE) data. *J. Geophys. Res. Solid Earth* 115, B08407. <http://dx.doi.org/10.1029/2009JB007018>.
- Steckler, M.S., B. Oryan, C.A. Wilsan, C. Grall, S.L. Nooner, D.R. Mondal, S.H. Akhter, S. DeWolf, S.L. Goodbred, Synthesis of the Distribution of Subsidence of the Lower Ganges-Brahmaputra Delta, Bangladesh, *Earth-Science Reviews*, 224, 103887, doi:10.1016/j.earscirev.2021.103887.
- Steiger, J., Gurnell, A.M. and Goodson, J.M. (2003). Quantifying and characterizing contemporary riparian sedimentation. *River Research and Applications* 19, 335-352. doi: <http://dx.doi.org/10.1002/rra.708>

- Syvitski, J.P.M., Kettner, A.J., Overeem, I., Hutton, E.W.H., Hannon, M.T., Brakenridge, R.G., Day, J., Vörösmarty, C., Saito, Y., Giosam, L., Nicholls, R.J., 2009. Sinking deltas due to human activities. *Nat. Geosci.* 2 (10), 681–686. <http://dx.doi.org/10.1038/ngeo629>.
- Syvitski J.P.M., Vörösmarty, C.J., Kettner, A.J., Green, P. (2005) Impact of humans on the flux of terrestrial sediment to the global coastal ocean. *Science* 308:376–380. doi:10.1126/science.1109454
- Terzaghi, K., Peck, R.B. (1967). *Soil Mechanics in Engineering Practice*, 2nd ed. Wiley, New York, 729pp.
- Tessler, Z., C. J. Vörösmarty, M. Grossberg, I. Gladkova, H. Aizenman, J.P.M. Syvitski, E. Foufoula-Georgiou (2015). Profiling risk and sustainability in coastal deltas of the world. *Science*, 349 (6248), 638-643.
- Tessler, Z. D., C. J. Vörösmarty, I. Overeem and J. P. Syvitski (2018) A model of water and sediment balance as determinants of relative sea level rise in contemporary and future deltas. *Geomorphology*.
- van Asselen, S. (2011). The contribution of peat compaction to total basin subsidence: Implications for the provision of accommodation space in organic-rich deltas. *Basin Res.* 23, 239–255
- van Asselen, S., G. Erkens, E. Stouthamer, H. Woolderink, R. Geeraert, and M.M. Hefting (2018) The relative contribution of peat compaction and oxidation to subsidence in built-up areas in the Rhine-Meuse delta, The Netherlands. *Science of the Total Environment* 636, 177–191, doi: 0.1016/j.scitotenv.2018.04.141.
- Wang, Y., Shyu, J.B.H., Sieh, K., Chiang, H.-W., Wang, C.-C., Aung, T., Lin, Y.N., Shen, C.-C., Min, S., Than, O., Lin, K.K., Tun, S.T., 2013. Permanent upper plate deformation in western Myanmar during the great 1762 earthquake: Implications for neotectonic behavior of the northern Sunda megathrust. *J. Geophys. Res. Solid Earth* 118, 1277–1303, doi: 10.1002/jgrb.50121.
- Webb, E. L., D. A. Friess, K. W. Krauss, D. R. Cahoon, G. R. Guntenspergen, and J. Phelps (2013), A global standard for monitoring coastal wetland vulnerability to accelerated sea-level rise, *Nat. Clim. Change*, 3, 458–465.
- Wilson, C.A., and S.L. Goodbred (2015). Construction and Maintenance of the Ganges-Brahmaputra Meghna Delta: Linking Process, Morphology, and Stratigraphy. *Annual Review of Marine Science*, 7, 67-88.
- Wilson, C., Goodbred, S., Small, C., Gilligan, J., Sams, S., Mallick, B., & Hale, R. (2017). Widespread infilling of tidal channels and navigable waterways in the human-modified tidal delta plain of Southwest Bangladesh. *Elementa-Science of the Anthropocene*, 5, 78. doi: 10.1525/elementa.263.
- Woods, C., I. Overeem, K. Tiampo, M. Steckler (2019) DInSAR Sentinel-1A time series analysis to map subsidence of the Ganges-Brahmaputra-Meghna Delta, Abstract G13B-0538 presented at AGU Fall Meeting, San Francisco, Dec 9-13, 2019.
- Zahid, K.M., Uddin, A. (2005). Influence of overpressure on formation velocity evaluation of Neogene strata from the eastern Bengal Basin, Bangladesh, *J. Asian Earth Sci.* 25, 419–429.

7 Supplemental Material

1-Hazipur Well

The boundary at 244 m depth in the 1960 Hazipur-1 well is ascribed to the top of the Dupi Tila Fm and overlain by undated Recent-subrecent deposits (Loske and Teigler, 2013). However, formations in the prograding GBD are very time transgressive (Najman et al., 2012). Najman et al. (2012) propose a seismic stratigraphy in which the base of Megasequence 3, generally corresponding to the “recent” deposits, is 0.4-1.9 Ma. The boundary that Alam (1996) note is corresponds to a dominantly clay to a dominantly sand transition (Loske and Teigler, 2013). This is likely a shift to more proximal deposits or a shift in fluvial pathways and cannot be confidently correlated to the base of the Holocene. Shallow seismic imaging and tube well sampling (Pickering et al., 2018; Grall et al., 2018) indicate the base of the Holocene at the well, which lies in the Brahmaputra incised lowstand valley, should be about 60 m below sea level. The Hazipur-1 well is situated slightly landward of the Hinge Zone (Fig. 1) where limited subsidence is expected and reworking of the deposits can easily produce a lithologic transition at ages before the beginning of the Holocene. We thus consider this date to be unreliable.

2- Table S1: Summary of papers on subsidence discussed in text

Full listing of all individual measurements up to 2015 can be found in Brown and Nichols (2015)

Source	Area	Timescale	Methods	Subsidence Rates (subsidence +ve)
Alam (1996)	Throughout Bangladesh and West Bengal	Millennial	Summary of earlier data; Radiocarbon ages; Hydrocarbon well stratigraphy	-0.3 to 4 mm/y 22 mm/y
Hoque and Alam (1997)	Throughout Bangladesh and West Bengal	Millennial	Summary of earlier data; Estimated tectonic subsidence (multiple methods) Peat and wood assumed 5000y age	0.1 to 3.35 mm/y + 21 mm/y (Sylhet) 0.24-5.48 mm/y
Allison et al. (2003)	Lower Delta Plain, Bangladesh	Millennial	Radiocarbon dates; 5 previously published dates 7 new dates	0.52-7.12 mm/y Average = 2.18 mm/y
Grall et al. (2018)	Throughout Bangladesh	Millennial	Radiocarbon dates on tube well samples over Holocene	0 to 4.5 mm/y
Ericson et al. (2006)	Global	Millennial, Decadal,	Rates from Alam (1996) and Haq (1997) who estimates 10-25 mm/y (4 mm/y natural + 13 mm/y water withdrawal)	Up to 25 mm/y
Brown and Nichols (2015)	Throughout Bangladesh and West Bengal	All Scales: Millennial, Centennial, Decadal	Compilation of 203 rates from 24 papers. Methods include archeology, wells, radiocarbon, geomorphology, GNSS, groundwater levels, InSAR, neotectonics, magnetostratigraphy, tank excavation	-1 to 44 mmy mean 5.6 mm/y median 2.9 mm/y; Rates decrease with increasing time interval

Source	Area	Timescale	Methods	Subsidence Rates (subsidence +ve)
Sarker et al. (2012)	SW Bangladesh	Centennial	Relative plinth elevation	-0.6 to 2.5 mm/y
Hanebuth et al. (2013)	Katka in Sundarbans	Centennial	Elevation relative to modern land level with 6 radiocarbon and 7 OSL dates	4.1 ± 1.1 mm/y
Syvitski et al. (2009)	Global	Decadal	Tides gauges from PSMSL; average rate 8.35 mm/y high rate at Khepupara 18 mm/y	8-18 mm/y
Ostanciaux et al. (2012)	Global	Decadal	Tides gauges from PSMSL; 5 sites India (-3.65 mm/y) 2 sites Bangladesh (Hiron Point, Khepupara; 12.33 mm/y)	-3.56 and 12.33 mm/y
Higgins et al. (2014)	Swath from north of Dhaka to Noakhali	Decadal	ALOS-1 InSAR for 2007-2011; Calibrated with GNSS	0 to 18 mm/y
Reitz et al. (2015)	Throughout Bangladesh	Decadal	18 GNSS with 3 in coastal zone; time series from 2003 or 2007 to 2013	3 to 8 mm/y in coastal zone
Becker et al. (2020)	Throughout Bangladesh and West Bengal	Decadal	Analysis of groups of tide gauges for subsidence	Expected maximum subsidence of 1.5 to 7.2 mm/y for different regions

3-Shakher Temple

Sarker et al. (2012) describes the temple as “the only standing ancient structure in the Sundarbans is located in Shakher Tek, about one kilometer away from the east bank of the Sibsa River. In the early 17th century, Raja Paratapaditya had established a township and a fort there during his reign in order to fend off Arakanese and Portuguese pirates. The temple itself was built by the Pratapaditya settlers. It is located in Dacope upazila of Khulna district. Made of brickwork, the temple is a temple for the goddess Kali of the Hindu religion.”

Paratapaditya was the last Hindu King of Jessore until his defeat by the Mughals in 1611. He ascended the throne in 1584. He built multiple forts including ones in the Sundarbans. The time of construction of the Shakher temple and the nearby fort is not known, but they were possibly built after 1602, when the Arakanese took control of Sandwip Island. It is worth noting that in the Rennell map of 1776 (Fig. S1), there is a split of the Murjuttah River (current Sibsa River) into multiple channels near where the fort and temple are. The fort and temple were likely built along the main channel on the natural levee of the island to control the channel, rather than 1 km inland from it as they are now.

We interpret the plinth level as being at a ridge at the base of the stairs (Fig. 6). This ridge is found around all sides of the temple. Furthermore, this position is consistent with the augering conducted by S. Goodbred and D. Mondal at the temple where they encountered a brick layer (Fig. S2) whose base we interpret as the original TPL level minus any excavation for preparing and leveling the site for construction. The depth of the base of the brick layer was at 1.5 ± 0.1 m below the surface.

The temple was likely built on the levee of the island to further protect against flooding, but is now in the interior. In the calculations 0.2 m is added to the subsidence to account for the change in ground surface. This is based on the GPS elevation data in Auerbach et al. (2015) showing a dropoff in elevation of this amount in the Sundarbans away from the channel.

We calculate the subsidence based on the elevation of the various reference layers and the depth to the base of the brick layer. In the calculations, we follow the Sarker et al. (2012) estimate of 0.25 m of relative sea level rise since the temple was built. This is subtracted off the RSLR to get the subsidence rate. We estimate the plinth level as 0.1 m above TPL level from our photos. We estimate original surface excavated by ~0.1 m to remove mud and plants and level ground.

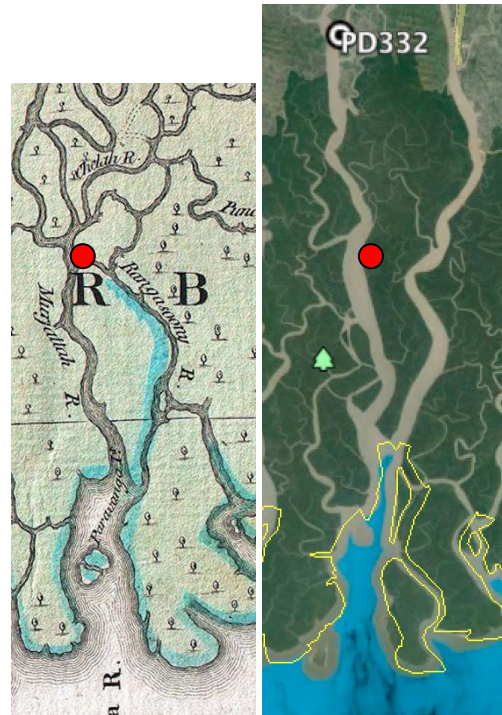


Figure S1. Comparison of segment of Rennell (1776) map and Google Earth image in the vicinity of the temple (red dot).

Using Sarker et al. (2012) method (Figure 5)

Original Plinth (PLS) = TPL + (1.2 to 1.8 m)
(augering yielded 1.6 m)

Current Plinth (PLE) = TPL + 0.1 m

Subsidence = PLS - PLE + Levee - Excavation - SLR

Subsidence = (1.2 to 1.8) - 0.1 + 0.2 - 0.1 - 0.25 = .95 to 1.55 m

at 400 y = 2.4 mm/y to 3.9 mm/y (for augering result = 3.4 mm/y).

Determination using auger results

Current base of bricks = TPL - 1.5 ± 0.1 m

Subsidence = (TPL - Bricks) + Levee - SLR - Excavation

Subsidence = 1.5 + 0.2 - 0.25 - 0.1 = 1.35 m

at 400 y = 3.4 mm/y ± 0.25 mm/y

or

Using Absolute elevations

Original TPL = 2.6 m (MHW from Auerbach et al. (2015))

Current TPL = 2.4 m (Fast static GPS result from Auerbach et al. (2015))

Current plinth = 2.4 - 1.5 = 0.9 m

Subsidence = OTPL - CTPL - SLR - Excavation

Subsidence = 2.6 - 0.9 - 0.25 - 0.1 m = 1.35 m

at 400 y = 3.4 mm/y ± 0.25 mm/y



Figure S2. Dhiman Mondal and others examine the auger, which contains a piece of brick.

The result is that estimates range from ~2.4-3.9 mm/y. If the observed elevation difference between the bricks and the plinth is used, the estimates are all 3.4 ± 0.5 mm/y. These estimates are not independent, but are consistent. It is lower if you do not assume that the temple was built on the island levee. The levee height of 0.2 m is equal to the observed elevation changes for the Sundarbans in the Auerbach et al. (2015) GPS survey. The interior elevation for the ground height at the temple is from a measurement during the same GPS survey, with the base stations 30 km to the north at PD32 (Figure S1).

4- Initial Core Logs

The figure on the following page shows the distribution of sand and mud deposits in the Holocene stratigraphy of the lower Bengal Delta. Data shown for four east-west core transects (G, H, J, K). Core locations shown on inset map and accompanying location table. The average proportion of mud across each transect is shown in Figure 8 on the main report and emphasizes the increase in mud in the fluvial-tidal delta (H, J, K) versus the fluvial delta (G).

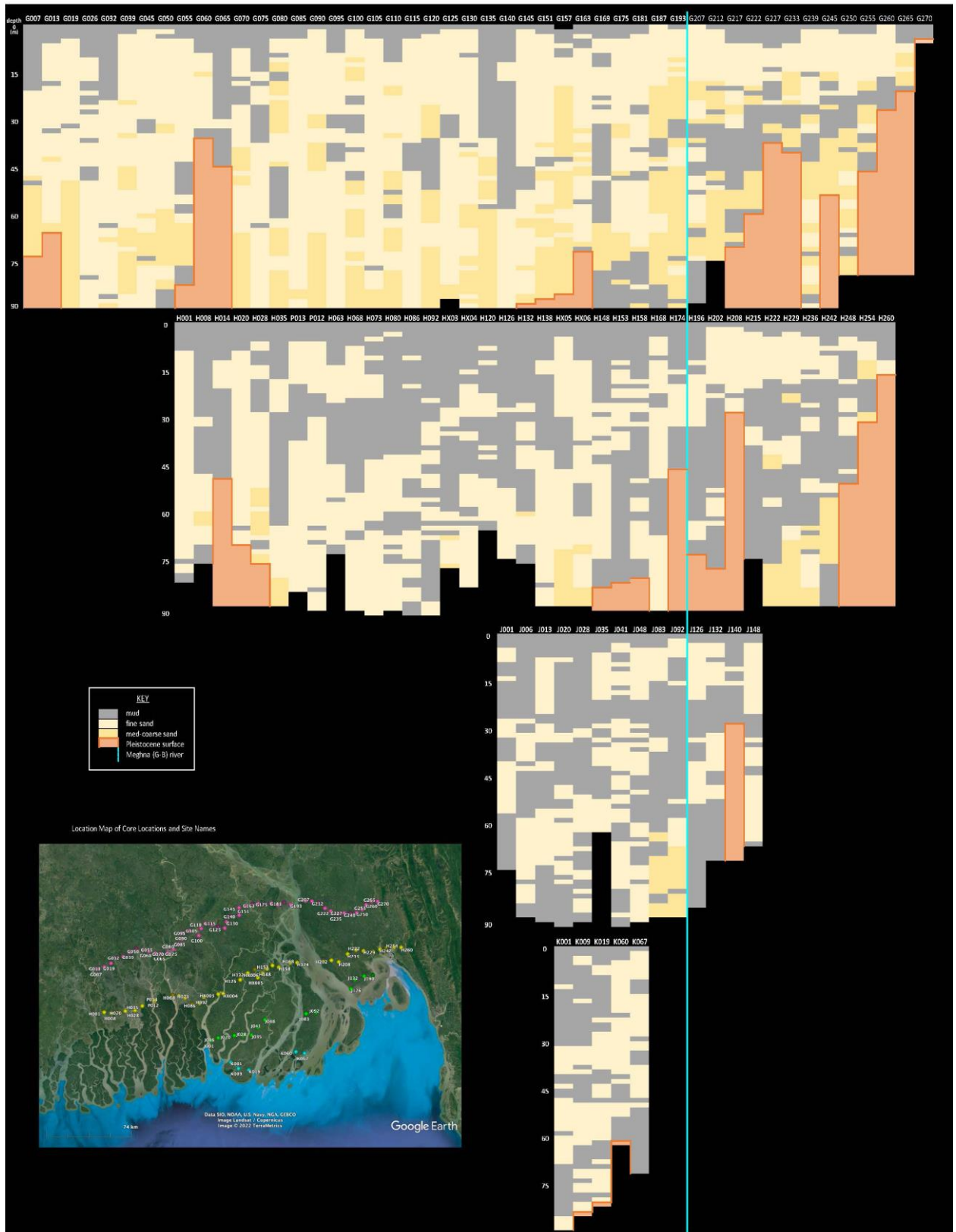


Figure S3. Distribution of sand and mud deposits in the Holocene stratigraphy of the lower Bengal Delta. Data shown for four east-west core transects (G, H, J, K).

5- Geodesy in GBD

GNSS systems have been used to examine tectonics of the IndoBurma subduction zone (e.g., Steckler et al., 2016, Mallick et al., 2019) and the Shillong Plateau (Mallick et al., 2020). Results indicate 13-17 mm/y of active eastward subduction across the IndoBurma subduction zone (Steckler et al., 2016, Mallick et al., 2019). However, Panda et al. (2020) suggest convergence is only 7-10 mm/y by referencing the motion to the stable Sunda block to the SE, rather than the Shan Plateau directly to the east. The Shillong Massif is rotating clockwise and overthrusting the Bengal Basin at rates reaching 5-8 mm/y in the eastern part of the plateau (Mallick et al., 2020). While these studies focused on the horizontal components of the velocity, the models predict 3-4 mm/y of subsidence from elastic loading and similar amounts of uplift farther east and north (Oryan et al., 2020). Reitz et al. (2015) examined the vertical component of GPS throughout Bangladesh for regional patterns and found both subsidence and uplift in the foldbelt reaching 7 mm/y. We have reprocessed all available data. Here we present subsidence rates for stations in southwestern Bangladesh. Figure S3 show the time series for all the stations in southwestern Bangladesh with the modeled subsidence, including seasonal corrections shown as thin lines. Values and locations for the stations are provided in Table S1.

Two of the sites with the longest records, PUST and KHUL/KHL2 had their original, intermittently working, outdated systems replaced. For PUST, a Trimble 400ssi was replaced with a Septentrio PolaRx5 in 2019 using the same antenna mount. For KHUL, a Trimble 400ssi was replaced with a Trimble NetR9 in 2014. The new antenna, KHL2, is ~200 m farther west.

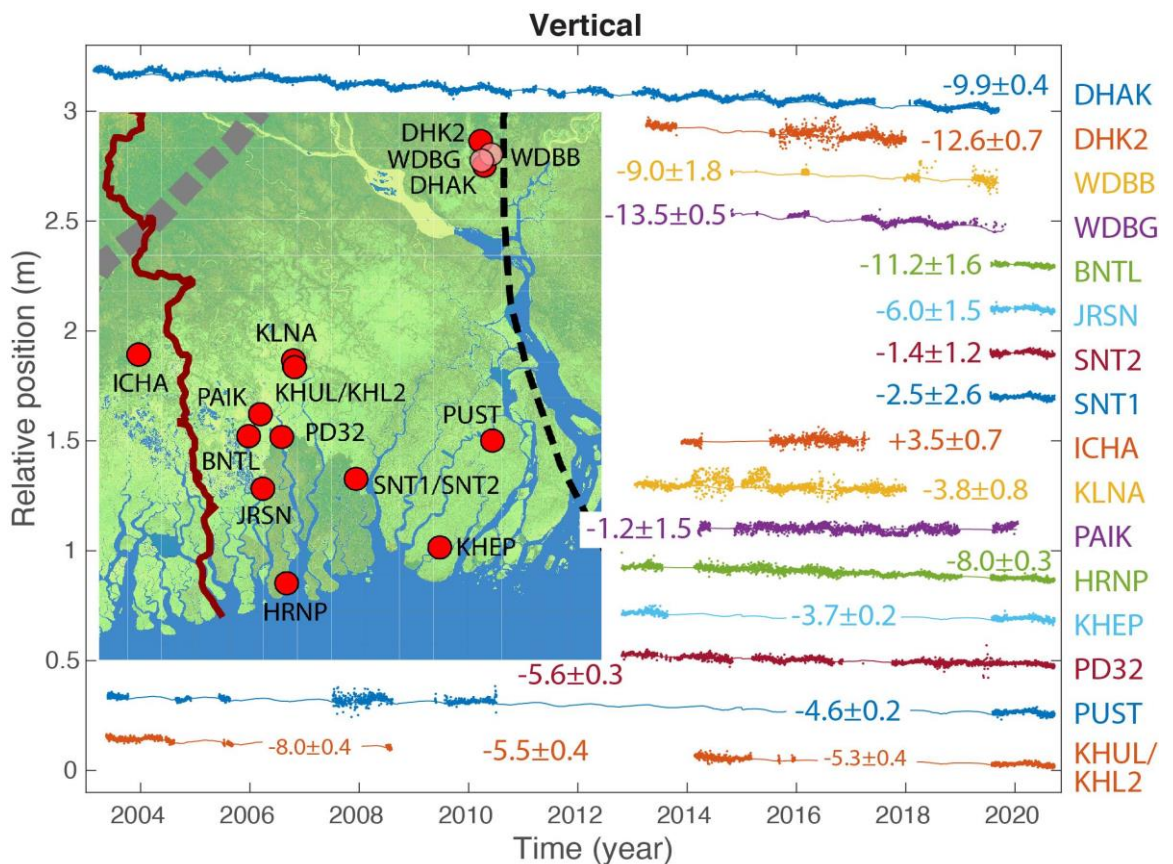


Figure S4. Vertical position time series for all of stations used in this paper. Colored dots and curves denoted daily GNSS measurement and long-term fitted behaviour for each station, respectively. We assigned an arbitrary constant shift to aid in visualization. The map shows the labelled position of each station.

Table S2: Locations and rates of subsidence measurements, along and installer and time span.

Site	Installer	Latitude	Longitude	Vertical Rate \pm	Years	No. Points
DHAK	LDEO/DUEO	23.7267	90.4013	-10.27 \pm 0.36	16.56	5249
DHK2	EOS	23.8047	90.3879	-13.28 \pm 0.67	4.75	989
WDBB	LDEO/DUEO	23.7887	90.4115	-9.56 \pm 0.57	4.91	287
WDBG	LDEO/DUEO	23.7529	90.3883	-12.12 \pm 0.67	5.01	794
BNTL	LDEO/BWDB	22.4981	89.2301	-6.78 \pm 0.77	2.67	831
JRSN	LDEO/BWDB	22.2480	89.3445	-2.05 \pm 0.80	2.67	885
SNT2	LDEO/BWDB	22.2556	89.8055	2.82 \pm 1.43	2.68	938
SNT1	LDEO/BWDB	22.2522	89.8051	-0.04 \pm 1.72	2.68	876
ICHA	EOS	22.8999	88.7360	2.30 \pm 0.81	3.42	743
KLNA	EOS	22.8526	89.5313	-4.73 \pm 0.62	4.96	1639
PAIK	BanD-Aid	22.5848	89.3194	-2.76 \pm 1.57	4.78	1480
HRNP	LDEO/DUEO	21.8164	89.4594	-7.37 \pm 0.29	9.43	2601
KHEP	LDEO/DUEO	21.9867	90.2197	-3.72 \pm 0.17	9.42	1085
PD32	LDEO/DUEO	22.5046	89.4359	-5.32 \pm 0.39	9.43	2601
PUST	LDEO/DUEO	22.4650	90.3833	-4.29 \pm 0.14	18.51	1598
KHUL/KHL2	LDEO/DUEO	22.8028/22.8021	89.5345/89.5327	-5.35 \pm 0.31	18.86	1447
KHLC	BanglaPIRE*	22.6717	89.5694	9 \pm 1	4.95	136-224
PD32 RSET	LSU	22.4520	89.4840	9.7 \pm 1.6	5	11
Shakher Temple		22.22	89.50	3.4 \pm 0.5	~400	2

LDEO = Lamont Doherty Earth Observatory

DUEO=Dhaka University Earth Observatory

BWDB=Bangladesh Water Development Board

BanD-Aid = Bangladesh Delta: Assessment of the Causes of Sea-level Rise Hazards and Integrated Development of Predictive Modeling Towards Mitigation and Adaptation

<http://belmont-bandaaid.org>

EOS=Earth Observatory of Singapore

BanglaPIRE= PIRE: Life on a Tectonically-Active Delta: Convergence of Earth Science and Geohazard Research in Bangladesh with Education and Capacity Building

<http://www.banglapire.org>

<https://www.researchgate.net/project/BanglaPIRE-Life-on-a-Tectonically-Active-Delta>

LSU = Louisiana State University

6 - RSET-MH measurements

Information regarding RSET-MH locations are compiled in Table S3. The longest running datasets analyzed for this report include 8 years of measurements in the Sundarbans mangrove forest at Sorbothkhali and Polder 32 at the village of Shrinagar (see Figures S4 & S5). Results are compiled in Table S4. For the RSET-MH installed for this project, plots of surface elevation and vertical accretion will be shown (see Figures S6 & S7), but the datasets are too short (3 years) for any meaningful analysis and calculation of shallow subsidence.

Table S3. Compilation of RSET-MH location (latitude/longitude), install dates, and geographic location notes.

RSET #	RSET LOCATION	BWDB Install site	Latitude °N	Longitude °E	Date Installed	Number of 4' rods installed	Notes
RSET-1	Sorbothkhali/P32	P32	22.45943	89.46863	10/26/2013	10	Sundarbans streambank
RSET-2	Sorbothkhali/P32	P32	22.45788	89.46806	10/27/2013	13	Sundarbans interior
RSET-3	Shrinagar/P32	P32	22.51961	89.49201	10/29/2013	8	Inside polder
RSET-4	Shrinagar/P32	P32	22.52029	89.49152	10/30/2013	8	Inside polder
RSET-5	Sorbothkhali/P32	P32	22.44785	89.50017	3/13/2015	10	Sundarbans interior
RSET-6	Sorbothkhali/P32	P32	22.4599	89.4764	3/14/2015	7	Sundarbans streambank
RSET-7	Shrinagar/P32	P32	22.51907	89.49034	10/5/2017	12	Inside polder
RSET-8	Shrinagar/P32	P32	22.51997	89.49043	10/9/2017	9	Inside polder
RSET-9	Katka	Katka	21.86285	89.77966	7/4/2018	9	Sundarbans streambank
RSET-10	Katka	Katka	21.863	89.77913	7/5/2018	13	Sundarbans interior
4A	Sarankhola/SNT1	Site 4	22.255623	89.805673	7/19/2019	20	Inside polder
4C	Sarankhola/SNT1	Site 4	22.24861	89.800921	7/20/2019	16	Outside polder
RSET-11	Hiron Point	Site 3	21.81892	89.45645	7/22/2019	20	Sundarbans interior
RSET-12	Hiron Point	Site 3	21.818385	89.456976	7/22/2019	19	Sundarbans streambank
RSET-13	Koyra/JRSN	Site 2	22.25625	89.33666	7/24/2019	19	Outside polder
RSET-14	Koyra/JRSN	Site 2	22.24704	89.343645	7/24/2019	20	Inside polder
RSET-15	Baintola/BNTL	Site 1	22.4978	89.23315	7/25/2019	19	Inside polder
RSET-16	Baintola/BNTL	Site 1	22.49867	89.25239	7/25/2019	16	Outside polder
RSET-17	Kuakata/KHEP	Site 6	21.85821	90.13929	7/30/2019	16	Outside polder
RSET-18	Kuakata/KHEP	Site 6	21.85627	90.13556	7/31/2019	14	Inside polder
RSET-19	Patuakhali/PUST	Site 5	22.42123	90.45152	8/2/2019	20	Outside polder
RSET-20	Patuakhali/PUST	Site 5	22.42041	90.44698	8/2/2019	18	Inside polder

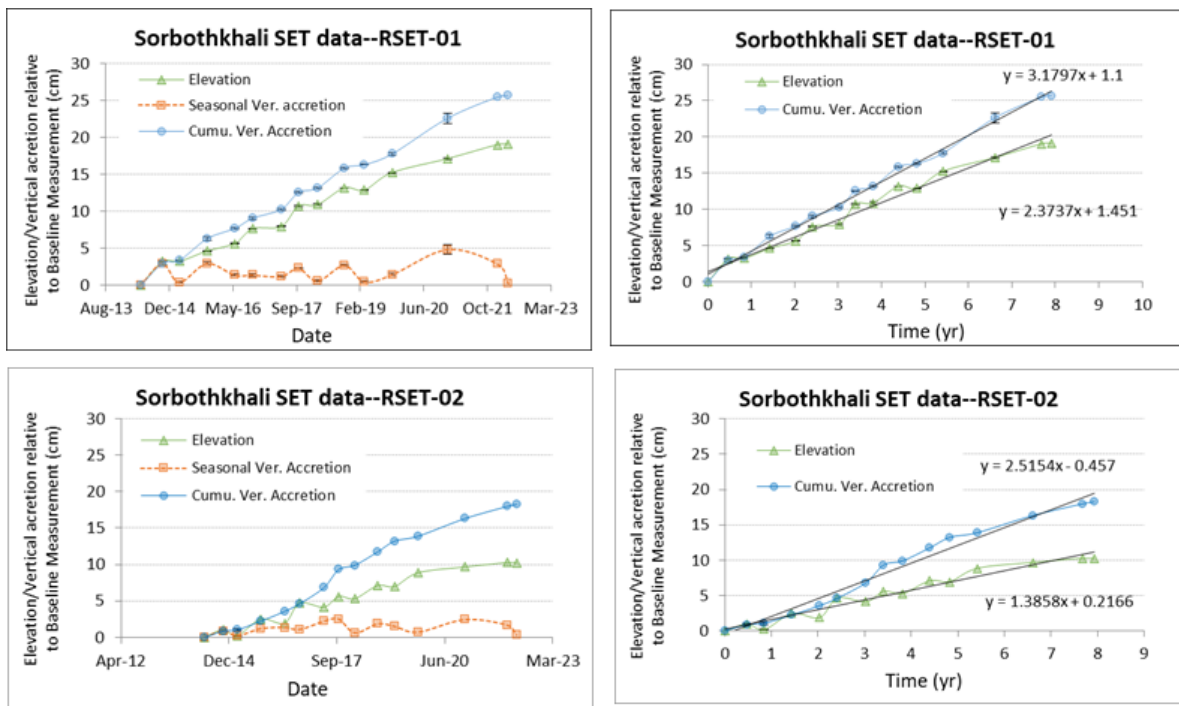


Figure S5. RSET-MH results for Sorbothkhali sites RSET-01 and RSET-02, our longest running datasets in the Sundarbans forest. Linear regression of elevation (SEC) and vertical accretion (VA) rates (shown at right) are used to calculate shallow subsidence (SS = VA - SEC). Shallow subsidence averaged from all sites is large but highly variable (9.7 ± 5.2 mm/yr). Results are compiled in Table S4.

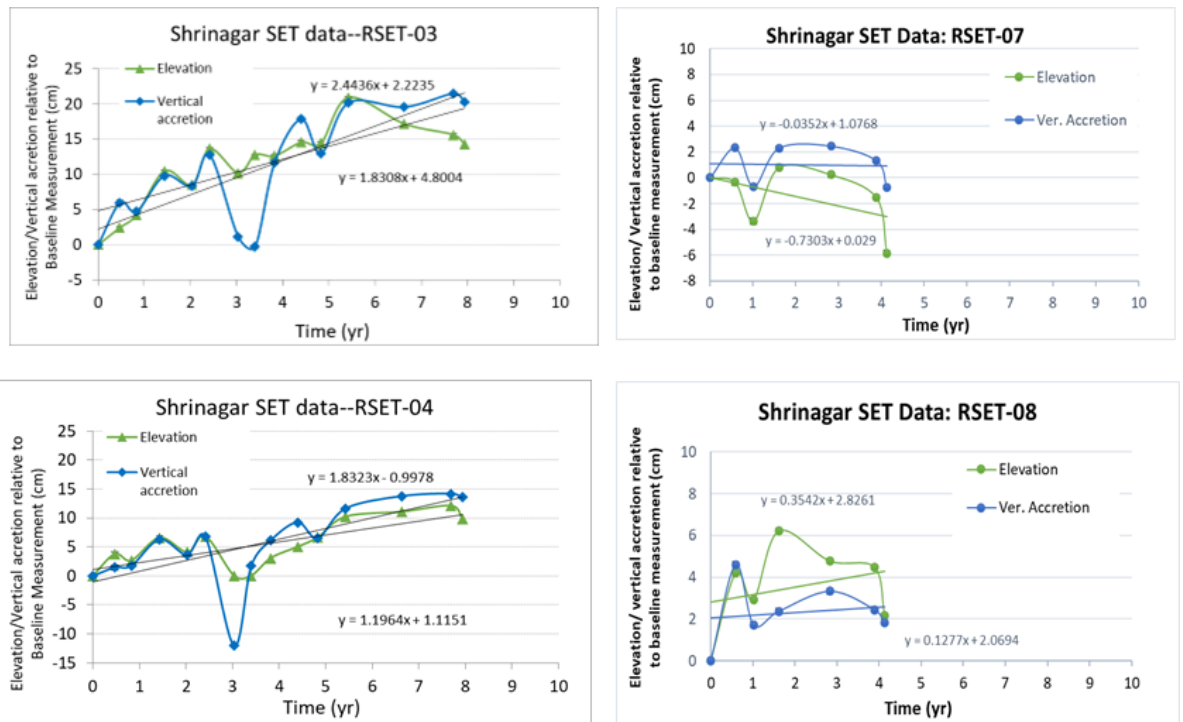


Figure S6. RSET-MH results for Polder 32 sites near Shrinagar: RSET-03 and RSET-04 are the longest running datasets, located proximal to the embankments, and RSET-07 and RSET-08 are located on the interior of the polder. Linear regression of elevation (SEC) and vertical accretion (VA) rates are used to calculate shallow subsidence ($SS = VA - SEC$). Shallow subsidence averaged from all sites is very slight but highly variable (4.3 ± 4.4 mm/yr), mostly due to shallow soil expansion occurring at RSET-08. Shallow subsidence from the creek bank sites has a slightly larger, more reasonable value (6.2 ± 0.2 mm/yr). Results are compiled in Table S4.

Table S4. Summary of RSET-MH results for the longest running datasets located in the Sundarbans (Sorbothkhali) and Polder 32 (Shrinagar). SEC = Surface Elevation Change, VA = Vertical Accretion, SS = Shallow subsidence.

Sundarbans (Shorbothkhali)		AVG (mm/yr)	STD (mm/yr)	Polder 32 (Shrinagar)		AVG (mm/yr)	STD (mm/yr)
(N=4)	Overall SEC	14.9	6.1	(N=4)	Overall SEC	6.6	11.1
	Overall VA	24.6	7.5		Overall VA	10.9	12.3
	Overall SS	9.7	5.2		Overall SS	4.3	4.4
Creek bank	SEC	17.5	8.8	Creek bank	SEC	15.1	4.5
	VA	29.5	3.3		VA	21.4	0.2
	SS	12	5.5		SS	6.2	0.2
Interior	SEC	12.6	1.8	Interior	SEC	-1.9	7.7
	VA	26.2	1.4		VA	0.5	1.2
	SS	7.4	5.5		SS	2.3	6.5

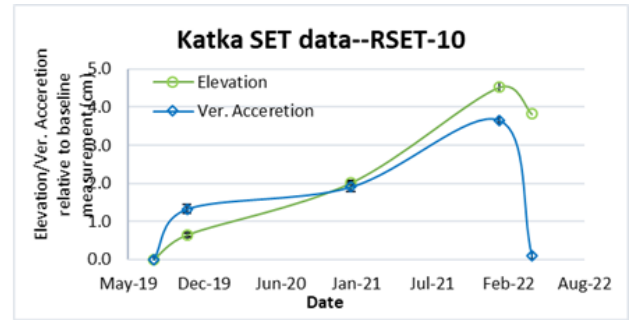
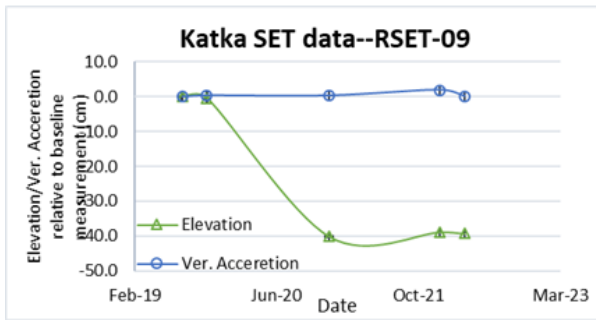


Figure S7. RSET-MH data from the Sundarbans Katka site. With only 3 years of data collection, analyses and calculation of shallow subsidence is not possible

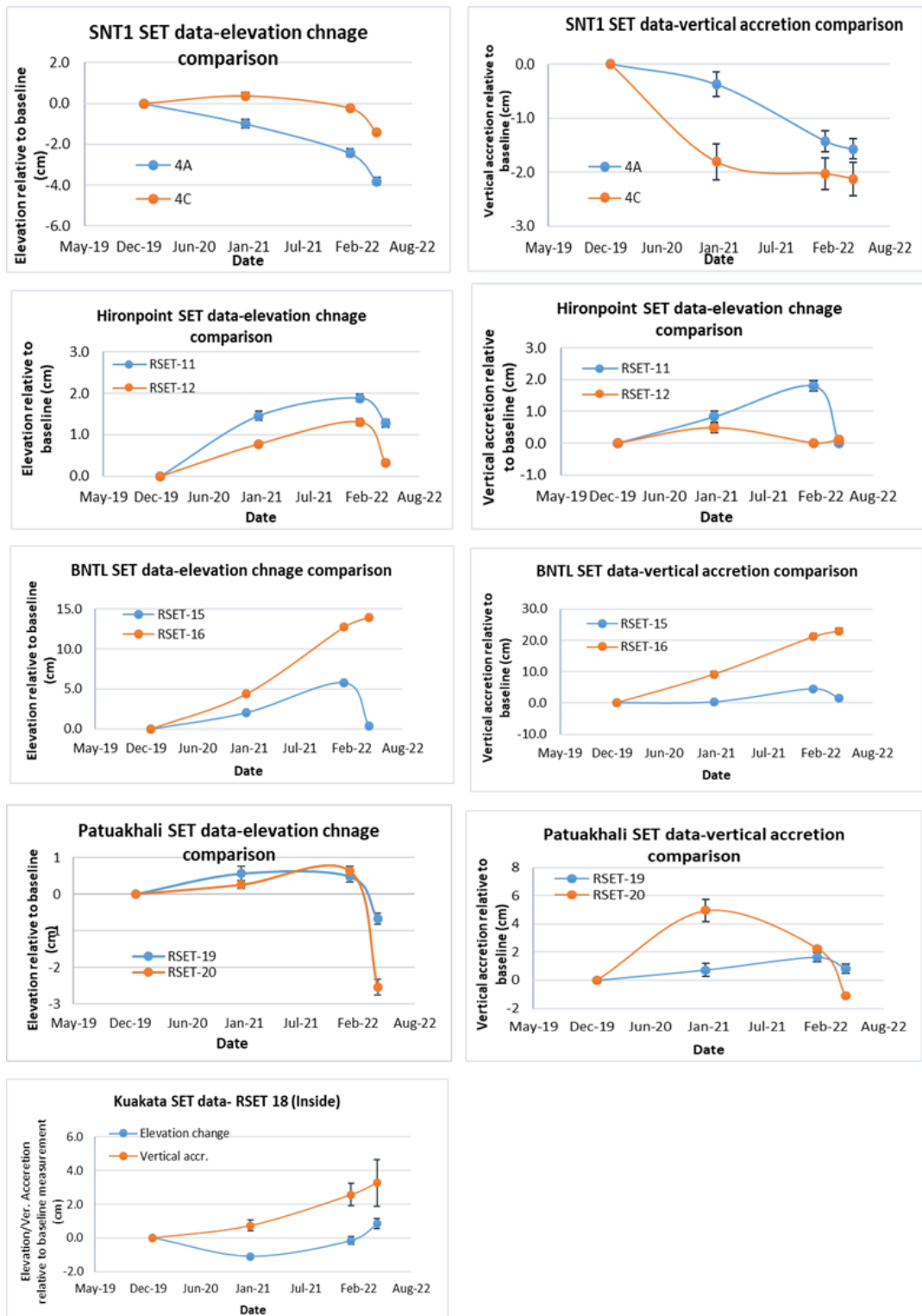


Figure S8. RSET-MH measurements for newly installed RSETs under this project. With only 3 years of data collection, analyses and calculation of shallow subsidence is not possible. RSET-17 located at Kuakata outside the embankment was destroyed by a marine vessel in 2020, thus only RSET-18 data is shown.

8 Additional References

- Haq, B.U., 1997. Regional and global oceanographic, climatic and geological factors in coastal zone planning. In: Haq, B.U., Haq, S. M., Kullenber, G., Stel, J.H. (Eds.), *Coastal Zone Management Imperative for Maritime Developing Nations*. Kluwer Academic Publishers, 55–74.
- Loske, B., and E.B. Teigler, (2013) FINAL REPORT – Preliminary Study on Shale Gas Potentiality in Bangladesh, DMT GmbH & Co. KG, 83 pp.
[http://hcu.portal.gov.bd/sites/default/files/files/hcu.portal.gov.bd/page/dd0582c2_bd5b_4331_b01f_2c9238621a56/FinalReport_Shale_Gas_Bangladesh_24_12_2013%20\(1\).pdf](http://hcu.portal.gov.bd/sites/default/files/files/hcu.portal.gov.bd/page/dd0582c2_bd5b_4331_b01f_2c9238621a56/FinalReport_Shale_Gas_Bangladesh_24_12_2013%20(1).pdf)
- Pickering, J.L., M.S. Diamond, S.L. Goodbred, C. Grall, J.M. Martin, L. Palamenghi, C. Paola, T. Schwenk, R.S. Sincavage, and V. Spieß (2018) Impact of glacial-lake paleofloods on valley development since glacial termination II: A conundrum of hydrology and scale for the lowstand Brahmaputra-Jamuna paleovalley system, *Geol. Soc. Amer. Bull.*, 131, 58–70, doi:10.1130/B31941.1.
- Mallick R., J.A. Hubbard, E.O. Lindsey, K.E. Bradley, J.D.P. Moore, A. Ahsan, A.K.M.K. Alam and E.M. Hill (2020) Subduction Initiation and the Rise of the Shillong Plateau, *Earth and Planetary Science Letters* 543, doi: 10.1016/j.epsl.2020.116351
- Najman, Y., Allen, R., Willett, E.A.F., Carter, A., Barfod, D., Garzanti, E., Wijbrans, J., Bickle, M.J., Vezzoli, G., Ando, S., Oliver, G., Uddin, M.J. (2012). The record of Himalayan erosion preserved in the sedimentary rocks of the Hatia Trough of the Bengal Basin and the Chittagong Hill Tracts, *Bangladesh. Basin Res.* 24, 499–519. doi:10.1111/j.1365-2117.2011.00540.x
- Panda, D., B. Kundu, V.K. Gahalaut, C. Rangin (2020). India-Sunda plate motion, crustal deformation and seismic hazard in the Indo-Burmese Arc, *Tectonics*, 39, e2019TC006034. doi: [10.1029/2019TC006034](https://doi.org/10.1029/2019TC006034)